



MDOT RC-1527

**CONDITION ASSESSMENT AND METHODS
OF ABATEMENT OF PRESTRESSED
CONCRETE BOX-BEAM DETERIORATION**

Phase II

**FINAL REPORT
VOLUME II**



MichiganTech

Center for Structural Durability
A Michigan DOT Center of Excellence

Research

Intentionally left blank

CONDITION ASSESSMENT AND METHODS OF ABATEMENT OF PRESTRESSED CONCRETE BOX- BEAM DETERIORATION

Phase II

Project Manager: Mr. Steve Kahl, P.E.

Submitted to



Submitted by



Western Michigan University
Department of Civil & Construction Engineering
College of Engineering and Applied Sciences
Kalamazoo, MI 49008
Fax: (269) – 276 – 3211

Dr. Haluk Aktan, P.E.
Professor & Chair
(269) – 276 – 3206
haluk.aktan@wmich.edu

Dr. Upul Attanayake
Assistant Professor
(269) – 276 – 3217
upul.attanayake@wmich.edu

Mr. Evren Ulku
Graduate Research Assistant
(313) – 577 – 3785
evren@eng.wayne.edu

MichiganTech

Michigan Technological University
Dept. of Civil & Environmental Engineering
1400 Townsend Drive
Houghton, MI 49931
Fax: (906) – 487 – 1620

Dr. Theresa M. Ahlborn, P.E.
Associate Professor
(906) – 487 – 2625
tess@mtu.edu

Dr. Yogini Deshpande
Post Doctoral Researcher
(906) – 487 – 1474
yogini@mtu.edu

Intentionally left blank

Contents

TABLE OF TABLES.....	iv
TABLE OF FIGURES.....	vi
7 Analytical Modeling of Box-Beam Sub-Assemblages	1
7.1 Objective and Approach	1
7.2 Sub-Assemblage Models of Box-Beams	1
7.2.1 The Effect of Shear Key Material Properties and Number of Diaphragms ...	3
7.2.2 Bridge Width Effect on Clamping Stress Distribution	11
7.3 Summary and Conclusions	12
8 Analytical Modeling: Construction Simulation and Service Load Analysis.....	15
8.1 Overview.....	15
8.2 Construction Process Simulation and Analysis Results	19
8.3 Service Load Analysis	23
8.3.1 Load Combination 1: 1.0 DEAD + 1.0 NTG.....	23
8.3.2 Load Combination 2: 1.0 DEAD + 1.0 PTG	25
8.3.3 Load Combination 3: 1.0 DEAD + 1.0 LL	28
8.4 Summary and Conclusions	32
9 Rational Transverse Posttension Design	35
9.1 Overview.....	35
9.2 Construction Monitoring.....	35
9.3 Macromechanical Model	38
9.4 Rational Posttension Design Procedure	42
9.4.1 Overview.....	42
9.4.2 Analysis and Design Procedure	44
9.5 Construction Simulation with Staged Posttension.....	49
9.5.1 Service Load Analysis	55
9.6 Summary and Conclusions	67

10 Capacity Evaluation of a Box-Beam Bridge with Distressed Beams.....	71
10.1 Overview.....	71
10.2 Flexure Critical Distress and Associated Box Beam Capacities	78
10.3 Shear Critical Distress and Box Beam Capacities	85
10.4 Influence of Grout Loss and Broken Posttension Strands	85
10.5 Summary and Conslusions.....	90
11 Summary and Conclusions	95
11.1 Recommendations.....	98
12 Suggestions for Future Research	101
13 References.....	103

Intentionally left blank

TABLE OF TABLES

Table 8-1. Material Properties of Prestressing Strands.....	17
Table 9-1. Averaged Transverse Moment, N-m/m (in-lb/in)	47
Table 9-2. Geometric Parameters of Diaphragms and Transverse Posttension Locations along Beam Height	48
Table 9-3. Posttension Force Requirement for the Sample Bridge	49
Table 10-1. Distress Level Summary in FE Analysis.....	72
Table 10-2. Distress Observed During Field Inspection and Used in FE Models.....	72
Table 10-3. Service Moment Capacities for Box-beams at Various Distress Levels (ft-kips)	79
Table 10-4. Nominal Moment Capacities of Box-beams with Various Distress Levels (ft- kips)	81
Table 10-5. Moment Demands for Distress Levels One through Four at Mid-span	81
Table 10-6. Moment Demands for Distress Levels One through Four at Quarter Point	82
Table 10-7. Rating Factors for Distress Levels One through Four at Mid-span.....	84
Table 10-8. Rating Factors for Distress Levels One through Four at Quarter Points.....	84
Table 10-9. Moments due to Dead and Live Loads, Nominal Moment Capacities, and Rating Factors for Distress at Mid-span.....	87
Table 10-10. Nominal Moment Capacity and Load Demands Based on FE Results (Distress at Mid-span).....	91
Table 10-11. Nominal Moment Capacity and Load Demands Based on the AASHTO LRFD (2004) (Distress at Mid-span).....	91
Table 10-12. Rating Factors for Distress Levels One through Four at Mid-span Obtained from FE Results	92
Table 10-13. Rating Factors for Distress Levels One through Four at Mid-span Obtained Analytically Using AASHTO LRFR Specifications for Lower Bound Dead Load Demand.....	92
Table 10-14. Rating Factors for Distress Levels One through Four at Mid-span Obtained Analytically Using AASHTO LRFR Specifications for Upper Bound Dead Load Demand.....	93

Intentionally left blank

TABLE OF FIGURES

Figure 7-1. Front view of the sub-assembly with three box-beams	2
Figure 7-2. Isometric view of the box-beam sub-assembly	2
Figure 7-3. Clamping stress along the length of shear key for different grout materials (Note: stresses are taken at mid-depth of the beam)	3
Figure 7-4. Stresses YY along shear key length for different number of diaphragms (Note: stresses are taken at mid-depth of the beam)	4
Figure 7-5. Deflection profile of the mid-span transverse section bottom fiber under concentrated load. (Note: solid – with posttension and dash – without posttension)	5
Figure 7-6. Deformed shape at mid-span transverse section under concentrated load: (a) with and (b) without posttension	6
Figure 7-7. Mid-span transverse section vertical deflection at the bottom fiber of the sub-assembly made with grout material of 1000 ksi modulus under concentrated load and posttension	6
Figure 7-8. Mid-span transverse section vertical deflection at the bottom fiber under dead load with and without posttension	7
Figure 7-9. Deformed shape of mid-span transverse section under dead load: (a) with posttension and (b) without posttension	7
Figure 7-10. Deflection plot of the bottom fiber under concentrated load at mid-span transverse section for three diaphragm configuration	8
Figure 7-11. Clamping stress distribution at the mid-span transverse section under concentrated load: (a) without and (b) with posttension	9
Figure 7-12. Clamping stress distribution along the bottom fiber under concentrated load at mid-span transverse section with and without posttension.....	9
Figure 7-13. Clamping stress distribution along the bottom extreme fiber at mid-span transverse section under concentrated load with posttension	10
Figure 7-14. Clamping stress distribution along the mid-span transverse section bottom extreme fiber under concentrated load with posttension for different diaphragm configurations	11

Figure 7-15. Isometric view of sub-assembly model with four beams	11
Figure 7-16. Clamping stress variation along the length of shear keys	12
Figure 8-1. Transverse section of box-beam assemblage model	16
Figure 8-2. Isoparametric view of the box-beam assemblage model	16
Figure 8-3. 27 × 36 box beam geometry	17
Figure 8-4. Axle and lane load positions for two-lane-loaded configuration	18
Figure 8-5. Positive and negative temperature gradient loads	18
Figure 8-6. Stress development under prestressing and self-weight of beams (note: only beam and strand components are active)	19
Figure 8-7. Deformed shape under prestressing and beam self-weight	20
Figure 8-8. Clamping stress distribution in grout layers after posttension application (note: deck is still free from stresses)	20
Figure 8-9. (a) Clamping stress in grout under posttension and deck dead load and (b) clamping stress distribution along the length of the shear key (stresses are extracted using shear key mid-height nodes)	21
Figure 8-10. Cast-in-place concrete deck stresses under barrier loading (a) top and (b) bottom surfaces	22
Figure 8-11. Transverse stress distribution (a) at the top surface of the deck and (b) along the width of the deck top surface over mid-span (Section B-B) and end-diaphragm (Section A-A) under Service I load combination 1	24
Figure 8-12. Transverse stress distribution (a) at the bottom surface of the 6-in thick deck and (b) along the width of the deck bottom surface over mid-span (Section B-B) and end-diaphragm (Section A-A) under Service I load combination 1	25
Figure 8-13. Transverse stress distribution (a) at the top surface of the deck and (b) along the width of the deck top surface over mid-span (Section B-B) and end-diaphragm (Section A-A) under Service I load combination 2	26
Figure 8-14. Transverse stress distribution (a) at the bottom surface of the deck and (b) along the width of the deck bottom surface over mid-span (Section B-B) and end- diaphragm (Section A-A) under Service I load combination 2	27
Figure 8-15. (a) Clamping stress distribution of grout layers under positive thermal gradient loading and (b) clamping stress distribution along the length of grout layers with	

and without the effect of positive gradient loading (stress plots are extracted using shear key top fiber nodes)	28
Figure 8-16. Transverse stress distribution (a) at the deck top surface and (b) along the width of the deck top surface over mid-span (Section B-B) and end-diaphragm centerline (Section A-A) under Service I load combination 3 with live load on a single lane	29
Figure 8-17. Transverse stress distribution (a) at the deck bottom surface and (b) along the width of the deck bottom surface over mid-span (Section B-B) and end-diaphragm centerline (Section A-A) under Service I load combination 3 with live load on a single lane	30
Figure 8-18. Transverse stress distribution (a) at the deck top surface and (b) along the width of the deck top surface over mid-span (Section B-B) and end-diaphragm (Section A-A) under Service I load combination 3 with live load on both lanes	31
Figure 8-19. Transverse stress distribution (a) at the deck bottom surface and (b) along the width of the deck bottom surface over mid-span (Section B-B) and end-diaphragm (Section A-A) under Service I load combination 3 with live load on both lanes	32
Figure 9-1. Location of the new bridge	36
Figure 9-2. (a) Shear-key between beams 11 and 12 and (b) discontinued top posttension strands	37
Figure 9-3. Shear-key interface cracking observed on May 14 th (a) before and (b) after posttension	37
Figure 9-4. Shear-key interface cracks observed on June 4 th	38
Figure 9-5. Deck cracking observed on June 22 nd	38
Figure 9-6. Concept of macromechanical model development procedure	40
Figure 9-7. Notations – forces and moments acting on a plate element	41
Figure 9-8. Side-by-side box-beam configuration	43
Figure 9-9. Cross-section of the RVE (a) without and (b) with deck.	43
Figure 9-10. Diaphragm and shear key locations.	45
Figure 9-11. New Jersey Type 4 barrier (Note: 1 in. = 25.4 mm)	46
Figure 9-12. Position of a single HS-20 truck	46

Figure 9-13. Transverse posttension locations along the beam height	49
Figure 9-14. Clamping stress (a) contours at shear key after the first stage posttension and (b) distribution along the length of the shear key with or without staged posttension (stresses are extracted using shear key mid-height nodes)	50
Figure 9-15. Clamping stress distribution along the shear key between fascia and the first interior beams under (a) posttension and (b) posttension and deck dead load	51
Figure 9-16. Clamping stress distribution along the length of the shear key with or without staged posttension (stresses are extracted using shear key mid-height nodes; compression-negative, tension-positive)	52
Figure 9-17. Transverse stress distribution (a) at the deck top surface and (b) along the width of the deck top surface over mid-span (Section B-B) and end-diaphragm (Section A-A) after second stage posttension	53
Figure 9-18. Transverse stress distribution (a) at the deck bottom surface and (b) along the width of the deck bottom surface over mid-span (Section B-B) and end- diaphragm (Section A-A) after second stage posttension.....	54
Figure 9-19. Transverse stress distribution at the cast-in-place concrete deck top surface (a) before and (b) after the barriers are placed	55
Figure 9-20. Transverse stress distribution (a) at the top surface of the deck and (b) along the width of the deck top surface over mid-span (Section B-B) and end-diaphragm (Section A-A) under service I load combination 1	57
Figure 9-21. Transverse stress distribution (a) at the bottom surface of the 6-in thick deck and (b) along the width of the deck bottom surface over mid-span (Section B-B) and end-diaphragm (Section A-A) under service I load combination 1	58
Figure 9-22. Transverse stress distribution (a) at the top surface of the deck and (b) along the width of the deck top surface over mid-span (Section B-B) and end-diaphragm (Section A-A) under service I load combination 2	60
Figure 9-23. Transverse stress distribution (a) at the bottom surface of the cast-in-place deck and (b) along the width of the deck bottom surface over mid-span (Section B-B) and end-diaphragm (Section A-A) under service I load combination 2	61
Figure 9-24. Clamping stress (a) profile on grout layers under positive thermal gradient loading and (b) distribution along the length of grout layers with and without	

positive gradient loading (stress plots are extracted using shear key top fiber nodes; compression-negative, tension-positive).....	62
Figure 9-25. Transverse stress distribution (a) at the deck top surface and (b) along the width of the deck top surface over mid-span (Section B-B) and end-diaphragm centerline (Section A-A) under service I load combination 3 with a single lane live load	63
Figure 9-26. Transverse stress distribution (a) at the 6-in. deck bottom surface and (b) along the width of the deck bottom surface over mid-span (Section B-B) and end-diaphragm centerline (Section A-A) under service I load combination 3 with a single lane live load	64
Figure 9-27. Transverse stress distribution (a) at the deck top surface and (b) along the width of the deck top surface over mid-span (Section B-B) and end-diaphragm (Section A-A) under service I load combination 3 with live load on two lanes	65
Figure 9-28. Transverse stress distribution (a) at the 6-in. deck bottom surface and (b) along the width of the deck bottom surface over mid-span (Section B-B) and end-diaphragm (Section A-A) under service I load combination 3 with live load on two lanes	66
Figure 9-29. Transverse stress distribution along the width of the 6-in cast-in-place concrete deck bottom surface with and without staged posttension under service I load combination 2	68
Figure 9-30. Transverse stress distribution along the width of the deck top surface with and without staged posttension under service I load combination 1	68
Figure 9-31. Transverse stress distribution along the width of the deck top surface with and without staged posttension under service I load combination 3 with a single lane live load	69
Figure 9-32. Clamping stress distribution along the length of the shear key top surface with and without staged posttension under positive gradient loading	69
Figure 10-1. Finite element model of distress levels 2 and 3: (a) enlarged view of half of the distressed zone along length and (b) section view of the distressed zone (note: broken strands are not visible).....	73

Figure 10-2. Finite element model of distress level 4: (a) enlarged view of half of the distressed zone along length and (b) section view of the distressed zone (note: broken strands are not visible).....	73
Figure 10-3. LRFR decision making flow chart (AASHTO LRFR 2003)	74
Figure 10-4. Axle load configuration of HL-93 generating maximum moment at mid-span (Note: Lane load that generates additional 200 ft-kips moment at mid-span is not shown).....	75
Figure 10-5. Axle load configuration of HL-93 generating maximum moment at quarter point (Note: Lane load that generates additional 150 ft-kips moment at quarter point is not shown).....	75
Figure 10-6. Axle load configuration of HL-93 generating maximum shear 1 ft away from the support (Note: Lane load that generates additional 15.36 kips shear 1 ft away from the support is not shown)	76
Figure 10-7. Axle load configuration of Truck 21 generating maximum moment at mid-span and quarter point	76
Figure 10-8. Axle load configuration of Truck 21 generating maximum shear 1 ft away from the support	77
Figure 10-9. 3D view of the model showing distress on fascia beam and design lanes	78
Figure 10-10. a) A portion of shear key grout remain intact with the beam and (b) beam surface after shear key grout cleanly fall off	86
Figure 10-11. Shear key grout loss	86
Figure 10-12. Shear key grout loss definition.....	86
Figure 10-13. Distress at shear key between a fascia and the first interior beam at mid-span	87
Figure 10-14. Normal stress distribution through the depth of deck-beam composite cross-section under dead load + prestress (tensile +; compression -)	89
Figure 10-15. Normal stress distribution through the depth of deck-beam composite cross-section under service loads that develop 424 psi extreme fiber tensile stress (Tensile +, Compressive -)	89
Figure 10-16. Normal stress distribution through the depth of deck-beam composite cross-section only under 100 percent live load (Tensile +, Compressive -)	90

Intentionally left blank

7 ANALYTICAL MODELING OF BOX-BEAM SUB-ASSEMBLAGES

7.1 OBJECTIVE AND APPROACH

The objective of finite element modeling and dead and live loads analysis is to evaluate the impact of transverse connection design and material parameters on the performance behavior of side-by-side precast prestressed concrete box-beam bridges. The transverse connection design and material parameters used for this purpose are: shear key grout mechanical properties, posttension force magnitude and location, number of diaphragms, and the bridge width.

Box-beam sub-assembly models are developed with three and four beams to study the effect of changing bridge width on posttension distribution (Figure 7-1). The shear key grout material modulus and number of diaphragms are varied to identify their influence on the load response of the bridge. The results presented from the FE analyses include the transverse normal stress (clamping stress) distribution at the shear key location along the beam (i. e., stress YY – refer to Figure 7-2 for the definition of the coordinate system used in the analysis) and the vertical displacement profile of the mid-span cross-section (i.e., at $x=25$ ft). Clamping stress distributions are compared between three and four-beam widths to demonstrate bridge width influence.

7.2 SUB-ASSEMBLAGE MODELS OF BOX-BEAMS

The bridge FE models are based on a 27×36-in. box-beam section. This box section is the most common beam specified in Michigan bridges (Aktan et al. 2005). The FE models are developed in compliance with Section 6.65.13 of the MDOT Bridge Design Guide (2005) provisions. The models consist of three 50 ft long 27×36-in. box beams connected with full-depth shear keys. According to the MDOT Bridge Design Guide (2005), a 50 ft span is the limiting span for four transverse posttension locations. Spans that are greater than 50 ft require five posttension locations. In this analysis, for this 50 ft. limiting span, five posttension locations (1 @ each beam end, 1 @ each quarter point, and 1 @ center of beam) are used in order to evaluate the clamping stress distribution along the shear keys. The posttension force calculated for the HS-25 design load is applied to all five posttensioning locations at the mid-depth of beam (i.e., 104.5 kips). End posttension locations are 1.5 ft away from each beam end. Intermediate diaphragm

thickness is 14 inches. Posttension anchor plates (7.5×7.5×1.5-in.) are also modeled at every posttension location (Figure 7-1 and Figure 7-2).

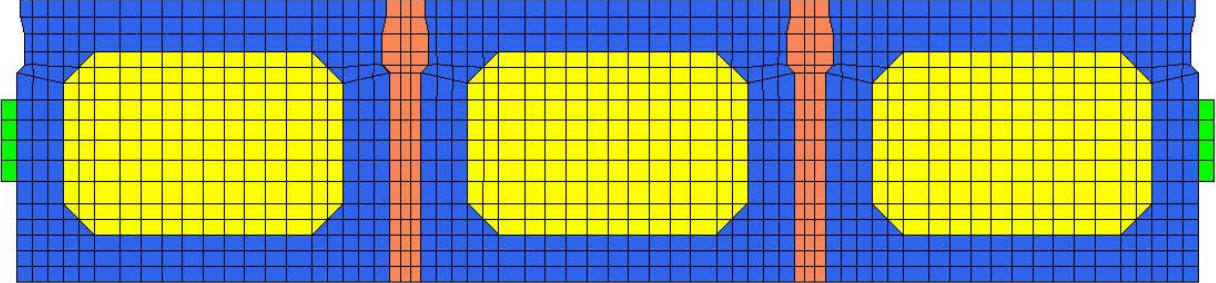


Figure 7-1. Front view of the sub-assembly with three box-beams

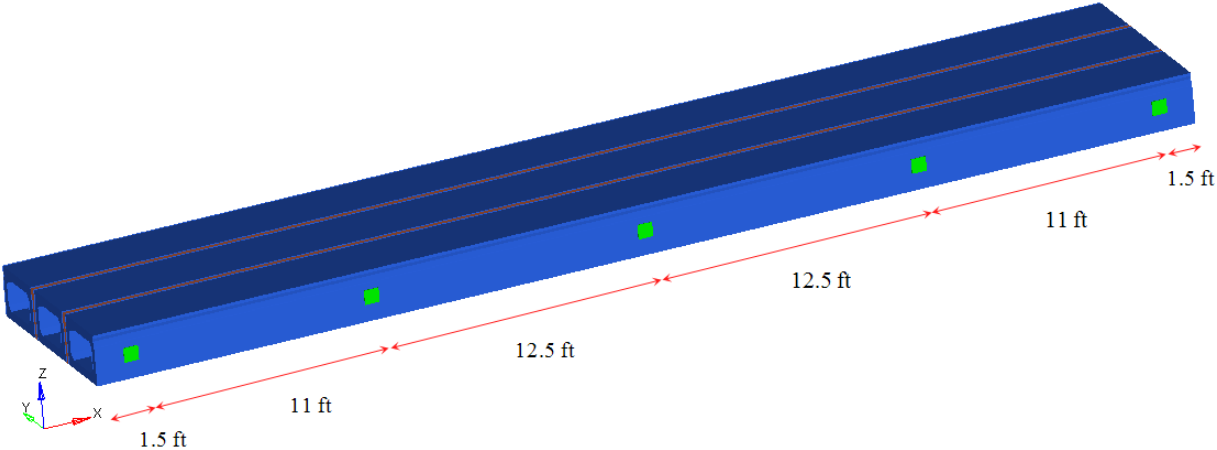


Figure 7-2. Isometric view of the box-beam sub-assembly

In the benchmark model, modulus of elasticity (E) of 5000 ksi and Poisson’s ratio of 0.2 are specified as the mechanical properties of concrete for the beam and shear key grout. The grout modulus of elasticity is high compared to that of R-2 grout used in Michigan bridges (Chapter 6). Grout properties are one of the parameters in analyzing the effects of the variation of shear key material properties on posttension stress (clamping stress) distribution and will be varied parametrically in other analyses. In the analysis, posttension is modeled unbonded and incorporated as a concentrated force of 104.5 kips applied to the anchor plates at each diaphragm location. The steel modulus of 29,000 ksi and Poisson’s ratio of 0.3 defined the material properties of the anchor plates. Live load is applied as a nodal vertical concentrated load of 25 kips at the middle beam’s mid-span. For dead load, both concrete and grout density is assumed to be 150 lb/ft³.

In the figures, tensile stresses are shown with positive (+) values, whereas negative (-) denotes compressive stresses. Downward deflections are presented with negative (-) values.

7.2.1 The Effect of Shear Key Material Properties and Number of Diaphragms

7.2.1.1 Posttension stress distribution along the shear-key

The influence of grout material properties on clamping stress distribution is investigated using five different elasticity modulus values ranging from 5000 ksi to 1000 ksi. The clamping stress variation along the length of the shear key at the beam mid-depth is presented in Figure 7-3. Stresses are calculated along a node line at beam mid-depth.

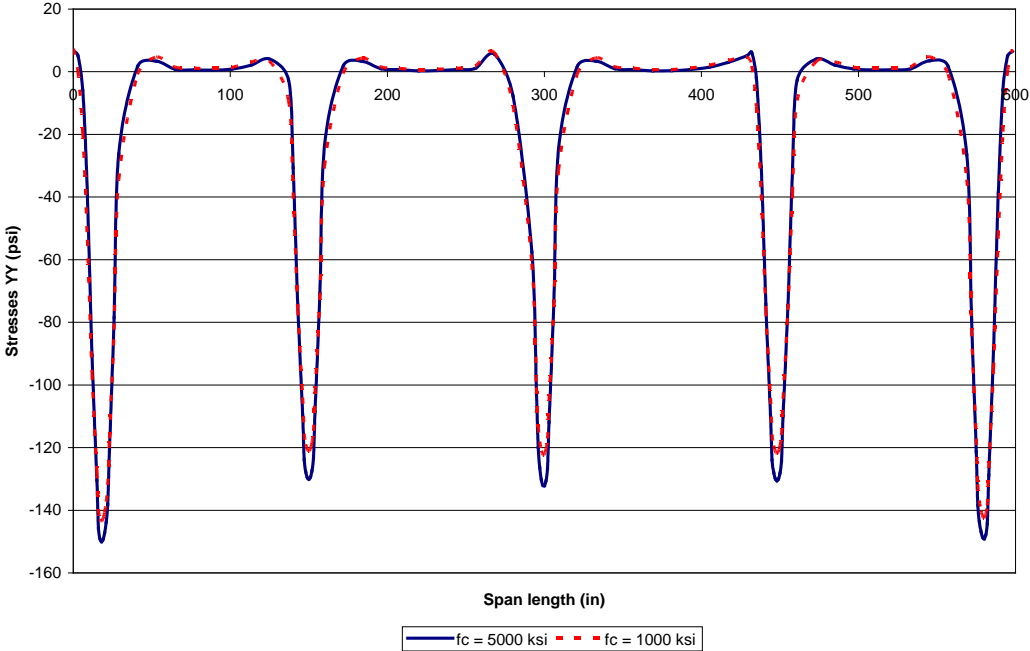


Figure 7-3. Clamping stress along the length of shear key for different grout materials (Note: stresses are taken at mid-depth of the beam)

As seen in the Figure 7-3, the clamping stress generated by the posttension forces is concentrated only within the diaphragm locations, and it is virtually zero or in tension between the diaphragm locations. Conversely, the AASHTO LRFD (2004) Section 5.14.1.2.8 requirement is that nominal transverse posttension stress (clamping stress) along the shear key, after all losses, shall not be less than 0.25 ksi. From Figure 7-3, it is clear that 0.25 ksi stress along the shear key could not be attained even within the diaphragm zone. The change in the elasticity modulus of grout material from 5000 ksi to 1000 ksi did not change the clamping stress variations along the

beam length. At diaphragm locations, the change in clamping stress levels are insignificant, with a 5000 ksi grout modulus generating 7 psi higher stress than that of a 1000 ksi grout modulus.

The impact of the number of diaphragms on the clamping stress distribution is investigated under live and dead loads. For this purpose three and five diaphragm configurations are compared while keeping the grout elasticity modulus constant at 5000 ksi. Clamping stress calculated along the length of the shear key at the beam mid-depth is presented in Figure 7-4.

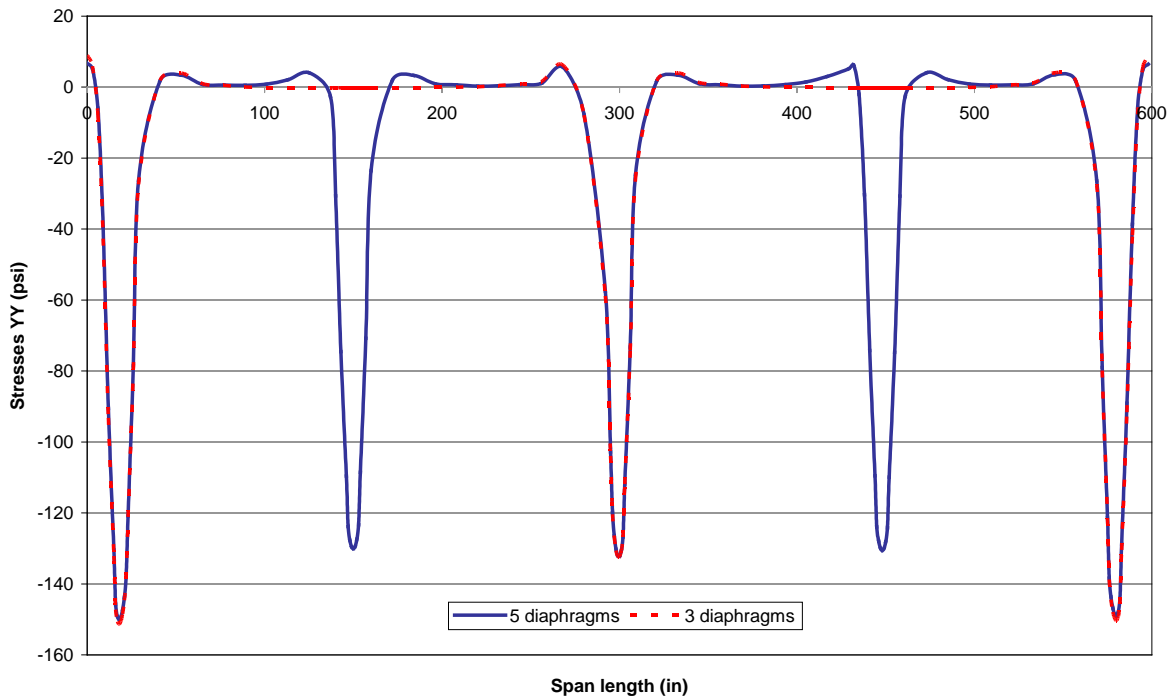


Figure 7-4. Stresses YY along shear key length for different number of diaphragms (Note: stresses are taken at mid-depth of the beam)

As seen in the Figure 7-4, the clamping stress distributions at the diaphragm locations remained identical.

7.2.1.2 Mid-span deflection

Mid-span vertical displacement profiles are calculated from a series of analyses performed to investigate relative displacement of beams with five and three diaphragms. The loading consisted of dead load and a 25 kips concentrated load applied at the center node of the mid-span cross-section. Although the concentrated load does not represent the design live load, it is placed to investigate the influence of the parameters on differential deflection. Both the concrete and grout elasticity modulus are taken as 5000 ksi unless otherwise noted.

Figure 7-5 shows the vertical displacements of a mid-span cross-section when beam sub-assembly with five diaphragms is directly subjected to a concentrated live load with and without transverse posttension. The displacements are extracted along the bottom nodes of the cross-section at mid-span. The shear key positions along the width of the cross-section are shown on Figure 7-5 as dotted lines. It is apparent from the figure that, with shear keys intact, posttension force does not help reduce the vertical displacements.

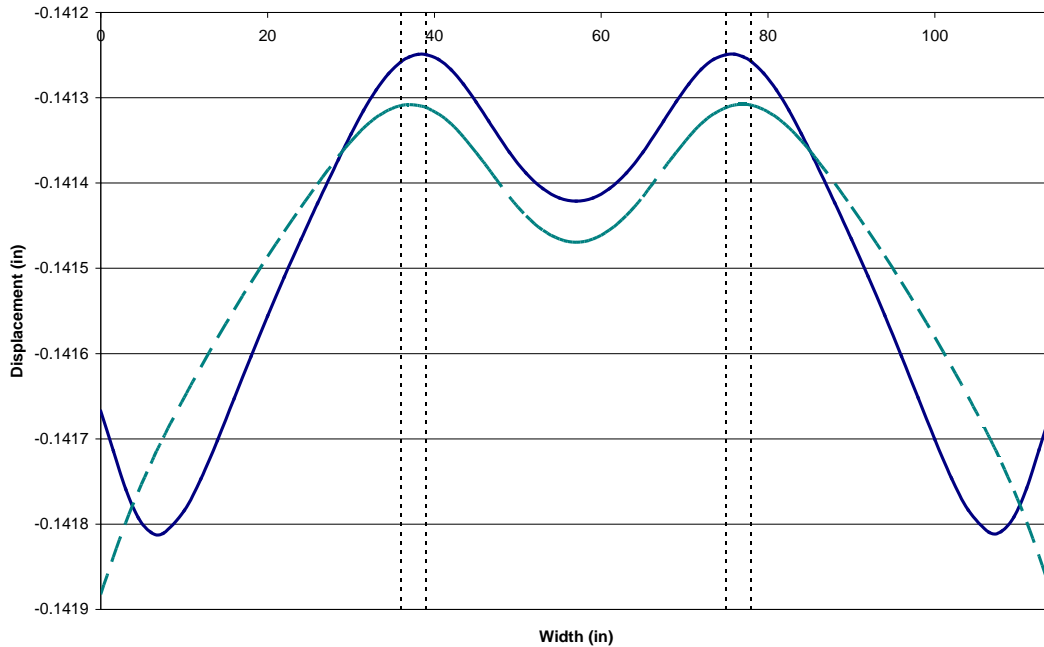


Figure 7-5. Deflection profile of the mid-span transverse section bottom fiber under concentrated load.
 (Note: solid – with posttension and dash – without posttension)

The deformed shapes of the mid-span cross-section with and without posttension are shown in Figure 7-6.

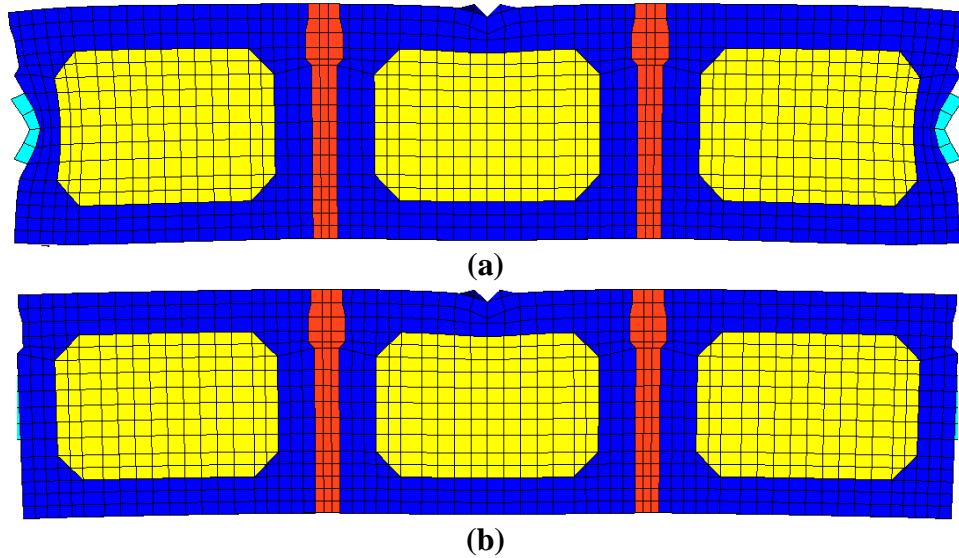


Figure 7-6. Deformed shape at mid-span transverse section under concentrated load: (a) with and (b) without posttension

The vertical displacement profile of the cross-section with five diaphragms and a grout modulus of 1000 ksi (lower bound) is shown in Figure 7-7. Although the deflected shape resembles the profile obtained in the case of 5000 ksi grout, a lower shear key modulus resulted in increased displacements. Sharp variations of vertical displacement within the shear key regions are also documented.

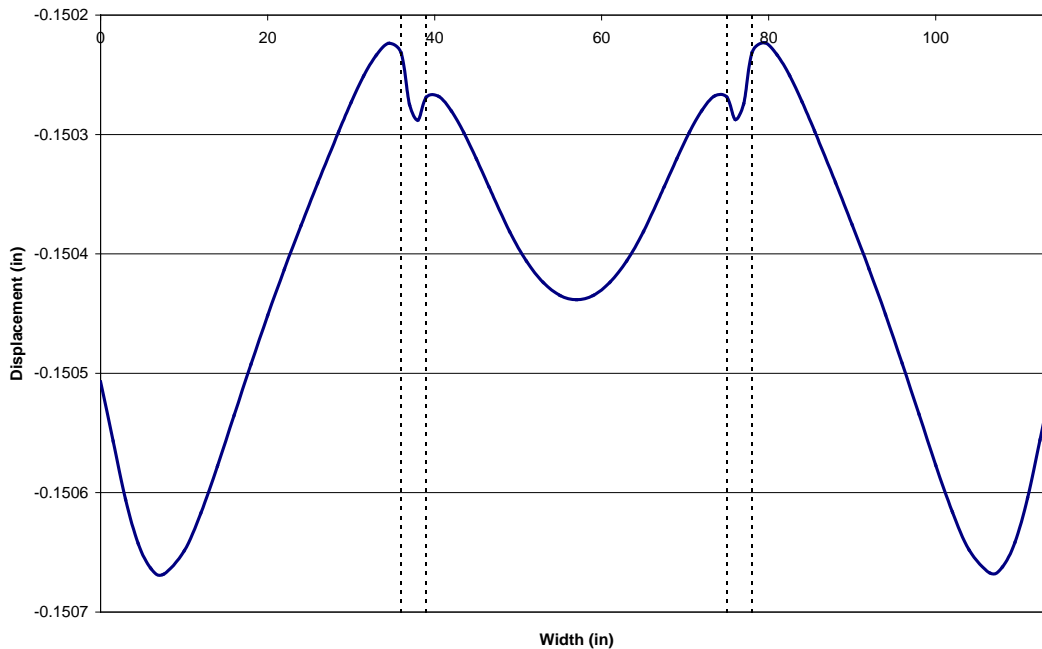


Figure 7-7. Mid-span transverse section vertical deflection at the bottom fiber of the sub-assembly made with grout material of 1000 ksi modulus under concentrated load and posttension

The box-beam sub-assembly with five diaphragms is analyzed under dead load with and without posttension. Figure 7-8 shows the vertical displacement profile of the mid-span cross-section. Figure 7-9 shows the deformed shape of the cross-section under dead load with and without posttension. As seen in Figure 7-9, when shear keys are intact, the application of transverse posttension did not influence the beam displacements.

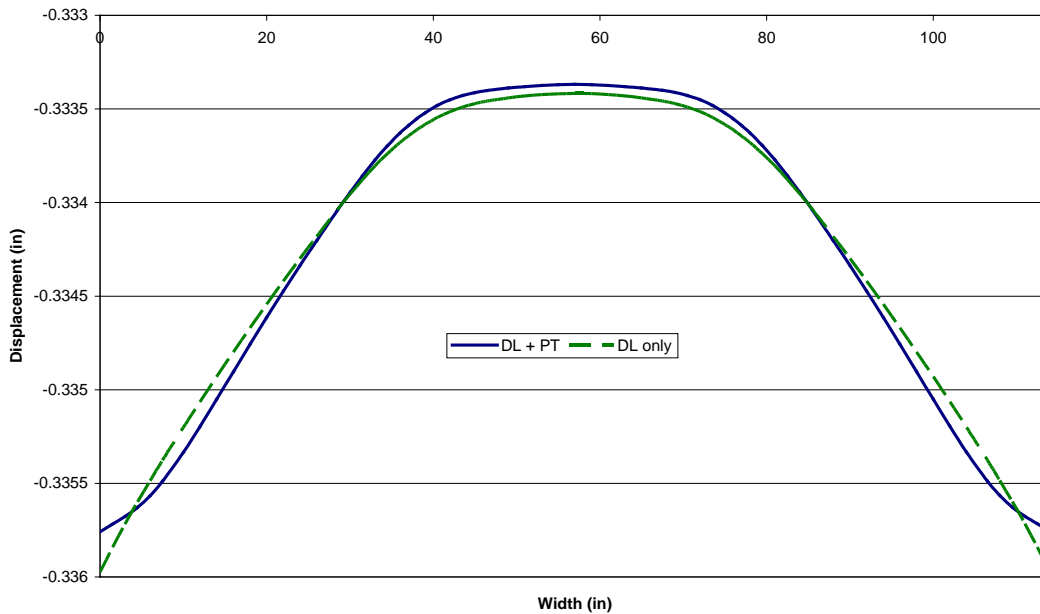


Figure 7-8. Mid-span transverse section vertical deflection at the bottom fiber under dead load with and without posttension

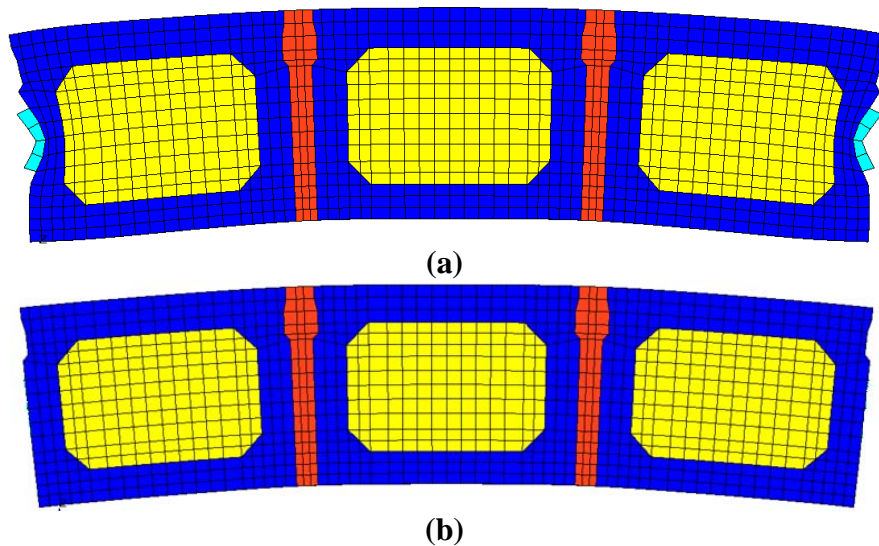


Figure 7-9. Deformed shape of mid-span transverse section under dead load: (a) with posttension and (b) without posttension

In order to evaluate the impact of the number of diaphragms on relative beam displacements, analysis results presented above with five-diaphragm configurations are compared to similar analyses on models with three diaphragms. Figure 7-10 shows the vertical displacement profile of the cross-section under concentrated load and posttension for the three diaphragm configuration. The deflected shape resembles the profile observed in the case of five diaphragms. Displacements are around 0.005-in. greater than those of the five-diaphragm configurations.

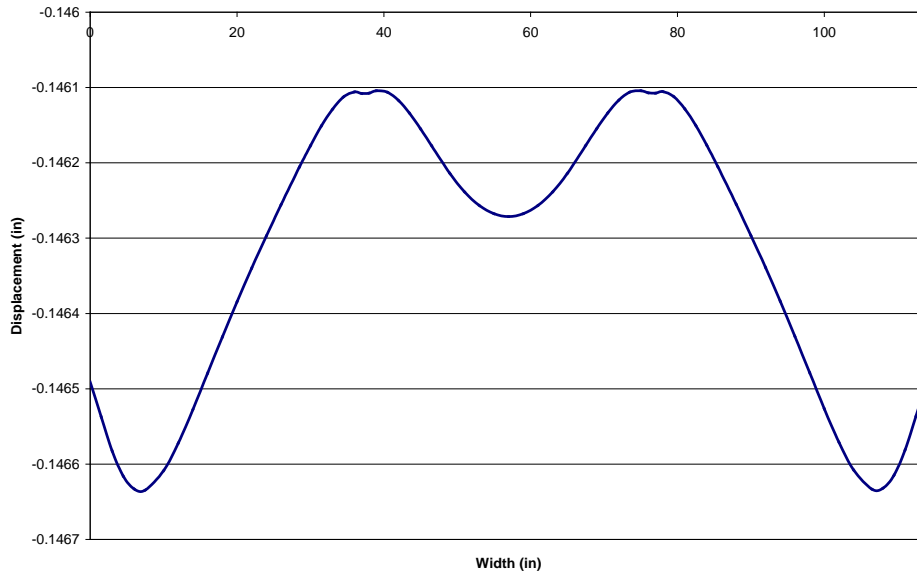


Figure 7-10. Deflection plot of the bottom fiber under concentrated load at mid-span transverse section for three diaphragm configuration

7.2.1.3 Clamping Stress Distribution in Transverse Direction

Figure 7-11 shows the clamping stress distribution within the bridge cross-section with or without posttension under a concentrated load. Figure 7-12 shows the stress profile of Figure 7-11 along the beam bottom fiber. In absence of transverse posttension, tensile stresses are developed at and near the bottom fibers of the cross-section. Application of transverse posttension eliminates most of the tensile stresses except near the boundaries.

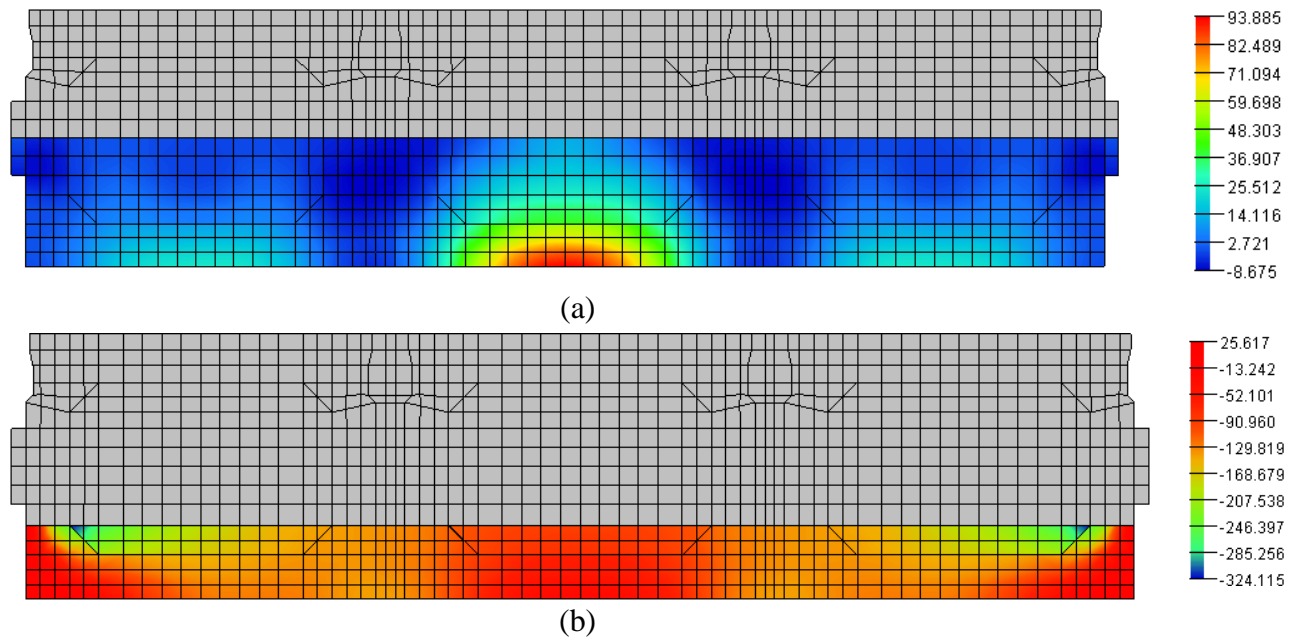


Figure 7-11. Clamping stress distribution at the mid-span transverse section under concentrated load: (a) without and (b) with posttension

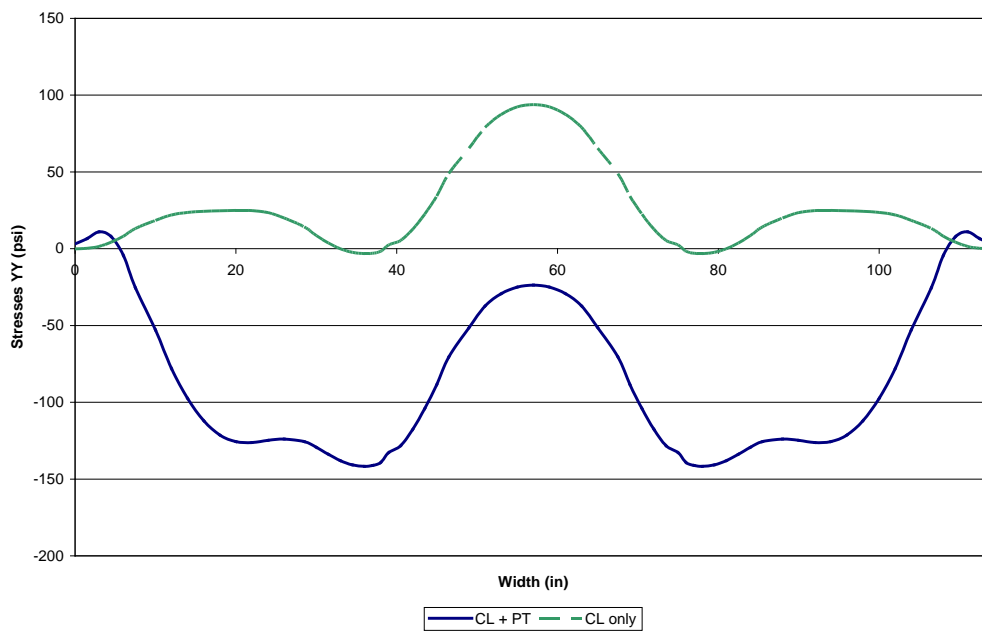


Figure 7-12. Clamping stress distribution along the bottom fiber under concentrated load at mid-span transverse section with and without posttension

Previously, the influence of the decrease in grout elasticity modulus on cross sectional deformations was investigated by comparing the analysis results with a grout modulus of 1000

ksi. The clamping stress profile is compared in Figure 7-13 for both grout modulus values along the beam bottom fiber of the bridge width. Displacements are increased and compressive stress maximum magnitudes near the bottom fiber are reduced with a lower grout modulus. The largest reduction in compressive stress is about 10 psi (i.e., about 7 percent). Results show that the difference between the stress profiles with a reduced grout elasticity modulus is negligible.

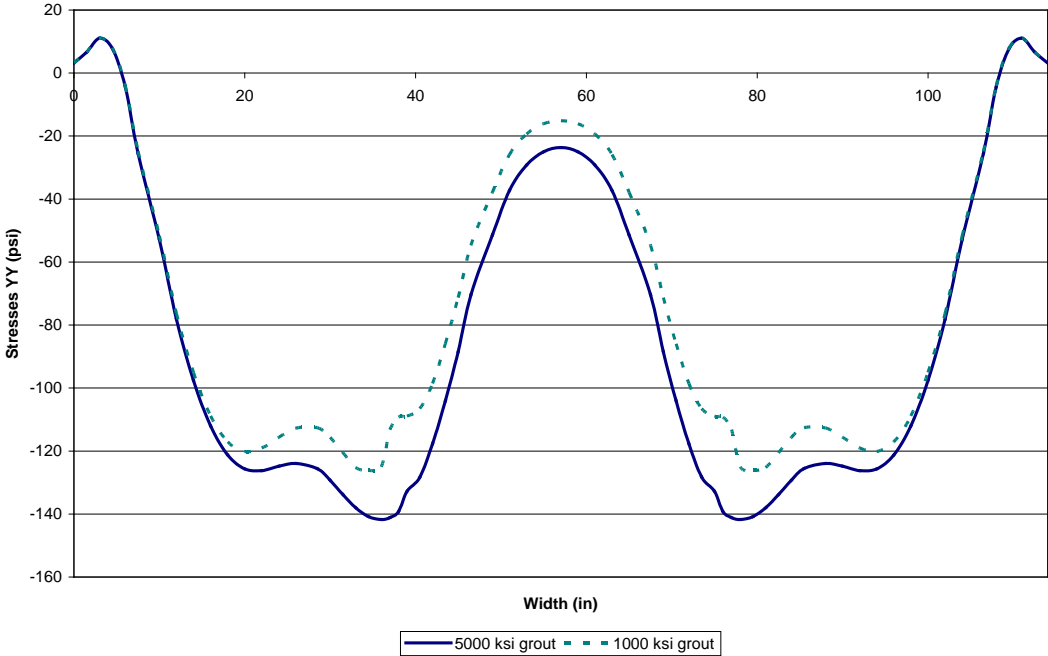


Figure 7-13. Clamping stress distribution along the bottom extreme fiber at mid-span transverse section under concentrated load with posttension

The clamping stress distribution of three and five diaphragm analysis models is compared. In both models there is a diaphragm at the mid-span. Figure 7-14 compares the clamping stress distribution at the mid-span transverse section under concentrated load and posttension along the bottom fibers with three and five diaphragm configurations. The stresses for three and five diaphragm configurations are almost identical.

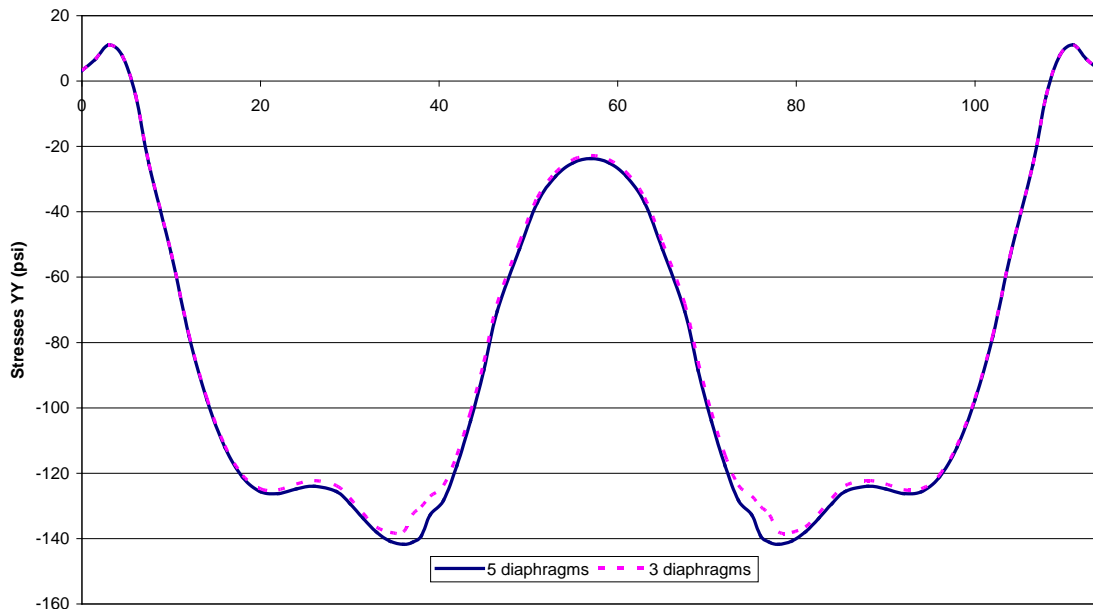


Figure 7-14. Clamping stress distribution along the mid-span transverse section bottom extreme fiber under concentrated load with posttension for different diaphragm configurations

7.2.2 Bridge Width Effect on Clamping Stress Distribution

El-Remaily et al. (1996) showed that the posttension force magnitude is a parameter of bridge width. In order to corroborate the effect of bridge width, a sub-assembly model with four beams is generated (Figure 7-15). Analysis results of four-beam and three-beam models are compared. The comparison of clamping stress along the bridge width shows that stress magnitudes are reduced with increasing bridge width (Figure 7-16). At diaphragm locations, the stress magnitudes at the shear key located at the mid-span transverse section (i.e., the shear key referred to as ‘mid’) are 20 to 40 psi lower than those of the shear key next to the fascia beam (i.e., the shear keys referred as ‘end’).

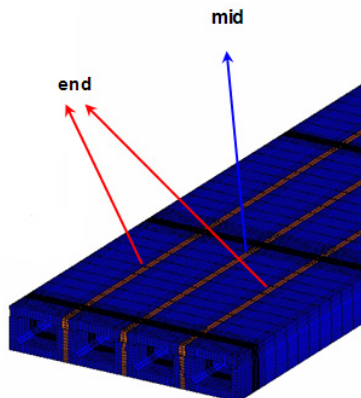


Figure 7-15. Isometric view of sub-assembly model with four beams

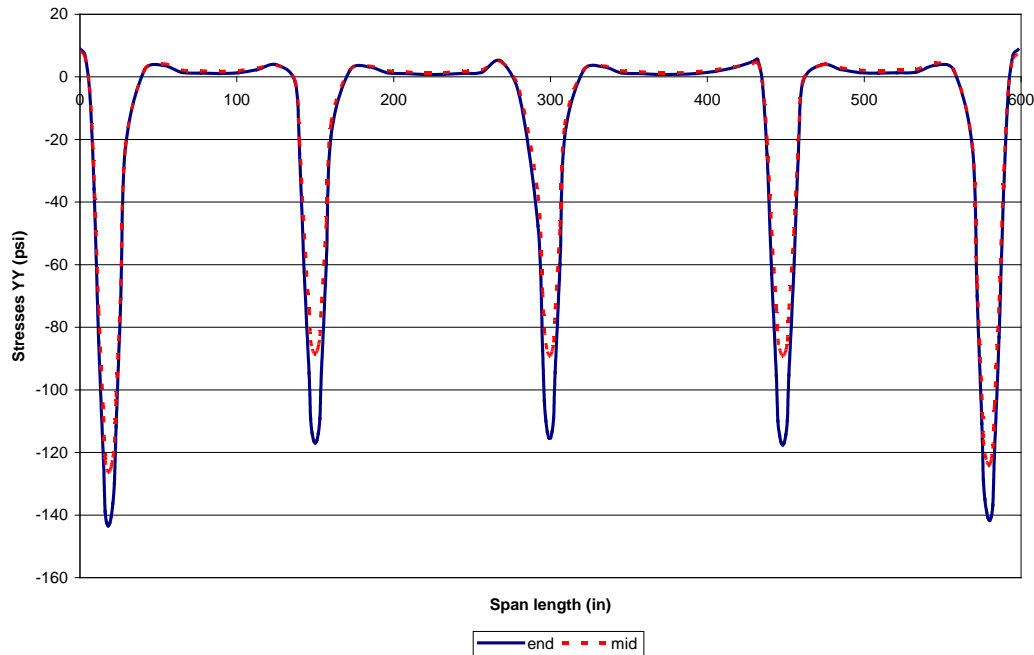


Figure 7-16. Clamping stress variation along the length of shear keys

7.3 SUMMARY AND CONCLUSIONS

FE analyses are carried out investigating the effects of transverse connection design and material parameters: grout modulus, posttension force magnitude, number of diaphragms, and the bridge width. Vertical displacement profiles at the mid-span transverse sections as well as the clamping stress distributions along the shear keys and at the mid-span transverse section are evaluated against the design parameters.

According to the results:

1. Clamping stress transfer is predominantly through the stiffer sections of the bridge superstructure (i.e., through the diaphragms). Shear keys in between the diaphragms are either under tension or zero stress, and are unable to develop a watertight seal without adequate compression.
2. The transverse posttension impact on mid-span deflections is minimal if the shear keys are intact. However, the transverse posttension is required to assure load transfer between girders and to increase the redundancy of the system.

3. AASHTO LRFD (2004) Section 5.14.1.2.8 recommendations regarding clamping stress distribution under transverse posttension are vague. To achieve a minimum stress or even a nominal stress of 250 psi at shear keys along the beam length would require a comprehensive redesign of transverse connection.
4. The transverse posttension force magnitude is a function of bridge geometry, number of diaphragms, shear key material modulus, and shear key width.

Intentionally left blank

8 ANALYTICAL MODELING: CONSTRUCTION SIMULATION AND SERVICE LOAD ANALYSIS

8.1 OVERVIEW

The objective of the refined analysis presented in this chapter is to simulate the construction procedure and sequences for verifying design assumptions and calculating stresses that develop within various components during construction. The analysis results will be used for fine-tuning the design assumptions. The analyses models developed are based on the MDOT Bridge Design Guide (2005) section 6.65.10A and 6.65.13 provisions.

The bridge used for this purpose consists of eight 50 ft long 27×36-in. box beams that are connected with full-depth shear keys, transverse posttension, and a six-inch thick cast-in-place concrete deck. The Bridge has two-lanes with a total width of 25.75 ft. There are five transverse posttension locations (1 @ each beam end, 1 @ each quarter point, and 1 @ center). Posttension force magnitude specified is for HS-25 design loading (i.e., 104.5 kips). Beam end posttension is located 10 in. away from each support centerline. The intermediate diaphragm thickness is 14 inches. The end diaphragm thickness is 26 inches, which satisfies the minimum 2 ft requirement. Posttension anchor plates (7.5×7.5×1.5-in.) are incorporated at each posttension location (Figure 8-1 and Figure 8-2).

Box-beams, diaphragms, shear keys, anchor plates, and deck are modeled with eight-node solid continuum elements (C3D8). These elements have three translational degrees of freedom (dof) at each node with a total of 24 dof. In the longitudinal direction, for the most refined elements, the maximum length is kept at 6 inches for an aspect ratio under six. Prestressing strands are modeled with two-node three dimensional truss elements (T3D2), again with three translational degrees of freedom at each node. Strands are embedded into the solid beam elements and constrained to have equal displacement profiles at coinciding nodes. Prestress is applied as an initial stress in the strand components. The same type of truss elements (T3D2) are used to model posttensioning strands. Also, for accurate representation of the construction sequence, strands are not embedded into the solid elements and are debonded from solid beam, diaphragm, and shear key components.

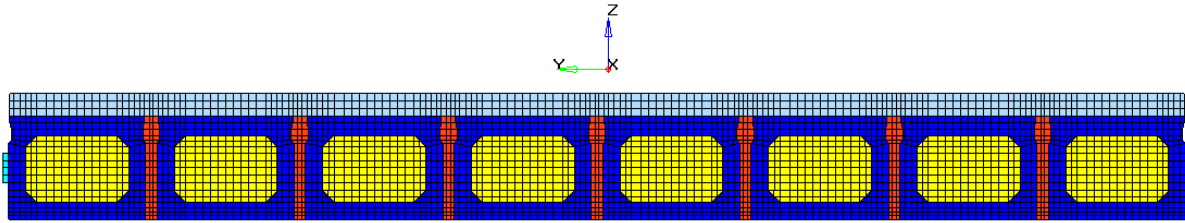


Figure 8-1. Transverse section of box-beam assemblage model

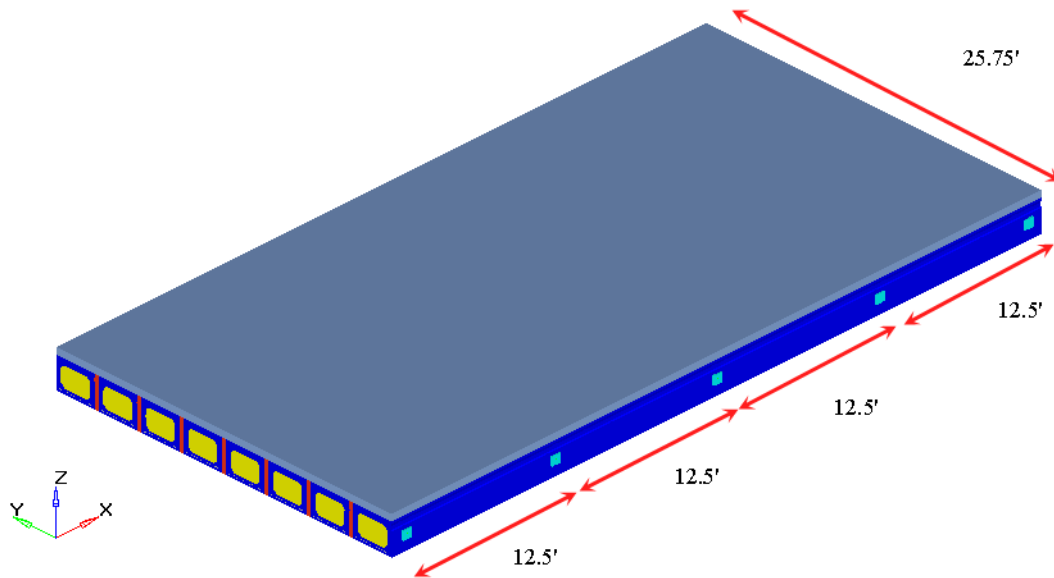


Figure 8-2. Isoparametric view of the box-beam assemblage model

The compressive strength (f'_c) of 5000 psi, modulus of elasticity of 4031 ksi, and Poisson's ratio of 0.2 are specified for both deck and girder concrete. Shear key grout material properties specified are: compressive strength (f'_c) of 4000 psi, modulus of elasticity (E_c) of 3600 ksi, and Poisson's ratio of 0.2. Prestressing strands with a nominal diameter of 1/2-inch and an area of 0.153 in² are embedded in the girders. A total of 10 strands are distributed along the bottom flange of each box girder. Strands are placed with a 2-in. cover as per the MDOT Bridge Design Guide (2005) section 6.65.10 provisions (Figure 8-3). The initial prestress value is 186.3 ksi, calculated after losses due to shrinkage and creep from the initial prestressing stress. The final prestressing after further losses due to relaxation of tendons and elastic shortening is calculated as 163.4 ksi (Table 8-1). UngROUTED posttension ducts are simulated for accurately simulating construction sequence; hence, posttension strands are tied to anchor plates at each diaphragm location. The steel modulus of 29,000 ksi and Poisson's ratio of 0.3 are the material properties of the anchor plates.

Table 8-1. Material Properties of Prestressing Strands

Ultimate stress	270.0 ksi
Yield strength (85% of ultimate)	229.5 ksi
Initial prestressing	186.3 ksi
Final prestressing	163.4 ksi
Modulus of elasticity	28,500 ksi
Poisson's ratio	0.3

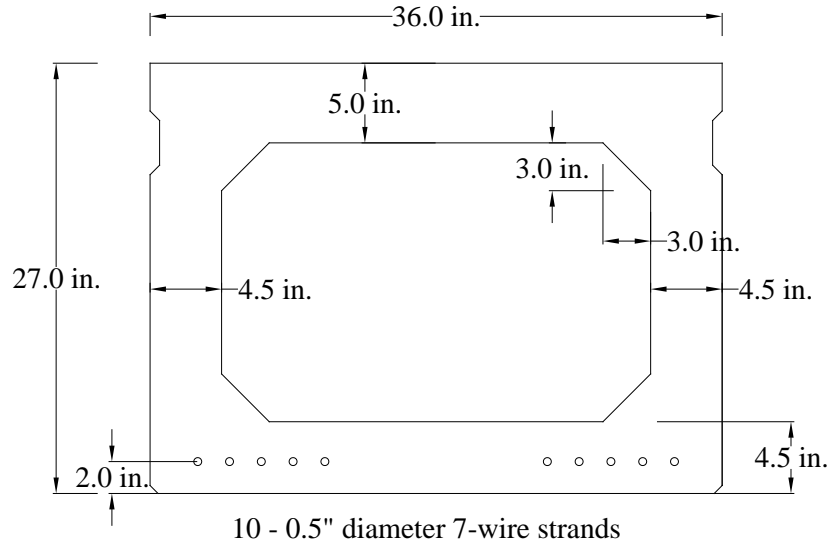


Figure 8-3. 27 × 36 box beam geometry

In the simulation analysis, HL-93 (AASHTO LRFD 2004) loading is placed to create maximum mid-span moment as given in Figure 8-4. The impact factor is taken as 1.75 from Section 3.6.2.1 of the AASHTO LRFD (2004) assuming shear keys act as joints. A lane load of 0.64 k/ft is used in addition to the axle loads, as per Section 3.6.1.3 of the AASHTO LRFD (2004). Multiple presence factors of 1.2 and 1.0 are used for one and two-lane loaded configurations, respectively (AASHTO LRFD Section 3.6.1.1 2004). The wheel load is distributed according to both tire contact area and FE mesh geometry limitations.

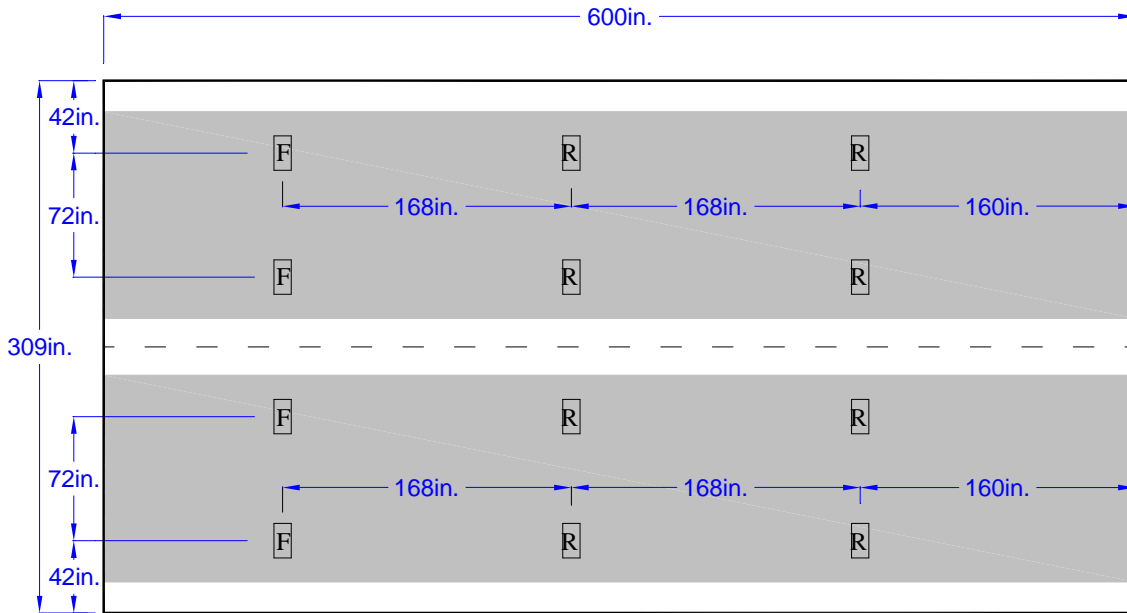


Figure 8-4. Axle and lane load positions for two-lane-loaded configuration

Thermal gradient loads applied in the analysis are for Zone-3 (AASHTO LRFD Section 3.12.3 2004). The negative temperature gradient is calculated in proportion to the positive temperature values by -0.30. Thermal gradient loads are shown in Figure 8-5 with height (h) being the bridge superstructure's full depth including the cast-in-place concrete deck. A uniform thermal expansion coefficient of 6.0×10^{-6} in./in./ $^{\circ}$ F is used for concrete and grout components.

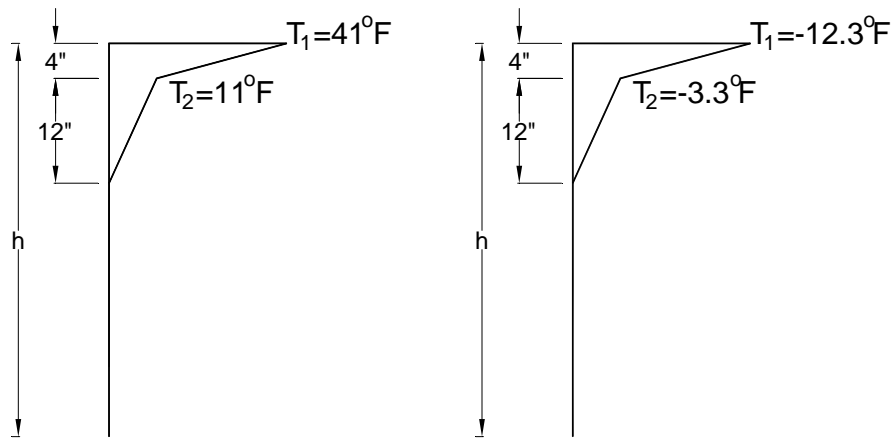


Figure 8-5. Positive and negative temperature gradient loads

The dead load effect is calculated from nominal dimensions and densities. The density of the concrete and grout components (i.e., girder, diaphragm, deck, and shear key) is 150 lb/ft^3 . New

Jersey type IV barrier loads of 475 lb/ft are distributed over 18 in. from the edges of the deck. Analyses do not include volume change loads such as heat of hydration thermal loads and drying shrinkage.

8.2 CONSTRUCTION PROCESS SIMULATION AND ANALYSIS RESULTS

In Michigan, the box-beam bridge superstructure system is constructed in five stages: first, placing precast and prestressed concrete box-beams adjacent to each other; second, grouting 3-in. thick full-depth shear-keys; third, applying transverse posttension; and fourth, casting a six-inch thick concrete deck with a single mat of reinforcement. Last, the barriers are placed and the bridge is opened to traffic. The finite element modeling and analysis sequence that follows the construction sequence is described below:

Step 1: Box-Beams Placement

Precast prestressed beams are erected; beams are subjected to self-weight and prestress only. No other components of the model except beams and prestressing strands are active in the model. Thus, prestressing only affects the beam and diaphragm components as shown in Figure 8-6.

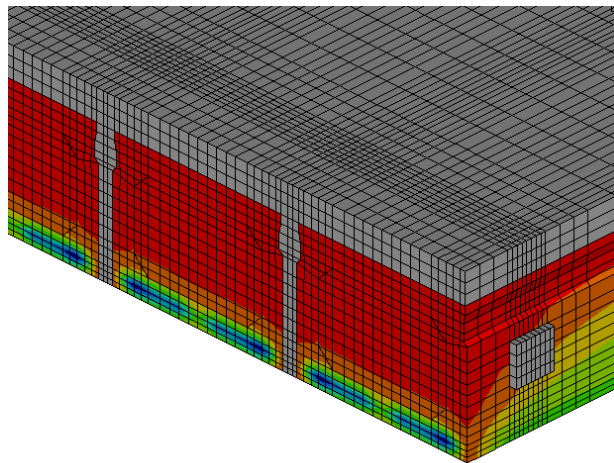


Figure 8-6. Stress development under prestressing and self-weight of beams (note: only beam and strand components are active)

FE analysis results show that beam camber under self-weight is 0.60 inches (Figure 8-7). This matches the analytical solution of 0.625 inches with 96% accuracy.



Figure 8-7. Deformed shape under prestressing and beam self-weight

Step 2: Shear key grout placement

Grout elements are activated. This step is vital. If all beams are modeled as connected to each other through shear keys, then the prestressing effect of each beam would be transferred to shear keys showing shear key stresses before load application. Shear keys should be stress free with proper modeling. Three-inch thick grout elements are activated, and their self-weight is distributed to beams. Beam camber deflection further reduces to 0.55 inches.

Step 3: Posttension application

The posttension application stage is simulated here, compressing/clamping the beam-shear key assemblage. Posttension and anchor plate components are activated. The deck is not placed; hence, deck elements are not activated. The maximum compressive clamping stress magnitude of the shear key elements, at the transverse posttension locations (i.e., at diaphragm locations), is calculated to be 150 psi. The highest shear key compressive clamping stress is observed between the fascia and the first interior beams. The maximum tensile stress of 6.6 psi is calculated at the interface. Clamping stress distribution in shear key grout is shown in Figure 8-8.

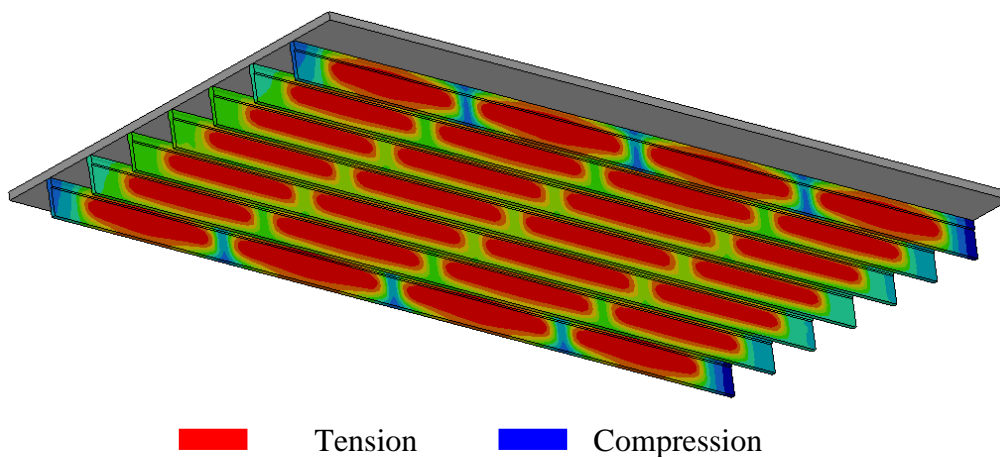


Figure 8-8. Clamping stress distribution in grout layers after posttension application (note: deck is still free from stresses)

Step 4: Deck is placed but not hardened

A dead load of six-inch thick cast-in-place concrete is applied on the assemblage; but deck elements are not active in the model. Upon loading, clamping stress magnitudes decreased in proportion to the distance to shear key from the fascia beam (Figure 8-9 a and b). Applying the deck dead load resulted in minor changes in the clamping stress magnitudes in grout layers. Compressive clamping stress magnitudes are increased to 157 psi from 150 psi; whereas tensile stress magnitudes are decreased to 6.4 psi from 6.6 psi.

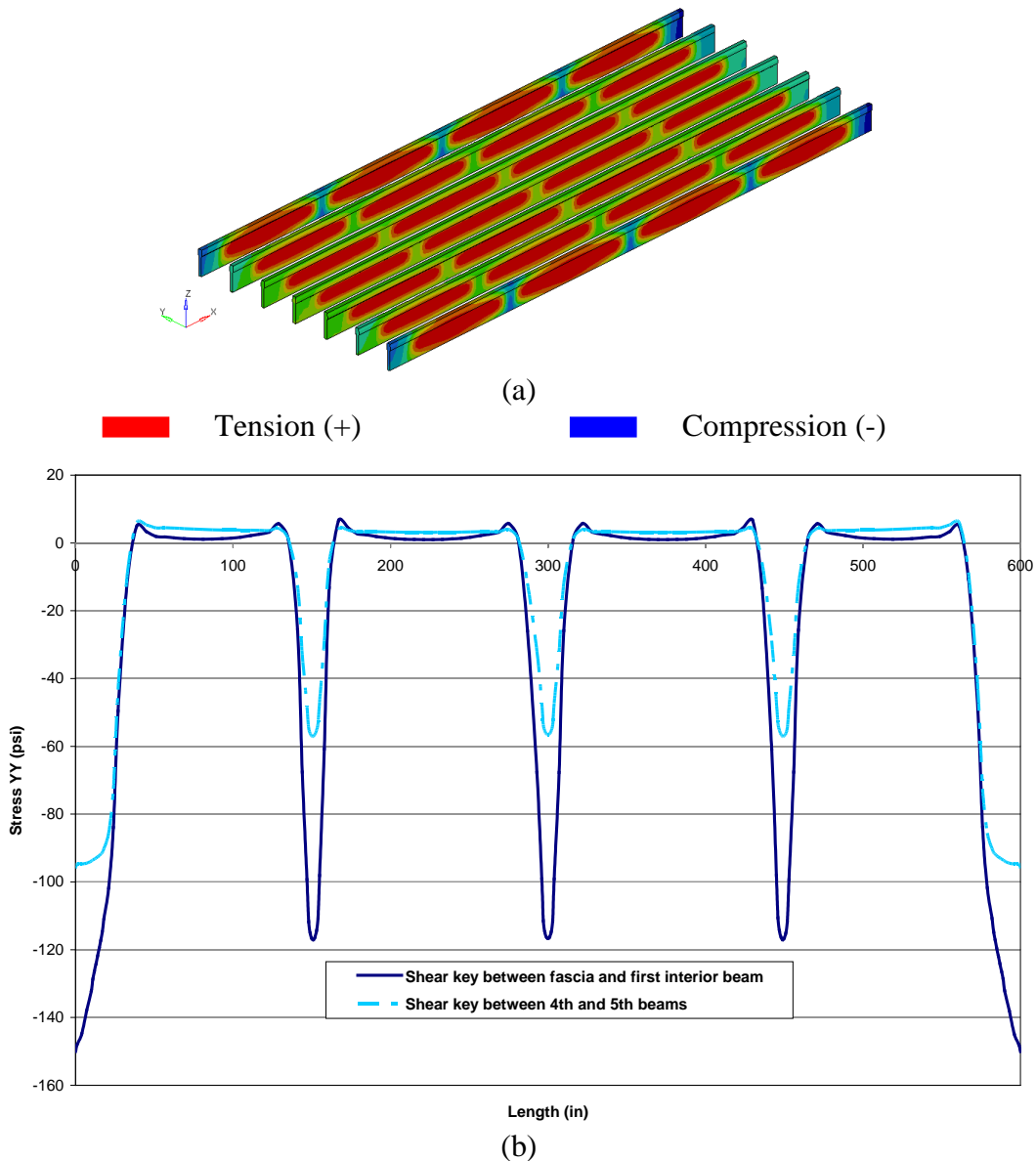


Figure 8-9. (a) Clamping stress in grout under posttension and deck dead load and (b) clamping stress distribution along the length of the shear key (stresses are extracted using shear key mid-height nodes)

Step 5: Deck is hardened and barriers are placed

Deck elements are activated in the model. Deck self-weight was applied in the previous sequence and will not generate deck stresses. Deck stresses are developed once the barrier load is applied. At the end of this step (step 5), all of the dead load components are now acting on the bridge.

Under full dead load, a large portion of the 6-in deck is under transverse tensile stresses, as observed in Figure 8-10. At the top fiber, the magnitude of transverse tensile stress is about 10 psi. The magnitude is reduced to about 5 psi at the bottom fiber. Barrier load effects on shear key grout stress magnitudes are minimal except on the grout layer between the fascia and first interior beam. In the grout layer, the maximum compressive clamping stress is increased to 164 psi from 157 psi; whereas the maximum tensile stress is increased to 6.5 psi from 6.4 psi.

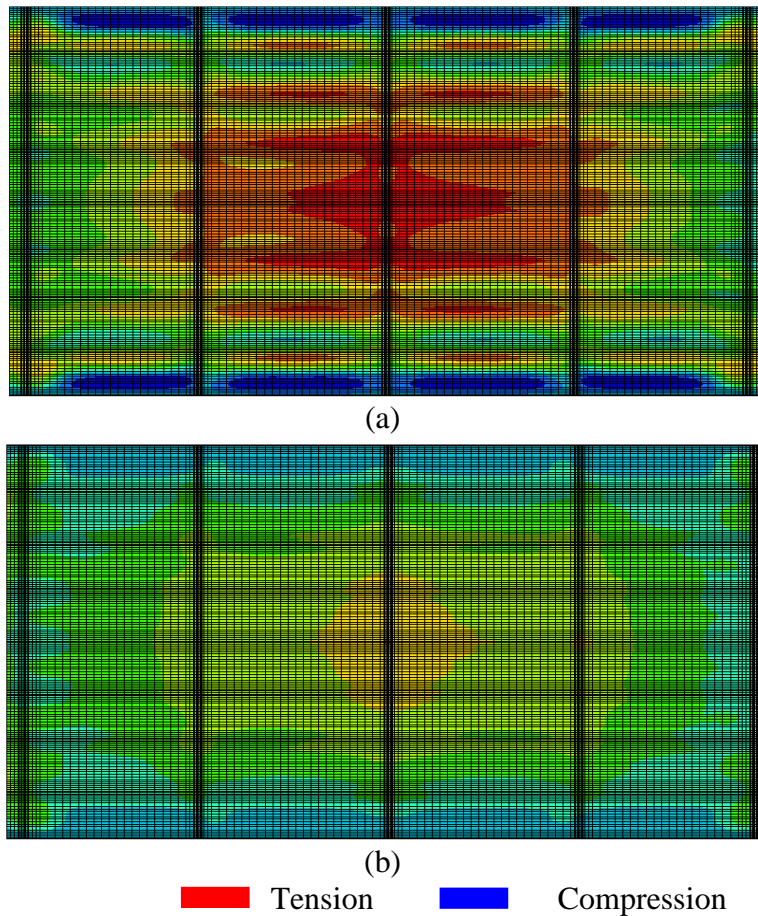


Figure 8-10. Cast-in-place concrete deck stresses under barrier loading (a) top and (b) bottom surfaces

8.3 SERVICE LOAD ANALYSIS

The service I limit state objective is to control cracking (AASHTO LRFD (2004)). As specified in Section 3.4.1 of the AASHTO (2004), γ_{TG} , load factor for temperature gradient may be taken as 1.0 and 0.5 when the live load is excluded or included in the service limit state. Subsequently, three critical load combinations are derived for the analysis. Service I load combination are:

Combo 1: 1.0 DEAD + 1.0 NTG

Combo 2: 1.0 DEAD + 1.0 PTG

Combo 3: 1.0 DEAD + 1.0 LL

where

NTG: Negative thermal gradient loading

PTG: Positive thermal gradient loading

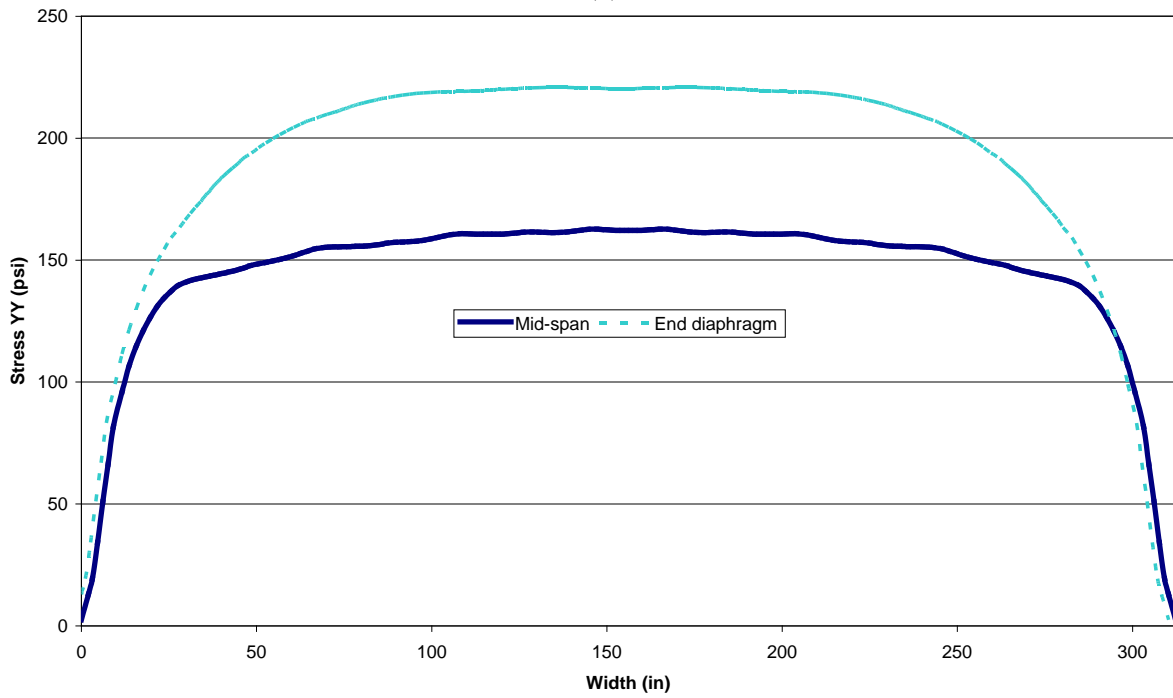
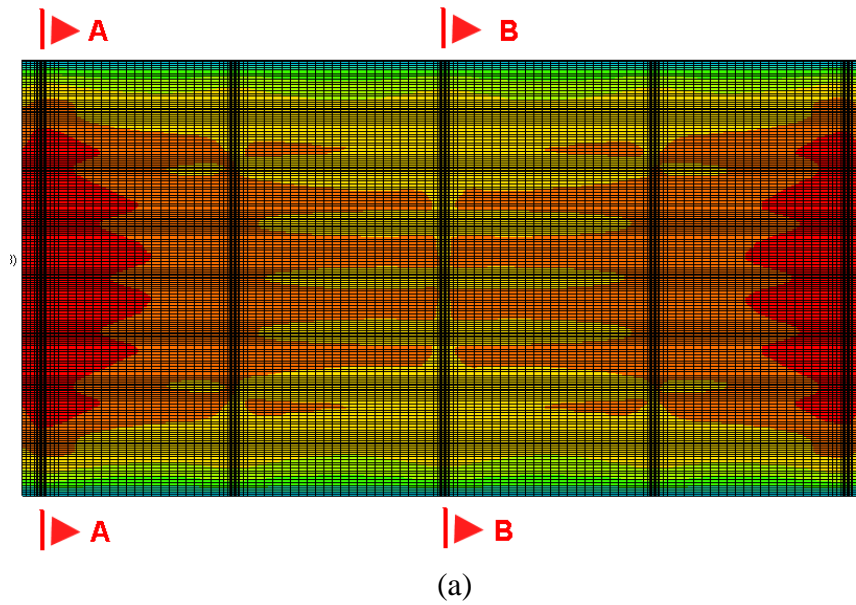
DEAD: Dead load of all components

LL: HL-93 live load with impact and multiple presence factors

Load combinations that include dead, live, and thermal gradient loading are not considered in the analysis. A discussion is presented at the end of the chapter, which explains the reasons for excluding such load combinations.

8.3.1 Load Combination 1: 1.0 DEAD + 1.0 NTG

Load combination consists of the application of negative thermal gradient loading while the stress state developed during construction stages is retained. Under negative thermal gradient loading, deck top fiber tensile stresses are significantly increased (Figure 8-11(a)). Figure 8-11 (b) depicts the stress distribution at the top surface of the deck directly over the end diaphragms (section A-A) and mid span diaphragms (section B-B). A tensile stress of 160 psi develops at mid-span close to the interior girders. Tensile stress further increases towards the supports reaching 230 psi over the end-diaphragms. At the bottom face of the 6-in cast-in-place slab, tensile stresses occur only at locations near the supports (Figure 8-12). Compressive clamping stresses developed in the shear keys are increased to 174 psi from 164 psi and are minimally affected by the negative thermal gradient loading. However, the tensile stress magnitude is increased to 11.6 psi from 6.5 psi along the beam interface, at a location between the fascia and the first interior.



■ Tension (+) ■ Compression (-)

Figure 8-11. Transverse stress distribution (a) at the top surface of the deck and (b) along the width of the deck top surface over mid-span (Section B-B) and end-diaphragm (Section A-A) under Service I load combination 1

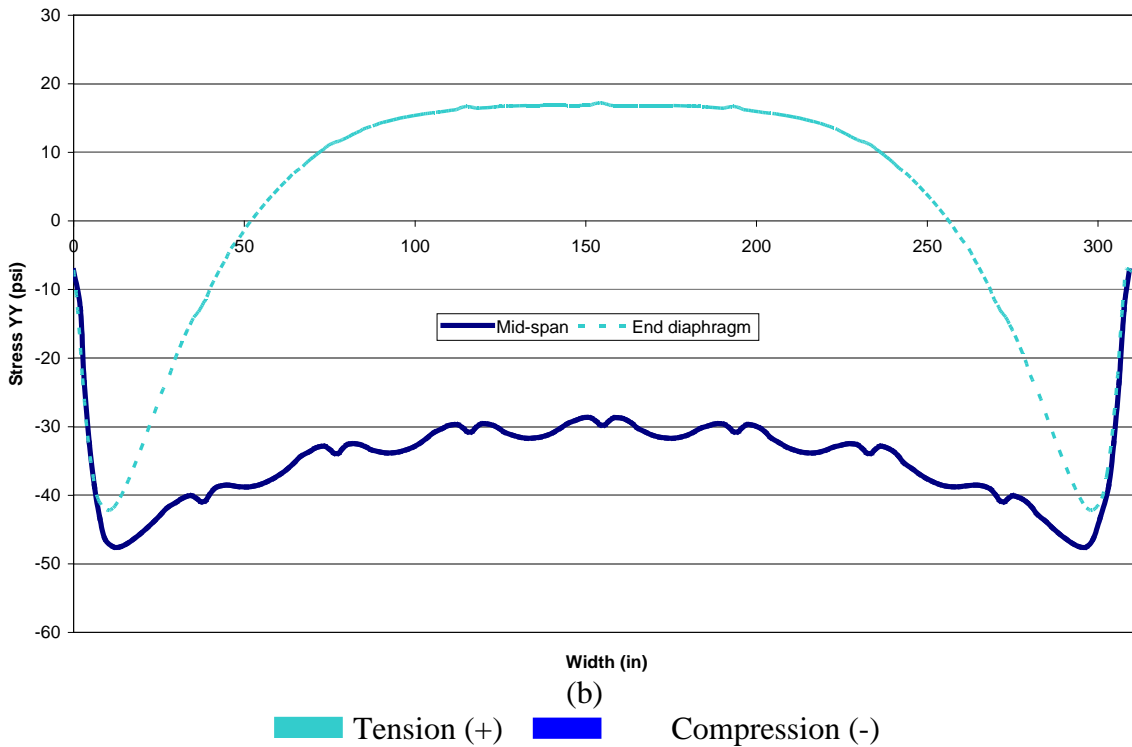
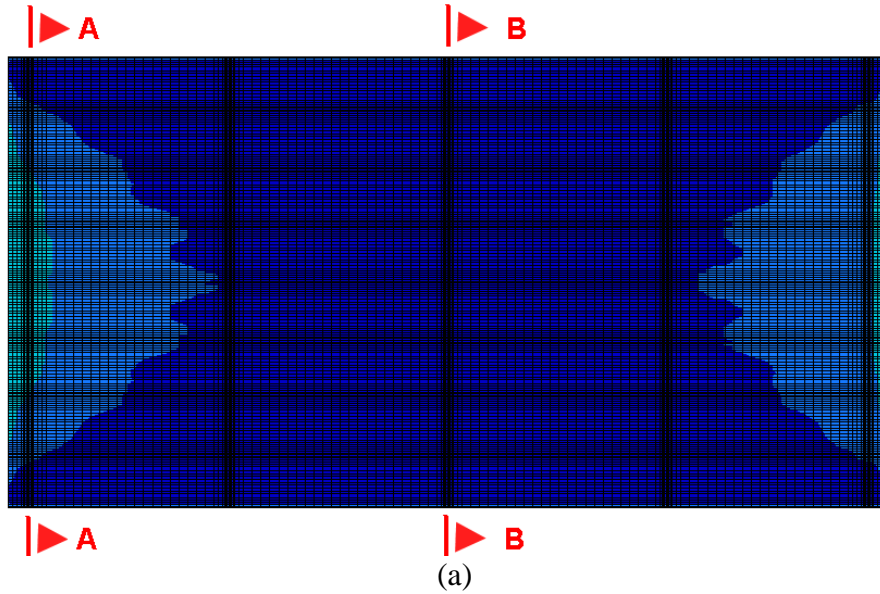


Figure 8-12. Transverse stress distribution (a) at the bottom surface of the 6-in thick deck and (b) along the width of the deck bottom surface over mid-span (Section B-B) and end-diaphragm (Section A-A) under Service I load combination 1

8.3.2 Load Combination 2: 1.0 DEAD + 1.0 PTG

In this combination, the system retains the stress state developed during construction, and positive thermal gradient loading is applied. Under this load, the deck's top fibers are now fully under compression (Figure 8-13) while tensile stresses forms on the bottom fibers of the 6-in.

thick deck (Figure 8-14). The maximum transverse tensile stress of 166 psi is documented at mid-span near the fascia beams (Figure 8-14). Tensile stresses are observed within the end diaphragms only at locations close to the fascia beams. Within the grout layers, between the fascia and the first interior beams, positive gradient loading increases both tensile and compressive stress magnitudes. Maximum tensile stress magnitudes increase to as much as 100 psi from -25 psi at the top of the shear key grout layers located between the fascia and the first interior beams (Figure 8-15).

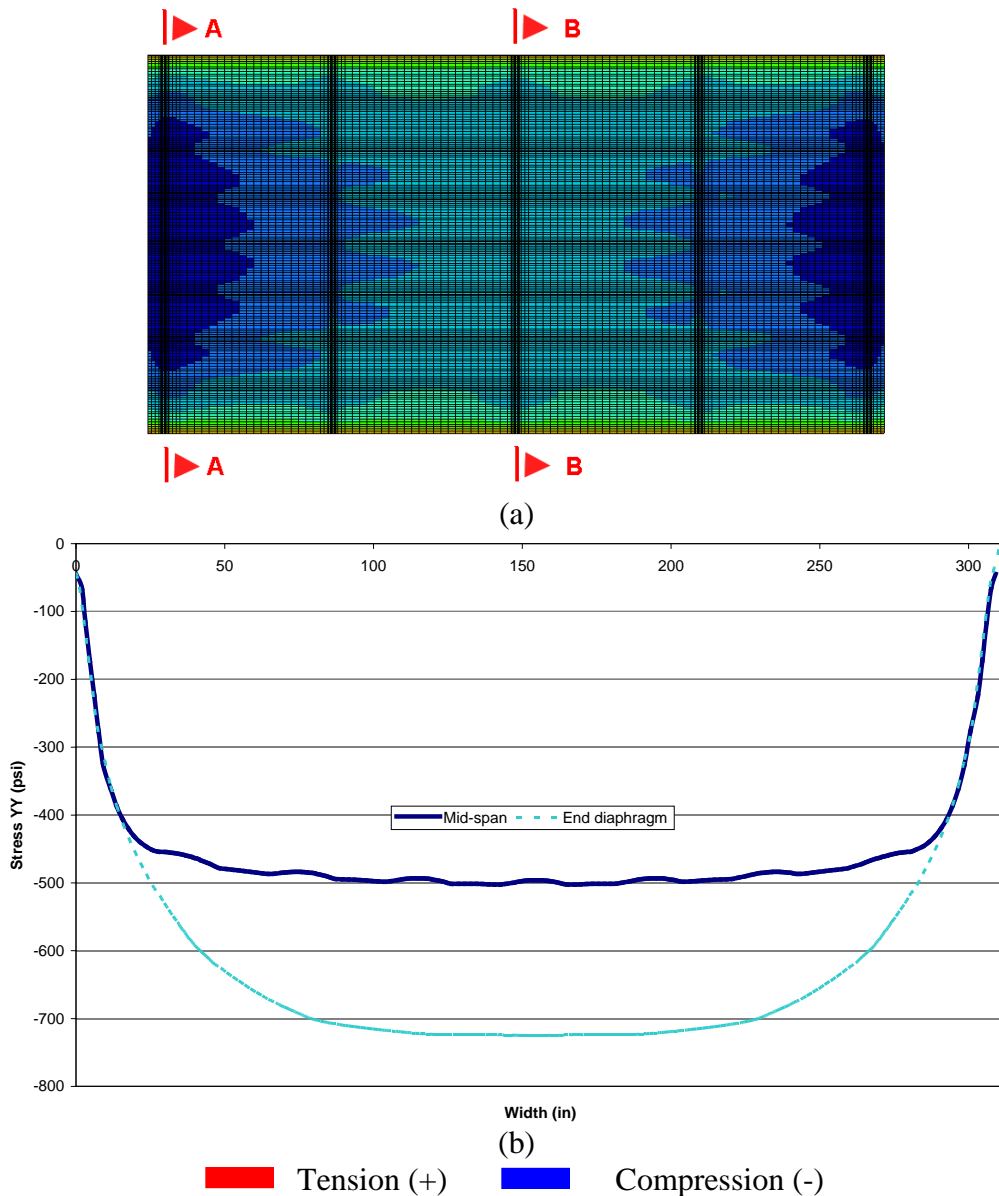
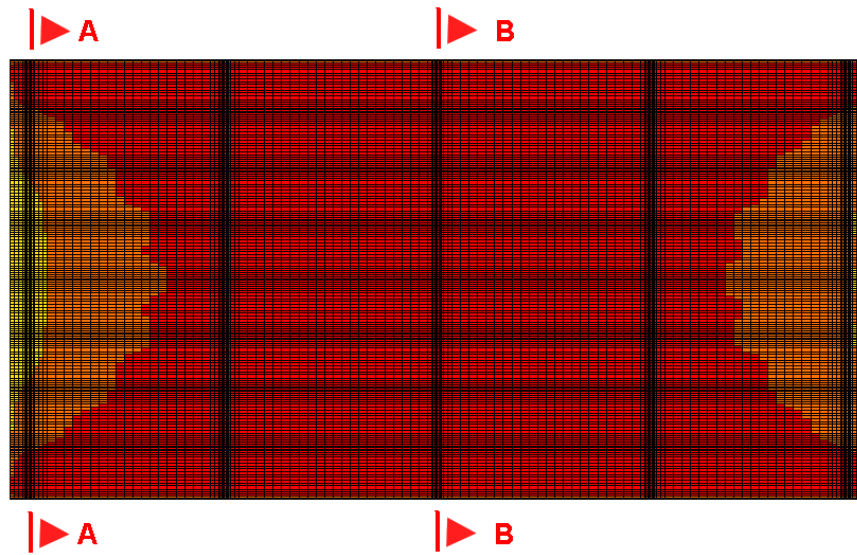
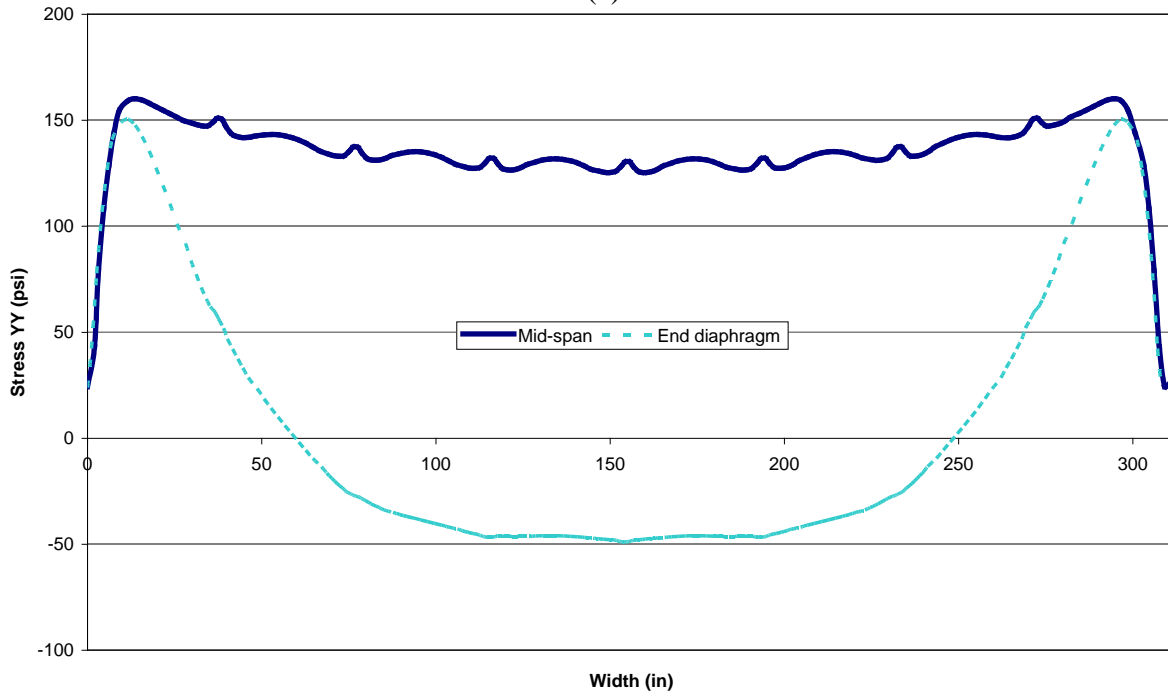


Figure 8-13. Transverse stress distribution (a) at the top surface of the deck and (b) along the width of the deck top surface over mid-span (Section B-B) and end-diaphragm (Section A-A) under Service I load combination 2



(a)



(b)

■ Tension (+) ■ Compression (-)

Figure 8-14. Transverse stress distribution (a) at the bottom surface of the deck and (b) along the width of the deck bottom surface over mid-span (Section B-B) and end-diaphragm (Section A-A) under Service I load combination 2

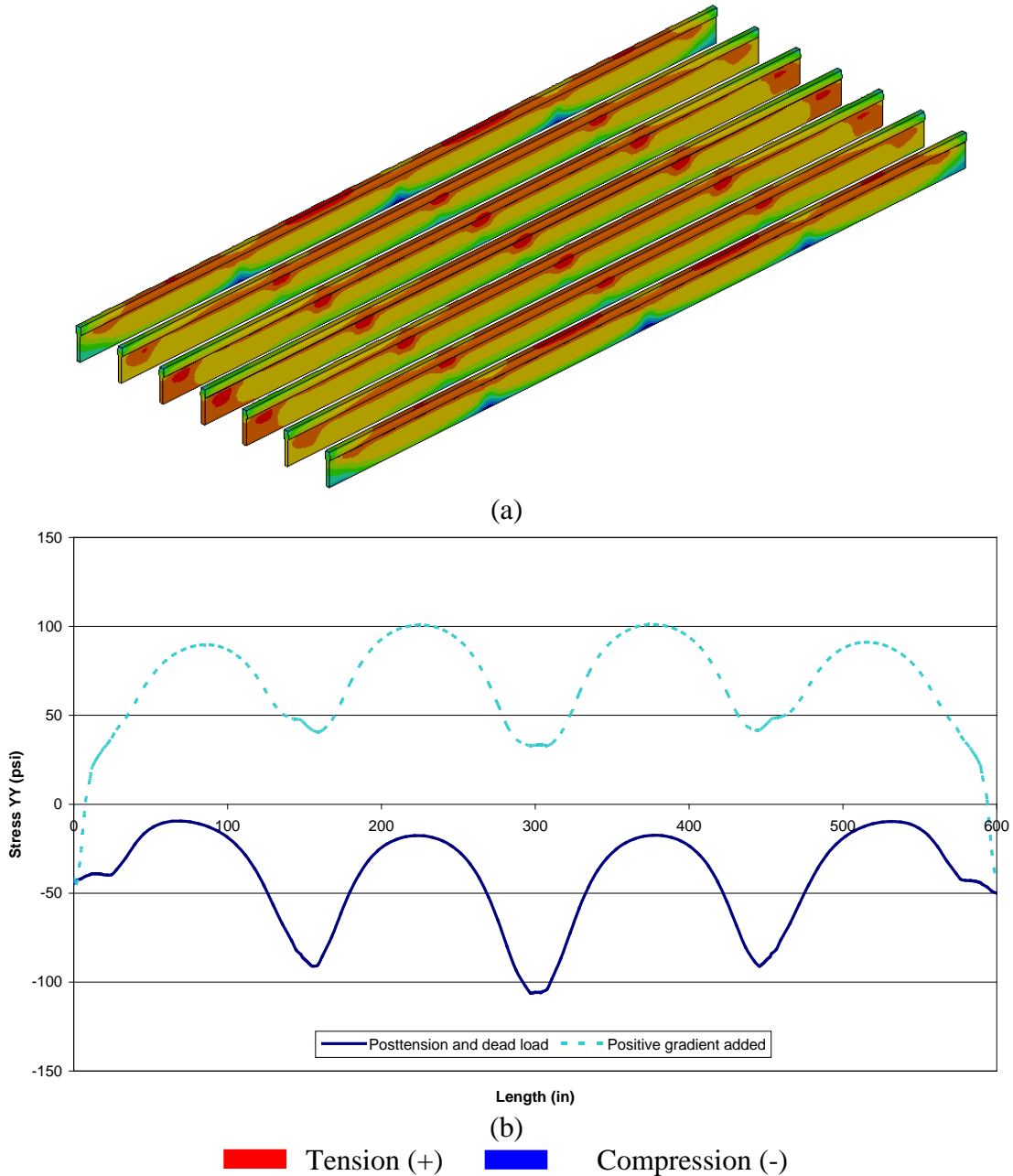


Figure 8-15. (a) Clamping stress distribution of grout layers under positive thermal gradient loading and (b) clamping stress distribution along the length of grout layers with and without the effect of positive gradient loading (stress plots are extracted using shear key top fiber nodes)

8.3.3 Load Combination 3: 1.0 DEAD + 1.0 LL

Single-Lane Loaded

In this combination, the system retains the stress state developed during construction, and HL-93 loading is applied on a single lane. This combination generated a maximum transverse tensile stress at the deck top fibers of about 32 psi over the end diaphragm and 22 psi at mid-span

(Figure 8-16). At the deck's bottom fibers, the maximum transverse tensile stresses are about 15 and 19 psi over the mid-span and end diaphragms, respectively (Figure 8-17). Live load on a single lane does not cause significant changes to grout clamping stresses. The maximum compressive clamping stress is increased to 189 psi from 164 psi; whereas tensile stress is increased to 16 psi from 6 psi.

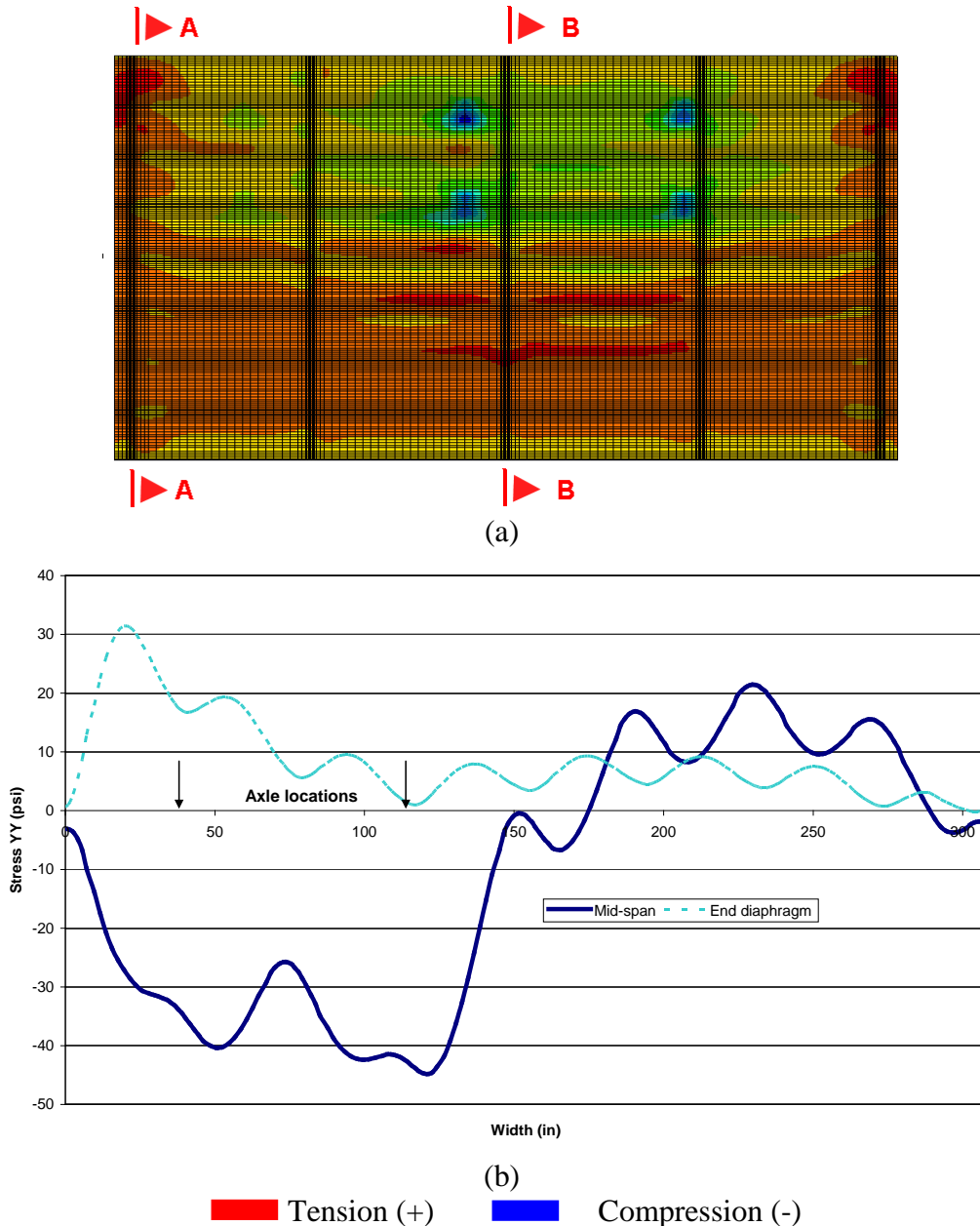


Figure 8-16. Transverse stress distribution (a) at the deck top surface and (b) along the width of the deck top surface over mid-span (Section B-B) and end-diaphragm centerline (Section A-A) under Service I load combination 3 with live load on a single lane

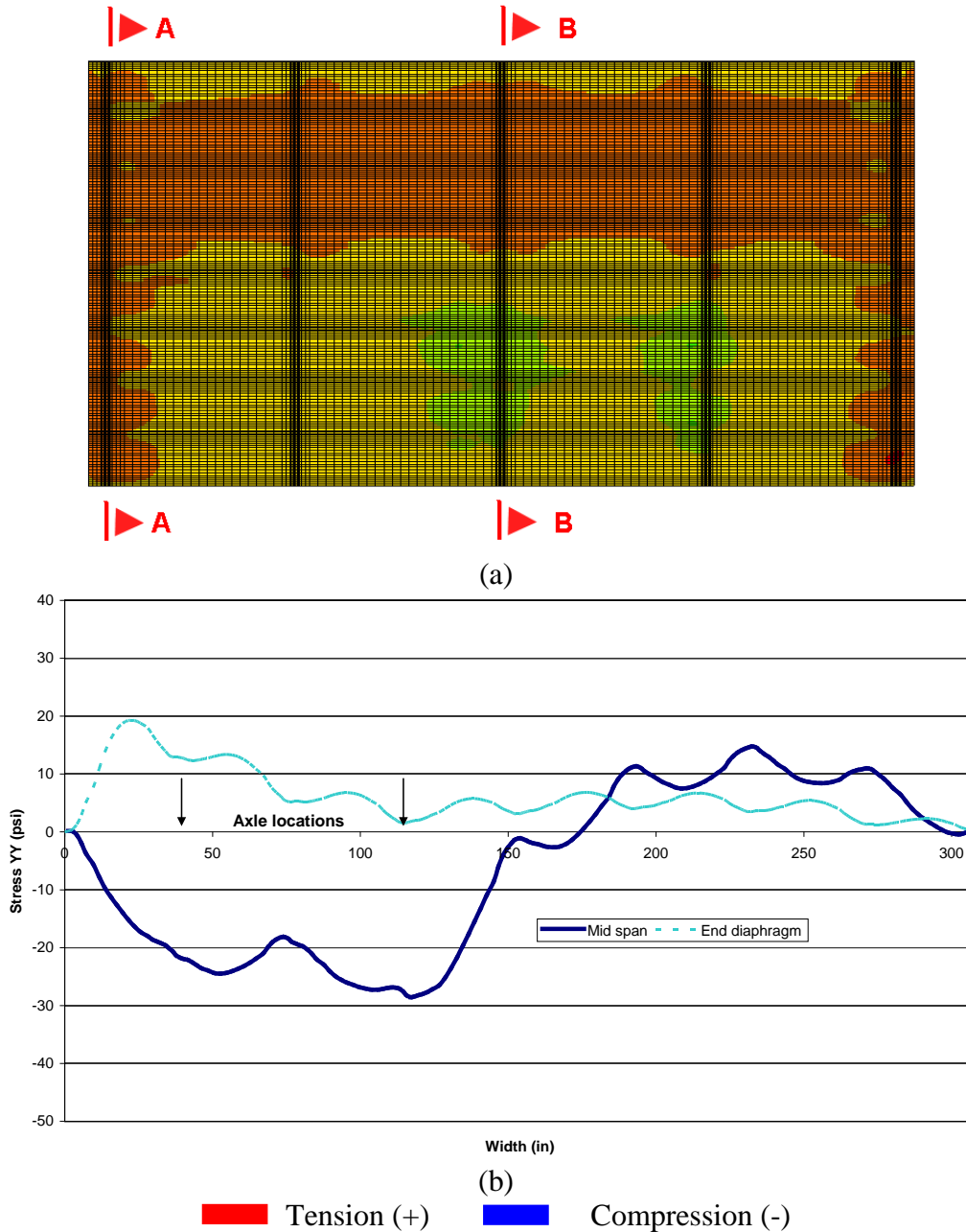


Figure 8-17. Transverse stress distribution (a) at the deck bottom surface and (b) along the width of the deck bottom surface over mid-span (Section B-B) and end-diaphragm centerline (Section A-A) under Service I load combination 3 with live load on a single lane

Two-Lane Loaded

In this combination, the HL-93 load is applied on both lanes. Under this load combination, the mid-span region is under compressive stress. However, both top and bottom surfaces of the 6-in thick deck located between two wheels of the same axle develop tensile stresses. Transverse tensile stress at these concentrated locations are no more than 10 psi at the top surface (Figure

8-18-a). Both top and bottom deck surfaces have transverse tensile stresses over the end diaphragms with maximum magnitudes of 25 and 15 psi, respectively (Figure 8-18 and Figure 8-19). The live load on both lanes does not significantly change clamping stresses developed in grout layers. The maximum compressive clamping stresses are within the grout layers located between the fascia and the first interior beams. Compressive stresses are increased to 189 psi from 164 psi; whereas tensile stresses are increased to 9.4 psi from 6.4 psi.

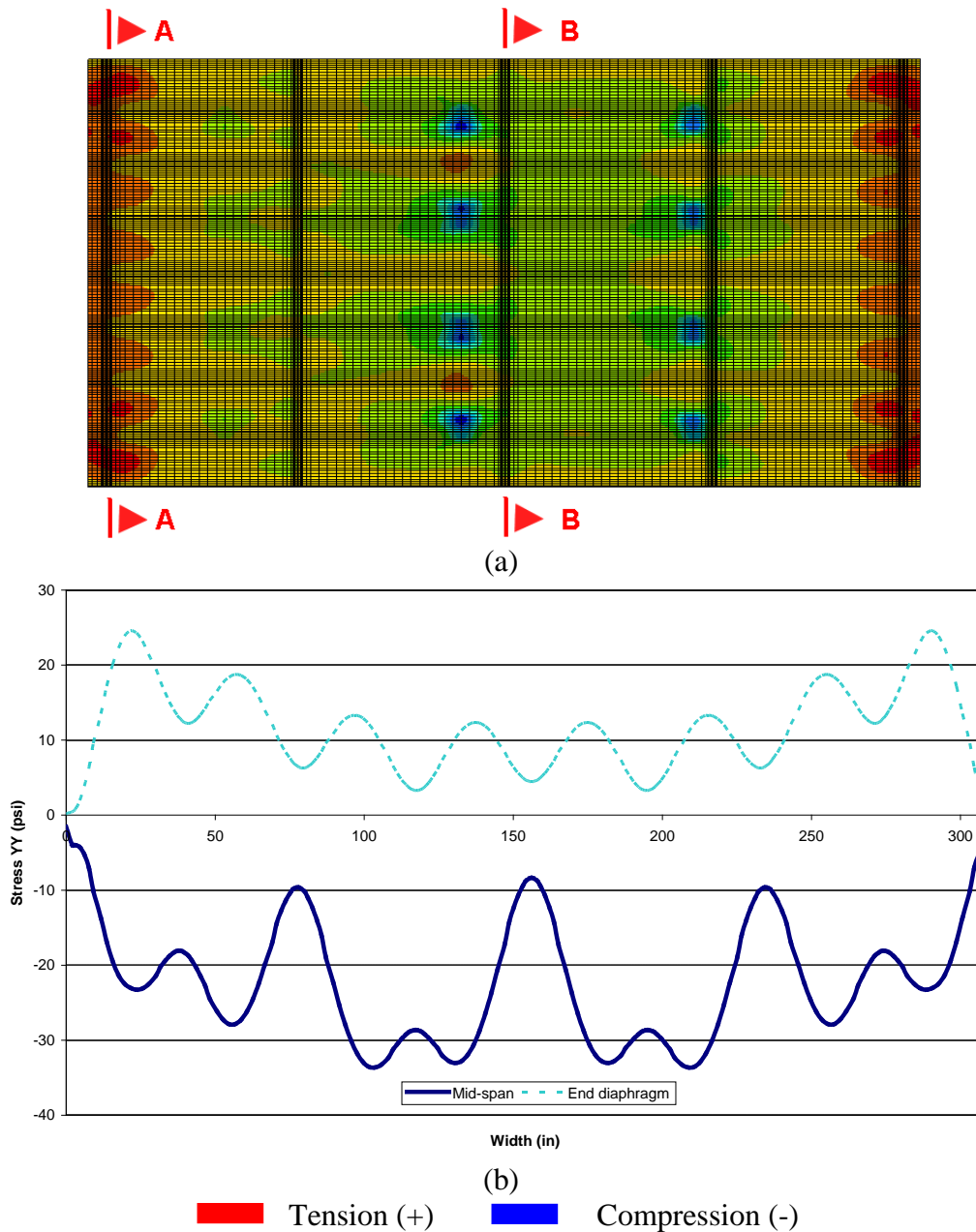


Figure 8-18. Transverse stress distribution (a) at the deck top surface and (b) along the width of the deck top surface over mid-span (Section B-B) and end-diaphragm (Section A-A) under Service I load combination 3 with live load on both lanes

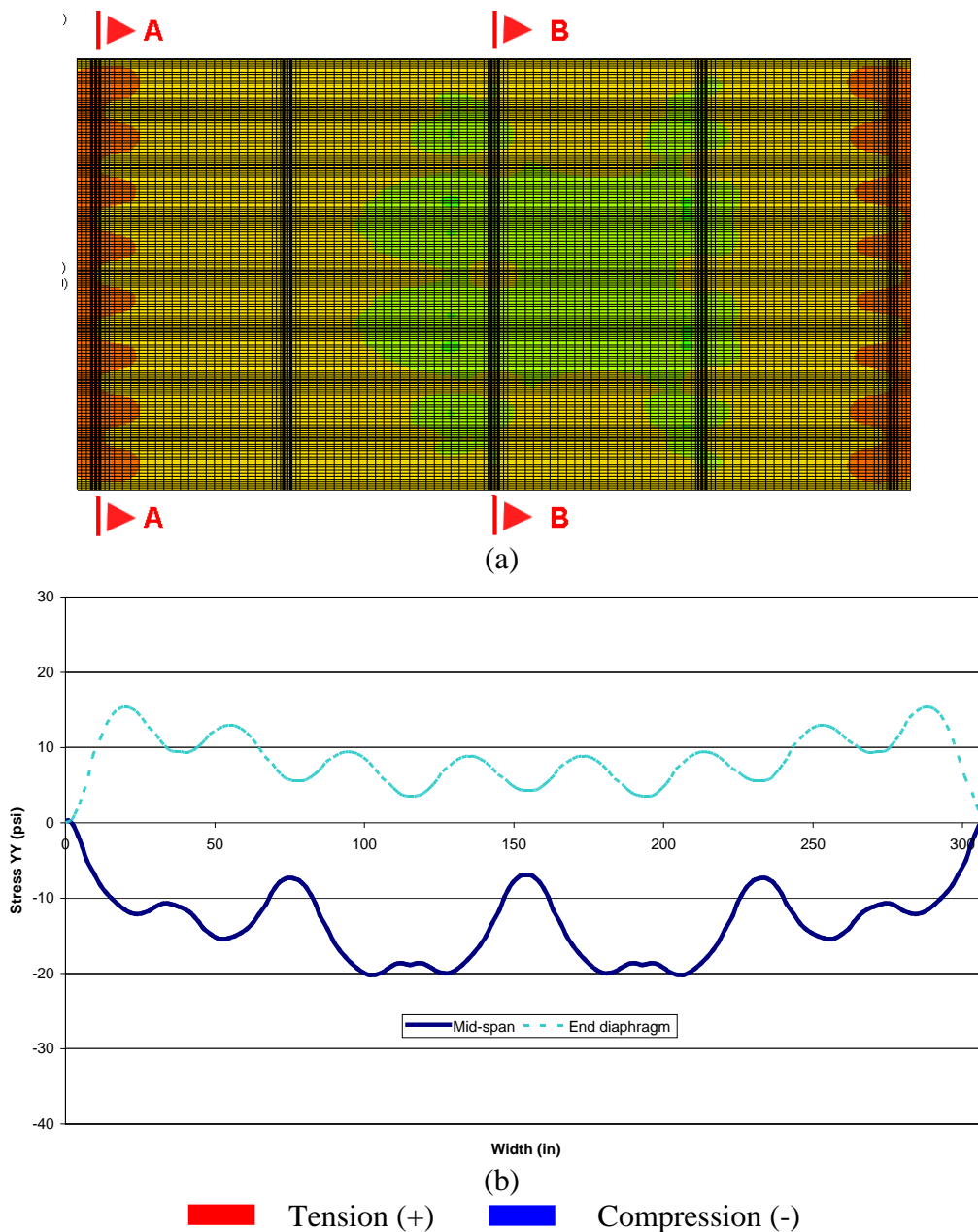


Figure 8-19. Transverse stress distribution (a) at the deck bottom surface and (b) along the width of the deck bottom surface over mid-span (Section B-B) and end-diaphragm (Section A-A) under Service I load combination 3 with live load on both lanes

8.4 SUMMARY AND CONCLUSIONS

FE analyses were carried out simulating the construction process sequences for the purposes of verifying the design assumptions that relate to performance expectations. Full 3-dimensional bridge models were subjected to the loads that develop during the stages of construction and later during operation of the bridge. Construction process sequences modeled are:

1. *Placing girders*
2. *Grouting shear keys*
3. *Applying posttension*
4. *Deck is cast but not hardened*
5. *Deck is hardened and barriers are placed.*

Service load analyses are performed considering the live and thermal gradient effects separately.

Load combinations were:

Combo 1: 1.0 DEAD + 1.0 NTG

Combo 2: 1.0 DEAD + 1.0 PTG

Combo 3: 1.0 DEAD + 1.0 LL

When thermal gradient and live load effects are considered simultaneously, the following load combinations are recommended in the AASHTO LRFD (2004):

Combo 4: 1.0 DEAD + 1.0 LL + 0.5 PTG or

Combo 5: 1.0 DEAD + 1.0 LL + 0.5 NTG

These combinations are not critical, and the combinations that include dead and thermal gradient effects (Combo 1 and Combo 2) generate much higher deck and grout stress magnitudes. Hence, Combo 4 and 5 were not considered in the analysis.

According to the analysis results:

1. Achieving a minimum clamping stress magnitude of 250 psi as required by the AASHTO at shear keys along the entire beam length would require a complete redesign of transverse posttension specifications.
2. Under posttensioning forces, clamping stresses are concentrated only within the width of diaphragms with the posttensioning strands.
3. Under posttensioning forces, clamping stress magnitudes within the shear keys increase towards the fascia beams (Figure 8-9 (b)).

4. Tensile stresses form both on top and bottom surfaces of the 6-in. deck under barrier loading, and increases potential for cracks reflecting from the shear keys (Figure 8-10).
5. The thermal gradient is the primary service loading that generates critical stresses within the deck and specific sections of shear key (Figure 8-11 through Figure 8-15).
6. Under negative thermal gradient loading, the top surface of the 6-in. deck is under tension; whereas bottom surface is under compression. Due to the fact that deck bottom surface is under compression, crack formation will be more random and not necessarily aligned with the shear keys (Figure 8-11 and Figure 8-12).
7. Under positive thermal gradient loading, the top surface of the 6-in. deck is under compression; whereas bottom surface is under tension (Figure 8-13, Figure 8-14 and Figure 8-15). Moreover, positive thermal gradient also creates tensile stresses at the top fibers of shear keys (Figure 8-15).
8. Under single lane loading, tensile stresses form both at mid-span and support regions of the 6-in. deck. With two-lane loading, tensile stresses only occur within the support regions (Figure 8-16 through Figure 8-19).

9 RATIONAL TRANSVERSE POSTTENSION DESIGN

9.1 OVERVIEW

Longitudinal reflective deck cracking is a recurring problem in Michigan and elsewhere even though many changes have been introduced to the empirical design procedures since 1950s (Aktan et al. 2005; Attanayake 2006). The finite element (FE) modeling and analysis of the construction sequences as well as post construction under live load discussed in chapter 8 showed that portions of the shear keys are under transverse tensile stresses. As a result, there is high potential for shear key-beam interface cracking and separation. A primary reason is that the shear keys are not uniformly compressed under transverse posttensioning. Conclusions derived from these analyses included the essential need to redesign the transverse posttensioning requirements. Moreover, it is documented that the transverse posttensioning requirements are based on empirical considerations without any regards to shear and moment demands and their variation on the shear keys. The shear key and deck longitudinal crack formation was observed and documented during construction monitoring of a side-by-side box-beam bridge project and is discussed in this chapter.

This chapter will present a rational analysis procedure for calculating the shear and bending moments at the shear keys from bridge load combinations. The rational analysis procedure is developed by the Western Michigan University project team and discussed in (Attanayake et al. 2008; Attanayake and Aktan 2008b; Attanayake 2006). This chapter will also present a rational design procedure based on the shear and moment demand envelopes at the shear key locations.

9.2 CONSTRUCTION MONITORING

Longitudinal reflective deck cracking was observed while monitoring the construction of a bridge that carries Oakland Drive over I-94 in Portage, Michigan (Figure 9-1). The construction scope included the full structure and substructure replacement. The bridge is straight and aligned in a north-south direction with two equal spans of 79 ft. There are six transverse posttension locations along each span. Each span width consists of 22 box-beams thus 21 shear keys. Each box-beam cross-section is 33×48-in. giving a full bridge width of 93 ft – 5 in. The bridge is designed for HS-25 loading; hence, posttension force magnitude applied at each location is 104.5 kips. There are two posttension locations at each diaphragm location. Therefore, the total

transverse posttension force magnitude is about 16 kips/ft. The bridge was originally designed for staged construction; hence, top posttension strands were discontinued at the bridge centerline while the bottom posttension strands were kept continuous (Figure 9-2). South span shear keys were grouted on May 11, 2007, and posttensioning was implemented on May 14, 2007. The project team inspected the shear keys on the same day just before and after posttensioning. Cracks along the interface between shear key and beam were observed before posttensioning and remained cracked after posttension (Figure 9-3). Shear keys were once again inspected three weeks after posttensioning (June 4th) but prior to deck placement. Cracks remained along the interface of every shear key (Figure 9-4).

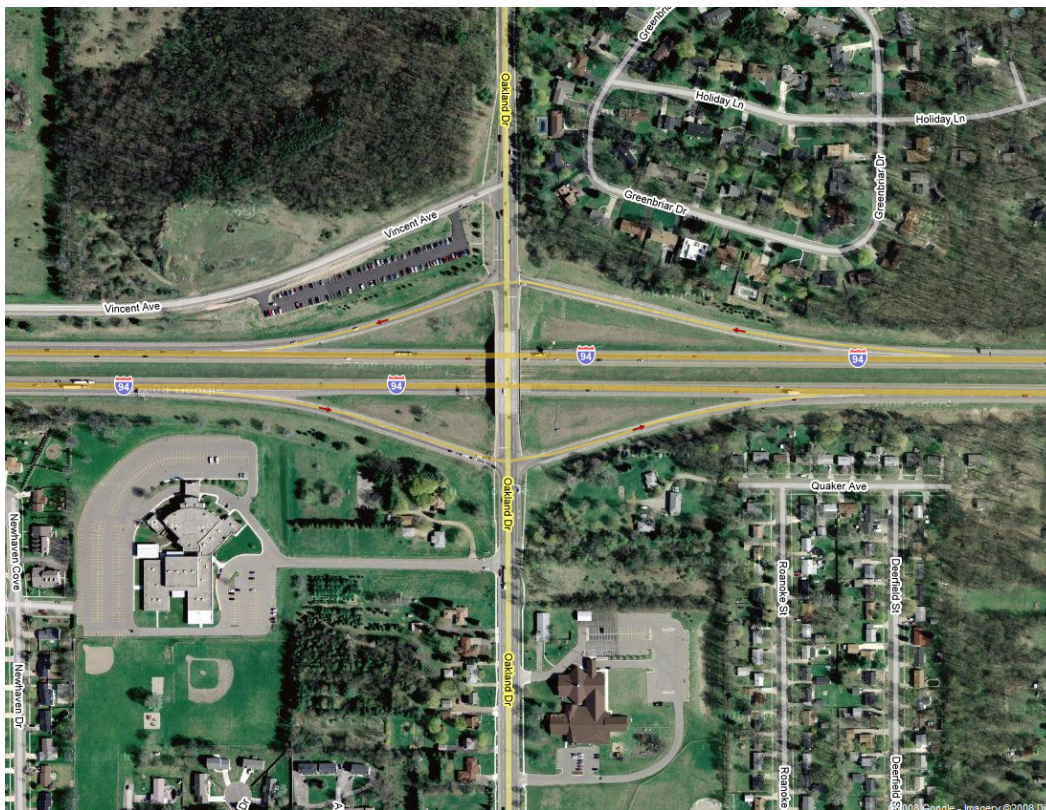


Figure 9-1. Location of the new bridge



Figure 9-2. (a) Shear-key between beams 11 and 12 and (b) discontinued top posttension strands

The bridge deck was placed on June 6th and June 8th on north and south spans, respectively. The deck was moist cured with burlap cover and bleed hoses for seven days. Bridge deck concrete with a water/cementitious material ratio of 0.45 is specified as MDOT Grade D. The deck concrete developed compressive strength in excess of 5500 psi in 5 days and 6400 in 28 days.

The deck surface was inspected on June 22nd. Cracks were documented that stemmed from the top surface of the deck above the abutments, and they aligned with the shear keys. These cracks were observed before the approaches and barriers were placed. Specifically, the cracks developed before any barrier or live loading on the bridge deck. During this time, the deck was not subjected to live loads, only intrinsic material actions such as the heat of hydration and drying shrinkage. Calculations showed that the tensile stresses that developed on the deck, from posttension losses during the period of June 6 (deck placement) and June 22, are not significant enough to cause cracking.



Figure 9-3. Shear-key interface cracking observed on May 14th (a) before and (b) after posttension



Figure 9-4. Shear-key interface cracks observed on June 4th



Figure 9-5. Deck cracking observed on June 22nd

9.3 MACROMECHANICAL MODEL

Construction process simulation results and observed performance of existing bridges show the need for a rational analysis model for orthotropic decks such as side-by-side box-beam bridge superstructures. Rational analysis model results will be utilized to rationally design transverse posttensioning. It should be mentioned that there is a rational transverse posttension design procedure given in the PCI Bridge Design Manual (2005) which is based on the grillage model proposed by El-Remaily et al. (1996). The grillage model, however, cannot sufficiently represent the load transfer response along the shear key due to simplified assumptions. Attanayake et al. (2008) developed a simple but refined analysis model using the concepts of mechanics of materials and macromechanics concepts. This model is referred to as the *macromechanical* model.

The first step in the macromechanical model development is to define the representative volume element (RVE) of the orthotropic deck; in this case, that is the side-by-side box-beam bridge deck (Figure 9-6). The RVE is defined by a shear key, halves of adjacent box-beams, and a portion of cast-in-place concrete deck. (Refer to the dashed box shown in Figure 9-6.) Hence, the width of the RVE is equal to the summation of a beam width and shear key thickness. In principle, the length of the RVE can be any value, yet it should be a reasonable ratio to the width since the RVE will be the building block of the bridge.

The analysis model development procedure from the RVE properties is depicted in Figure 9-6. The macromechanical modeling process is the calculation of stiffnesses of a finite portion of the original structure described by the RVE. The stiffnesses are normalized with respect to the length and width of the RVE. The normalized stiffness relations of RVE represent a thick plate with equal length and width dimensions of the orthotropic bridge superstructure system.

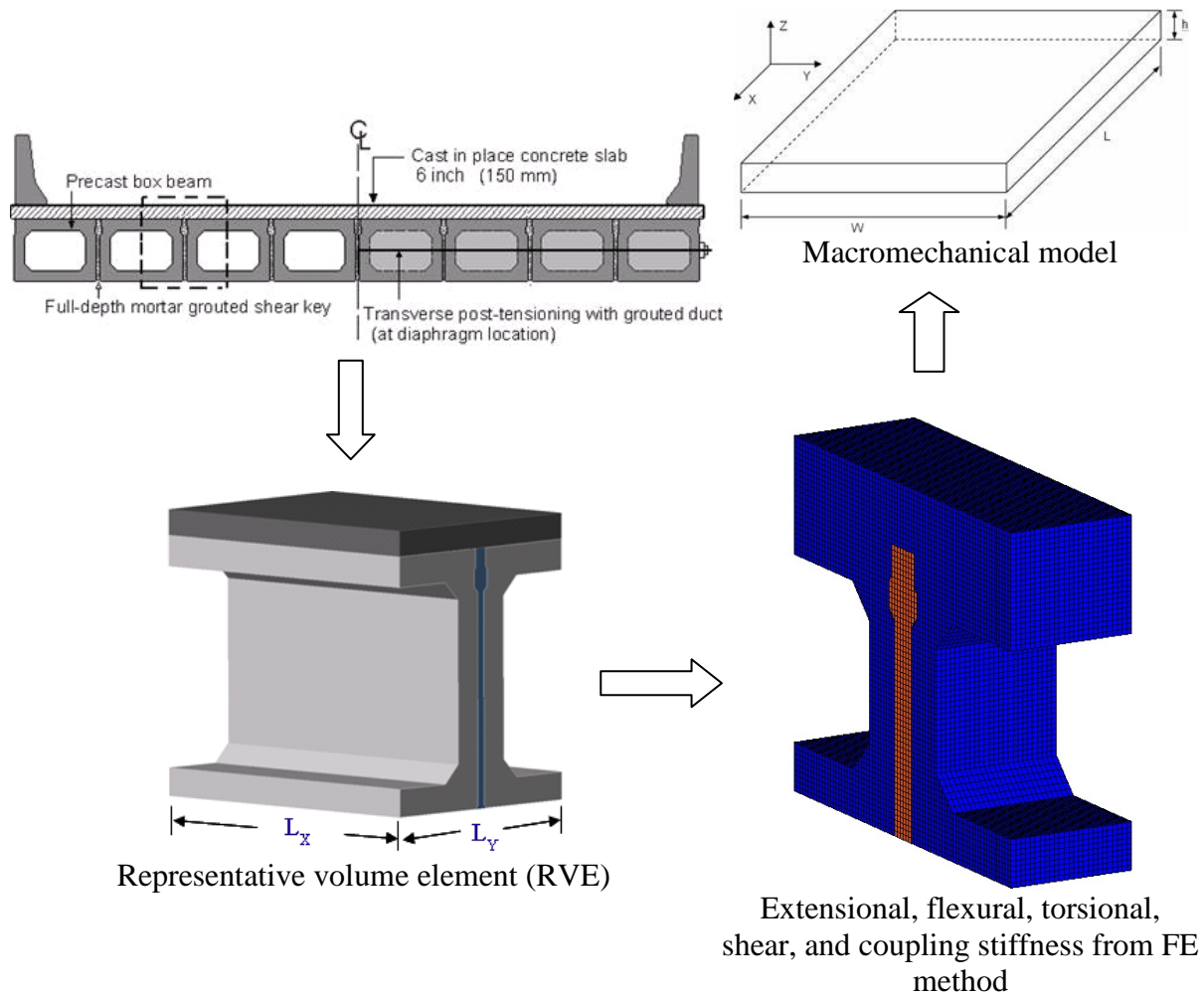


Figure 9-6. Concept of macromechanical model development procedure

The second step is to calculate the terms of the stiffness matrix given in Eq. 9-1 and Eq. 9-2. The stiffness matrix that is referred as the ABDE matrix consists of [A], [B], [D], and [E] sub matrices. The stiffness matrix defines the relationship between axial forces (N_1 and N_2) and axial strains (ϵ_1 and ϵ_2), in-plane shear force (N_{12}) and shear strain (γ_{12}), transverse shear forces (V_{13} and V_{23}) and transverse shear strains (γ_{13} and γ_{23}), moments (M_1 and M_2) and curvatures (k_1 and k_2), and torsional moment due to in-plane shear (M_{12}) and curvature (k_{12}). Definitions of forces and moments given in Eq. 9-1 are depicted in Figure 9-7. According to Eq. 9-1 and Eq. 9-2, the A_{ij} is in-plane stiffness, the B_{ij} is coupling stiffness, D_{ij} is flexural stiffness, and E_{ij} is the transverse shear stiffness (Kollar and Springer 2003; Jones 1975). The complete stiffness matrix of the RVE defined in Eq. 9-1 and Eq. 9-2 is referred to as the ABDE matrix.

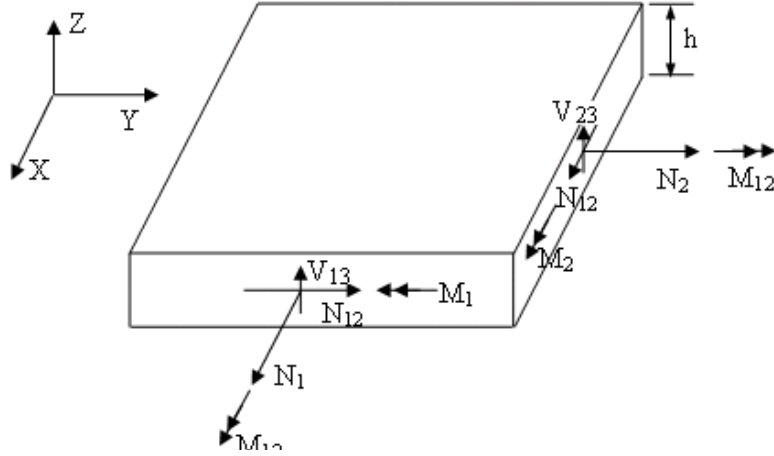


Figure 9-7. Notations – forces and moments acting on a plate element

The ABDE matrix of one RVE is established using the FE analysis. The FE model of the RVE is developed using continuum (8-node brick) elements with translational nodal degrees of freedom (ABAQUS 2008). Strains and curvatures are simulated with prescribed displacement profiles. Attanayake (2006) provides detailed procedure for developing ABDE matrix.

$$\begin{Bmatrix} N_1 \\ N_2 \\ N_{12} \\ M_1 \\ M_2 \\ M_{12} \\ V_{13} \\ V_{23} \end{Bmatrix} = \begin{bmatrix} A & B & 0 \\ B & D & 0 \\ 0 & 0 & E \end{bmatrix} \begin{Bmatrix} \varepsilon_1 \\ \varepsilon_2 \\ \gamma_{12} \\ k_1 \\ k_2 \\ k_{12} \\ \gamma_{13} \\ \gamma_{23} \end{Bmatrix} \quad (9-1)$$

where,

$$\begin{bmatrix} A & B & 0 \\ B & D & 0 \\ 0 & 0 & E \end{bmatrix} = \begin{bmatrix} A_{11} & A_{12} & A_{13} & B_{11} & B_{12} & B_{13} & 0 & 0 \\ A_{21} & A_{22} & A_{23} & B_{21} & B_{22} & B_{23} & 0 & 0 \\ A_{31} & A_{32} & A_{33} & B_{31} & B_{32} & B_{33} & 0 & 0 \\ B_{11} & B_{12} & B_{13} & D_{11} & D_{12} & D_{13} & 0 & 0 \\ B_{21} & B_{22} & B_{23} & D_{21} & D_{22} & D_{23} & 0 & 0 \\ B_{31} & B_{32} & B_{33} & D_{31} & D_{32} & D_{33} & 0 & 0 \\ 0 & 0 & 0 & 0 & 0 & 0 & E_{11} & 0 \\ 0 & 0 & 0 & 0 & 0 & 0 & 0 & E_{22} \end{bmatrix} \quad (9-2)$$

9.4 RATIONAL POSTTENSION DESIGN PROCEDURE

9.4.1 Overview

The rational transverse posttension design procedure is described in this report on a specific bridge design application. The bridge in this example is a side-by-side box-beam in length and width of 600 in. and 309 in., respectively. The bridge cross-section consists of eight 27 in. deep and 36 in. wide box-beams with 3 in. wide full-depth shear keys and a 6-in thick reinforced concrete deck as shown in Figure 9-8. Grouted joints (shear keys) transfer loads (moment and shear) while providing tight moisture seal between the beams. To assure tight moisture seal, the joint should not be allowed to develop cracks at the interface. Therefore, the grout-beam interface needs to be modeled as a tightly bonded joint. Current side-by-side box-beam superstructure configuration consists of rigid diaphragms at predefined locations that are established based on the span length. Intermediate diaphragms are provided to facilitate posttension applications. Posttension is to facilitate load transfer between the girders through the grouted shear keys. The service state expectation from the transverse posttension is to provide a box-beam assemblage that acts as a single unit without developing cracks at the joints. Assuming tightly bonded joints in the model satisfies the envisioned behavior by posttensioning; thus, diaphragms and posttension are not incorporated in the model.

Following the procedure discussed in Attanayake (2006), [A], [B], [D], and [E] matrices are developed for the RVE shown in Figure 9-9. Two different RVE configurations are considered in order to establish transverse posttensioning in two stages: with and without the cast-in-place concrete deck. Elasticity modulus of concrete (both cast-in-place deck and the box-beams) and grout are taken as 5000 psi and 3600 psi, respectively. Poisson's ratio of both concrete and grout is assumed 0.2. The resulting [ABDE] matrices for two different RVE configurations are given in Eq. 9-3 and Eq. 9-4. The coupling matrix [B] is zero (Attanayake 2006; Jones 1975; and Kollar and Springer 2003).

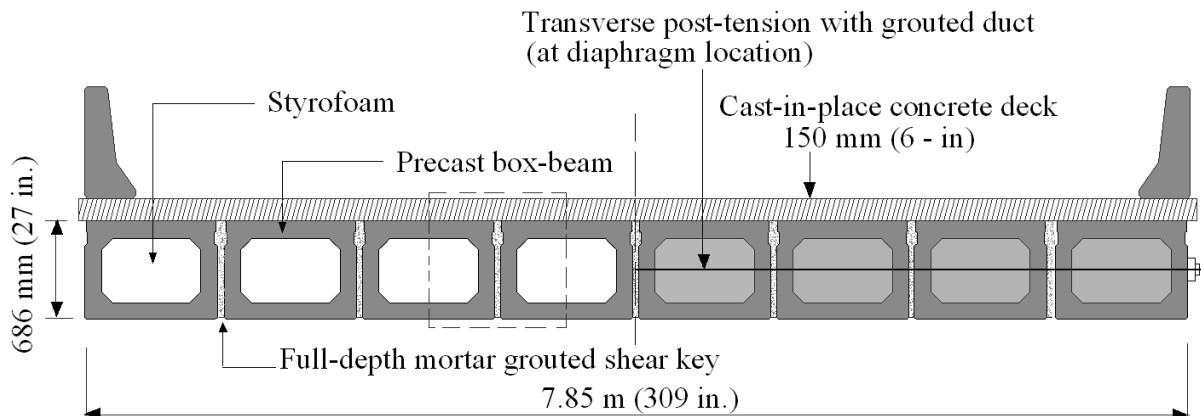


Figure 9-8. Side-by-side box-beam configuration

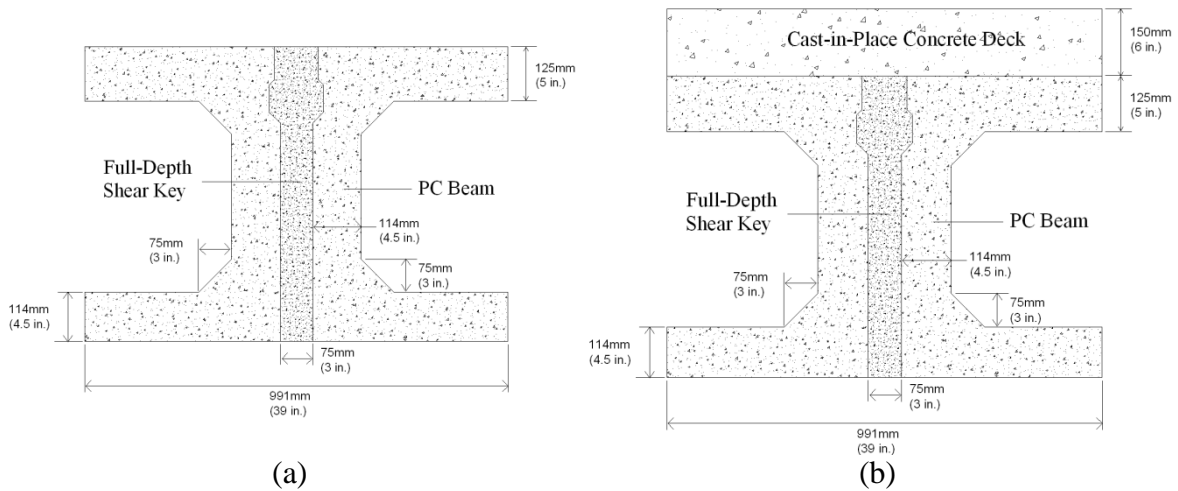


Figure 9-9. Cross-section of the RVE (a) without and (b) with deck.

Stiffness Matrix of RVE without Deck

$$\begin{bmatrix} A & B & 0 \\ B & D & 0 \\ 0 & 0 & E \end{bmatrix} = 10^7 \times \begin{bmatrix} 7.55 & 1.03 & 0 & 0 & 0 & 0 & 0 & 0 \\ 1.03 & 5.13 & 0 & 0 & 0 & 0 & 0 & 0 \\ 0 & 0 & 3.05 & 0 & 0 & 0 & 0 & 0 \\ 0 & 0 & 0 & 682.98 & 125.35 & 0 & 0 & 0 \\ 0 & 0 & 0 & 125.35 & 627.29 & 0 & 0 & 0 \\ 0 & 0 & 0 & 0 & 0 & 256.88 & 0 & 0 \\ 0 & 0 & 0 & 0 & 0 & 0 & 2.93 & 0 \\ 0 & 0 & 0 & 0 & 0 & 0 & 0 & 2.93 \end{bmatrix} \begin{matrix} lb/in \\ lb/in \\ lb/in \\ in-lb \\ in-lb \\ in-lb \\ lb/in \\ lb/in \end{matrix} \quad (9-3)$$

Stiffness Matrix of RVE with Deck

$$\begin{bmatrix} A & B & 0 \\ B & D & 0 \\ 0 & 0 & E \end{bmatrix} = 10^7 \times \begin{bmatrix} 10.68 & 1.67 & 0 & 0 & 0 & 0 & 0 & 0 \\ 1.67 & 8.35 & 0 & 0 & 0 & 0 & 0 & 0 \\ 0 & 0 & 4.30 & 0 & 0 & 0 & 0 & 0 \\ 0 & 0 & 0 & 1282.7 & 232.45 & 0 & 0 & 0 \\ 0 & 0 & 0 & 232.45 & 1162.8 & 0 & 0 & 0 \\ 0 & 0 & 0 & 0 & 0 & 477.4 & 0 & 0 \\ 0 & 0 & 0 & 0 & 0 & 0 & 4.31 & 0 \\ 0 & 0 & 0 & 0 & 0 & 0 & 0 & 4.31 \end{bmatrix} \begin{matrix} lb/in \\ lb/in \\ lb/in \\ in-lb \\ in-lb \\ in-lb \\ lb/in \\ lb/in \end{matrix} \quad (9-4)$$

9.4.2 Analysis and Design Procedure

The resulting analysis model assembled with the [ABDE] matrix (i.e., the macromechanical model) is simply a thick continuous plate. Live load combinations are applied satisfying the AASHTO LRFD (2004) requirements to generate maximum load effect without any restrictions. Analysis results under dead loads and HL-93 load represent the moment and shear distribution throughout the plate. Hence, moments and shear acting at the shear key locations can be determined. Knowing load demand at the longitudinal joints between precast beams (i.e., the shear key locations), any other joint detail can be developed.

In this example, the design procedure is illustrated using the most common transverse connection design configuration: i.e., the transverse posttension application through discrete diaphragms of the beams with full-depth grouted shear keys. The example uses five discrete diaphragms along the span: two 24 in. wide end diaphragms and three 14 in. wide intermediate diaphragms located at mid-span and one-fourth location along the span (Figure 9-10).

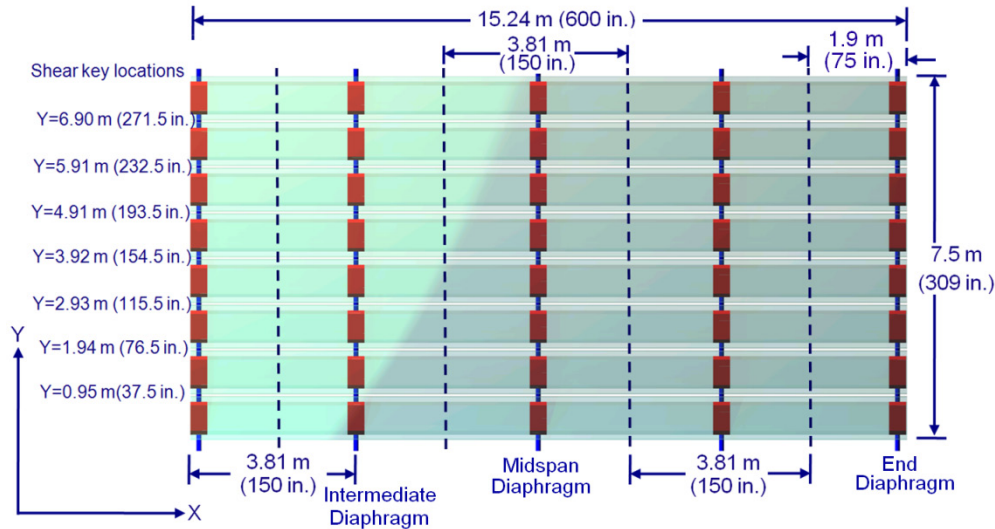


Figure 9-10. Diaphragm and shear key locations.

To determine the first stage of posttension, the macromechanical model with stiffness properties of RVE without a deck is analyzed under dead load corresponding to cast-in-place concrete deck. Concrete self weight is assumed to be 150 lb/ft^3 . For the second stage, the stiffness properties of RVE with a deck are assigned to the macromechanical model and analyzed under barrier load (New Jersey Type 4, Figure 9-11), and HS-20 truck and lane load (i.e., HL-93). HS-20 truck position on a single lane (Figure 9-12) and two lanes are considered. In order to determine the transverse posttension force requirement at each diaphragm location, the nominal moment acting within the half distance between diaphragms is calculated as given in Table 9-1. Critical moment combinations are recognized for calculating posttension force demand at the diaphragms before and after deck placement.

AASHTO LRFD (2004) does not provide an explicit service load criteria for longitudinal joint design. Hence, service I and III limit states are considered for limiting the stresses at the longitudinal joints. When load factors are considered, service I criteria obviously controls the design. The joint design criteria used here is crack prevention; hence, posttension is designed based on no tension. Based on AASHTO LRFD (2004) Section 3.6.1.1.2, multiple presence factors of 1.2 and 1.0 are considered for the condition of one and two lanes of vehicular live loads, respectively. Also, section 3.6.2.1 of AASHTO LRFD (2004) recommends using 1.75 as the dynamic load allowance factor for deck joints. Transverse posttension force magnitudes at each diaphragm location are calculated following service I limit state requirements, critical

transverse moments at the joints, and the AASHTO LRFD (2004) specification stipulations. The Michigan Bridge Design Guide (2005) specifies transverse posttension application at two locations along the height of 33 in. or deeper beams. Considering the impact of applying posttension at two locations along the beam height on moment transfer across the joint, a similar practice is maintained in this example as shown in Table 9-2.

Transverse posttension force magnitudes at each diaphragm location are calculated following Service I limit state requirements, critical transverse moments at the joints, and the AASHTO LRFD (2004) specification stipulations. The results are summarized in Table 9-3. A detailed calculation procedure developed by Attanayake and Aktan (2009) is provided in Appendix J.

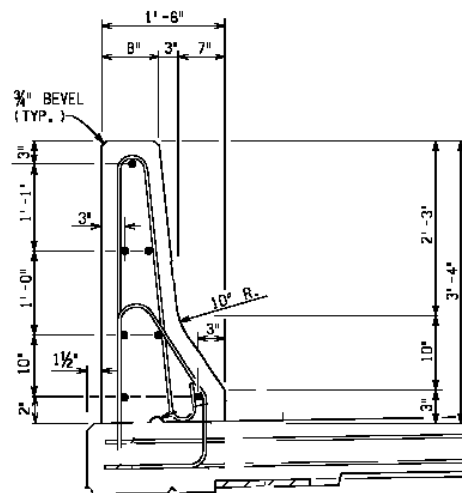


Figure 9-11. New Jersey Type 4 barrier (Note: 1 in. = 25.4 mm)

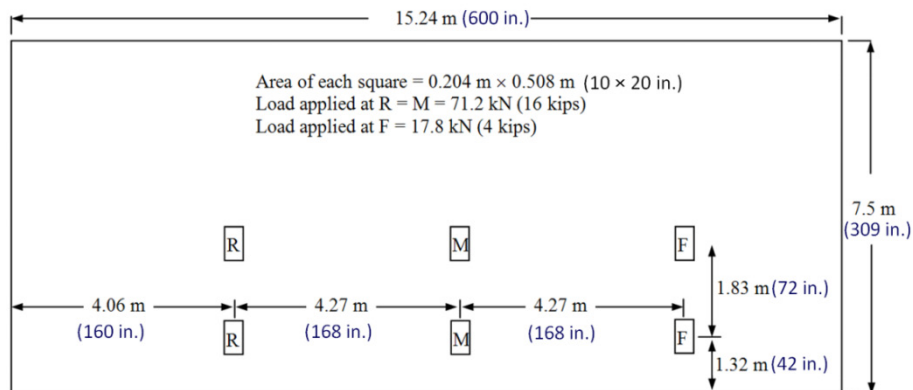


Figure 9-12. Position of a single HS-20 truck

Table 9-1. Averaged Transverse Moment, N-m/m (in-lb/in)

Row No.	Shear key location m (in.)	End Diaphragm Moment Averaged within 1.91m (75 in.)						Intermediate Diaphragm Moment Averaged within 3.81 m (150 in.)						Mid-span Diaphragm Moment Averaged within 3.81 m (150 in.)					
		Loads						Loads						Loads					
		Deck (a)	Barrier (b)	1 truck (c)	1 lane (d)	2 trucks (e)	2 lanes (f)	Deck (g)	Barrier (h)	1 truck (i)	1 lane (j)	2 trucks (k)	2 lanes (l)	Deck (m)	Barrier (n)	1 truck (o)	1 lane (p)	2 trucks (q)	2 lanes (r)
1	0.95 (37.5)	-730 (-164)	-2982 (-670)	-2728 (-613)	-547 (-123)	-1838 (-413)	-263 (-59)	2283 (513)	-2332 (-524)	8669 (1948)	2532 (569)	7432 (1670)	2078 (467)	3039 (683)	-2554 (-574)	10992 (2470)	3244 (729)	9372 (2106)	2657 (597)
2	1.94 (76.5)	779 (175)	-2439 (-548)	739 (166)	863 (194)	988 (222)	828 (186)	3974 (893)	-4303 (-967)	10805 (2428)	3872 (870)	9919 (2229)	3453 (776)	5224 (1174)	-5006 (-1125)	14098 (3168)	4873 (1095)	13087 (2941)	4406 (990)
3	2.93 (115.5)	1460 (328)	-2194 (-493)	1833 (412)	1095 (246)	2390 (537)	1077 (242)	5002 (1124)	-5304 (-1192)	13025 (2927)	3484 (783)	14374 (3230)	3698 (831)	6501 (1461)	-6439 (-1447)	16105 (3619)	4388 (986)	18165 (4082)	4810 (1081)
4	3.92 (154.5)	1606 (371)	-2140 (-481)	1384 (311)	360 (81)	2768 (622)	721 (162)	5345 (1201)	-5611 (-1261)	5994 (1347)	1571 (353)	11988 (2694)	3142 (706)	6920 (1555)	-6906 (-1552)	7939 (1784)	2145 (482)	15878 (3568)	4294 (965)
5	4.91 (193.5)	1460 (328)	-2194 (-493)	552 (124)	-18 (-4)	2390 (537)	1077 (242)	5002 (1124)	-5304 (-1192)	1348 (303)	209 (47)	14374 (3230)	3698 (831)	6501 (1461)	-6439 (-1447)	2060 (463)	423 (95)	18165 (4082)	4810 (1081)
6	5.91 (232.5)	779 (175)	-2439 (-548)	249 (56)	-36 (-8)	988 (222)	828 (186)	3974 (893)	-4303 (-967)	-886 (-199)	-414 (-93)	9919 (2229)	3453 (776)	5224 (1174)	-5006 (-1125)	-1010 (-227)	-467 (-105)	13087 (2941)	4406 (990)
7	6.9 (271.5)	-730 (-164)	-2982 (-670)	890 (200)	285 (64)	-1838 (-413)	-263 (-59)	2283 (513)	-2332 (-524)	-1237 (-278)	-454 (-102)	7432 (1670)	2078 (467)	3039 (683)	-2554 (-574)	-1620 (-364)	-587 (-132)	9372 (2106)	2657 (597)

Note: Negative (-) moments develop tension on top of the deck

Highlighted cells contain the critical moments for AASHTO LRFD (2004) Service I combination

Table 9-2. Geometric Parameters of Diaphragms and Transverse Posttension Locations along Beam Height

Transverse Posttension Locations along Beam Height		
Diaphragm Cross-Section without Deck		
	End Diaphragm (a)	Intermediate and Mid-span Diaphragms (b)
1. Cross-Section Area (A) mm ²	4.356×10^5	2.442×10^5
2. Moment of Inertia (I) mm ⁴	1.708×10^{10}	9.557×10^9
3. Neutral Axis Depth (y) mm	343	343
Diaphragm Cross-Section with Deck		
4. Cross-Section Area (A) mm ²	5.321×10^5	2.983×10^5
5. Moment of Inertia (I) mm ⁴	3.114×10^{10}	1.746×10^{10}
6. Miscellaneous Parameters		

Table 9-3. Posttension Force Requirement for the Sample Bridge

		Posttension Force at Diaphragm (P), kips		
		End Diaphragm	Intermediate Diaphragm	Middle Diaphragm
Before deck placement		7	41	52
After deck placement		63	105	130
Total		70	146	182
Total (empirical) MDOT ⁺	HS-20	82.5	82.5	82.5
	HS-25	104.5	104.5	104.5

+ Michigan DOT applies the highest level of posttension in the US. Posttension force magnitudes are recommended based on empirical methods and applied before deck placement (*Attanayake and Aktan 2008*)

9.5 CONSTRUCTION SIMULATION WITH STAGED POSTTENSION

Construction simulation discussed in chapter 8 is based on the current Michigan DOT practice. Transverse connection design, as specified in the MDOT design manual, is empirical and applied in a single stage. The rational design procedure discussed in section 9.4 recommends staged posttension to precompress the deck before casting barriers and applying live load. Finite element simulation of the proposed procedure and results are discussed in this section.

The first two stages of the construction process are the same as those discussed in Chapter 8. That is: beams are erected and then shear keys are grouted. Given below are the analyses performed for the following stages:

Stage 3: Posttension application before 6-in. thick deck placement

Following the proposed procedure, two posttension locations are considered along the beam height. The first posttension location is placed seven inches below the top of the beam. The second location is seven and a half inches above the bottom fiber of the beam (Figure 9-13). (Note: 7.5 in. distance is selected based on the limitations of the FE mesh size.) Posttension load magnitudes are established from the rational design example as given in Table 9-3.

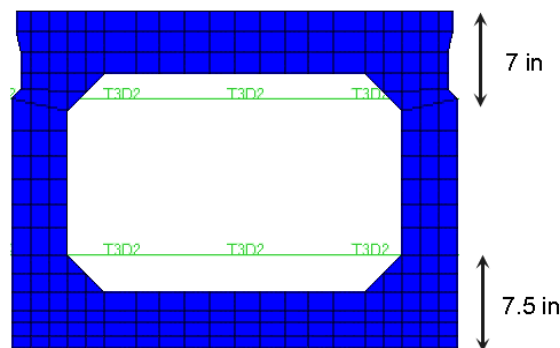


Figure 9-13. Transverse posttension locations along the beam height

Clamping stress distribution of the shear key located between fascia and the first interior beams is shown in Figure 9-14a. At the shear key located between fascia and the first interior beams, the maximum compressive clamping stress magnitude of 61 psi and tensile stress magnitude of 3.2 psi are obtained. The magnitude of posttension applied at the mid-span diaphragm is greater than the intermediate and end diaphragms; hence, the maximum clamping stress occurs at mid-span instead of end-diaphragms (Figure 9-14b).

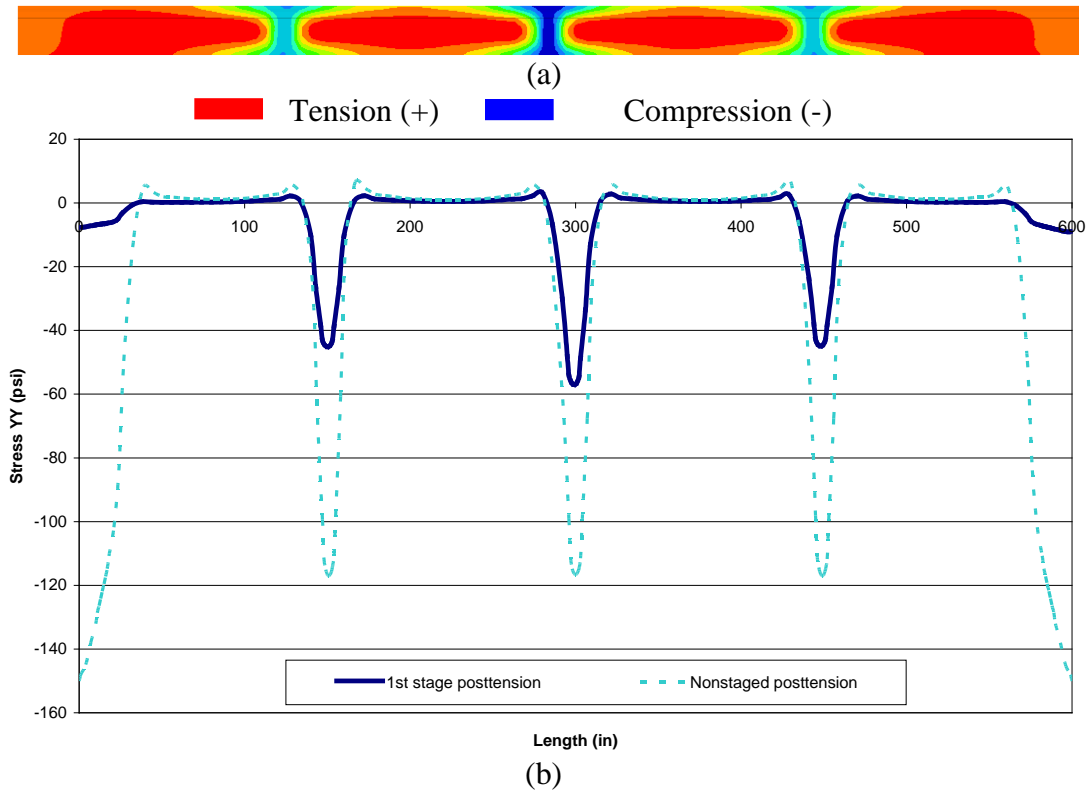


Figure 9-14. Clamping stress (a) contours at shear key after the first stage posttension and (b) distribution along the length of the shear key with or without staged posttension (stresses are extracted using shear key mid-height nodes)

Stage 4: Deck placement

After application of the first stage posttension, a 6-in. thick concrete deck is cast. Hence, dead load of the deck is acting on the beam-shear key system, but deck elements are not activated and are free of stresses. Applying deck as dead load causes minor changes to the shear key clamping stresses. Specifically, compressive clamping stresses are increased to 68 psi from 61 psi, whereas tensile stress magnitudes increased to 9 psi at locations close to end diaphragms where initial posttension magnitudes are low.

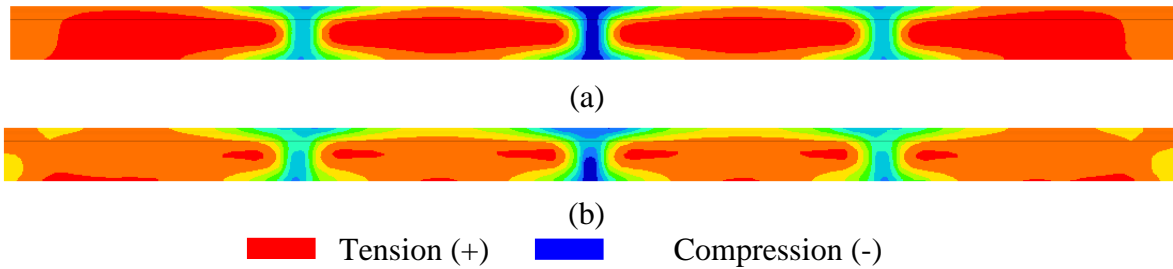


Figure 9-15. Clamping stress distribution along the shear key between fascia and the first interior beams under (a) posttension and (b) posttension and deck dead load

Stage 5: Deck concrete is hardened

To simulate the behavior of a bridge superstructure with hardened concrete deck, deck elements are activated. No loads are defined within this step. Any further loads applied will now act on the composite system.

Stage 6: Posttension application upon deck placement

Upon second stage posttension, clamping stress magnitudes at the shear key between fascia and the first interior beams are increased (Figure 9-16). Compressive clamping stress increases to 231 psi from 61 psi, whereas tensile stress magnitude remains the same at 9 psi. With the application of second stage posttension after deck placement, a greater part of the deck is compressed with maximum stress magnitude reaching 100 psi around mid-span. Maximum tensile stress magnitude of 18 psi develops in regions close to fascias at mid-span diaphragm location (Figure 9-17b). Tensile stresses that develop between the diaphragms (dark red contours in Figure 9-17a) and Figure 9-18a) correspond to magnitudes of less than 6 psi. Transverse stress distribution along the width of the deck is given in Figure 9-17 and Figure 9-18 for the top and bottom surfaces of the 6-in. thick cast-in-place deck, respectively.

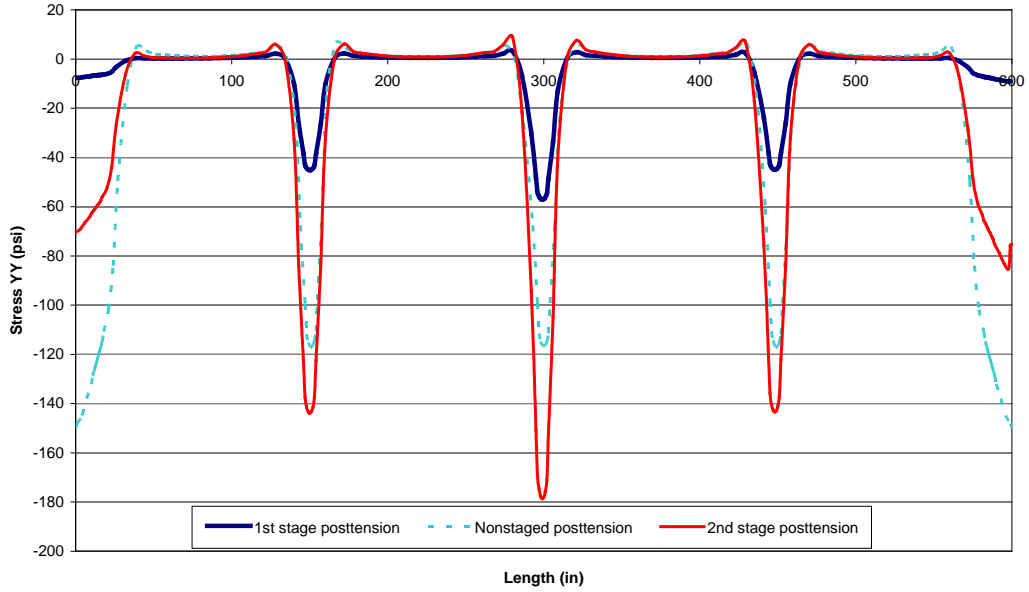


Figure 9-16. Clamping stress distribution along the length of the shear key with or without staged posttension (stresses are extracted using shear key mid-height nodes; compression-negative, tension-positive)

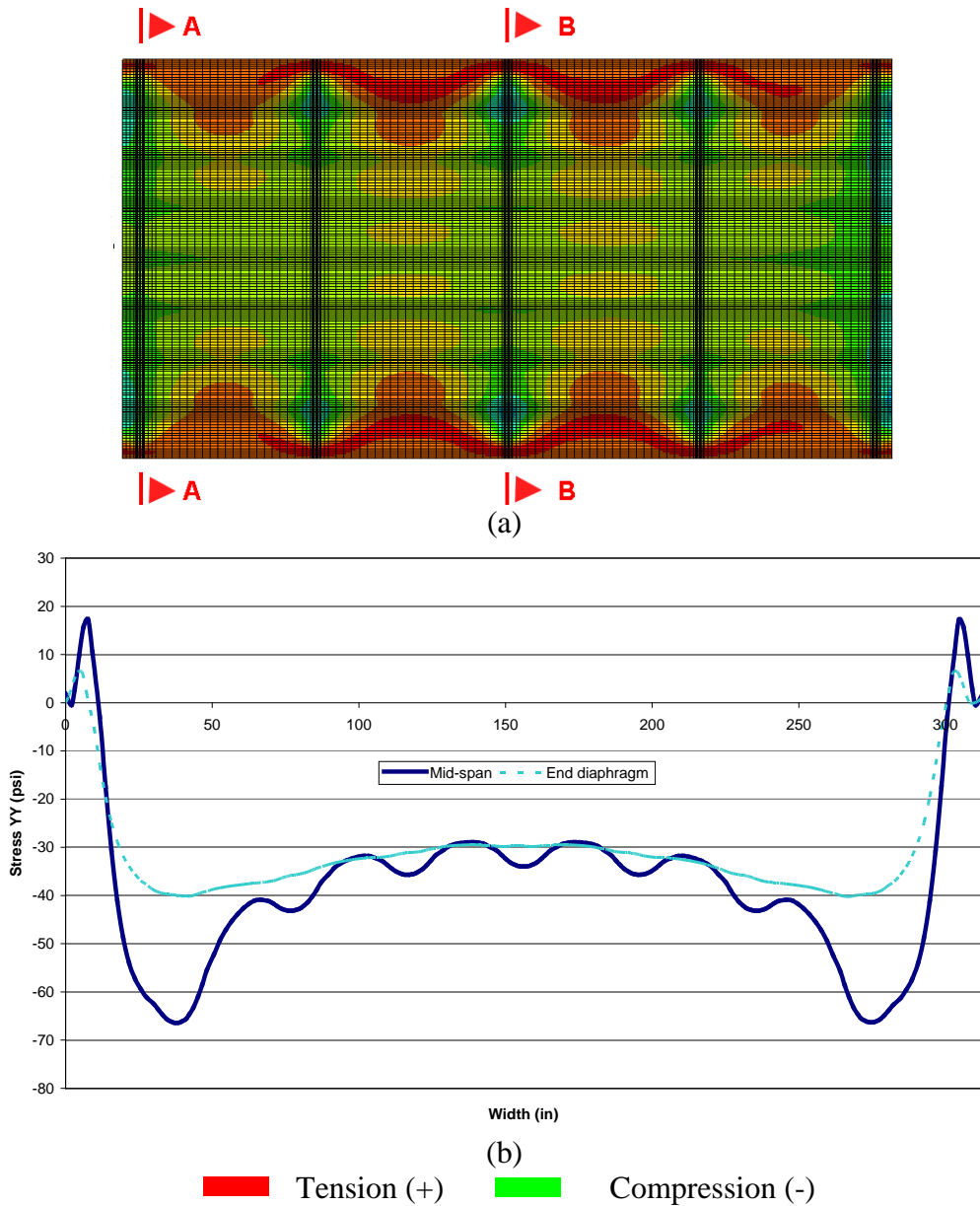


Figure 9-17. Transverse stress distribution (a) at the deck top surface and (b) along the width of the deck top surface over mid-span (Section B-B) and end-diaphragm (Section A-A) after second stage posttension

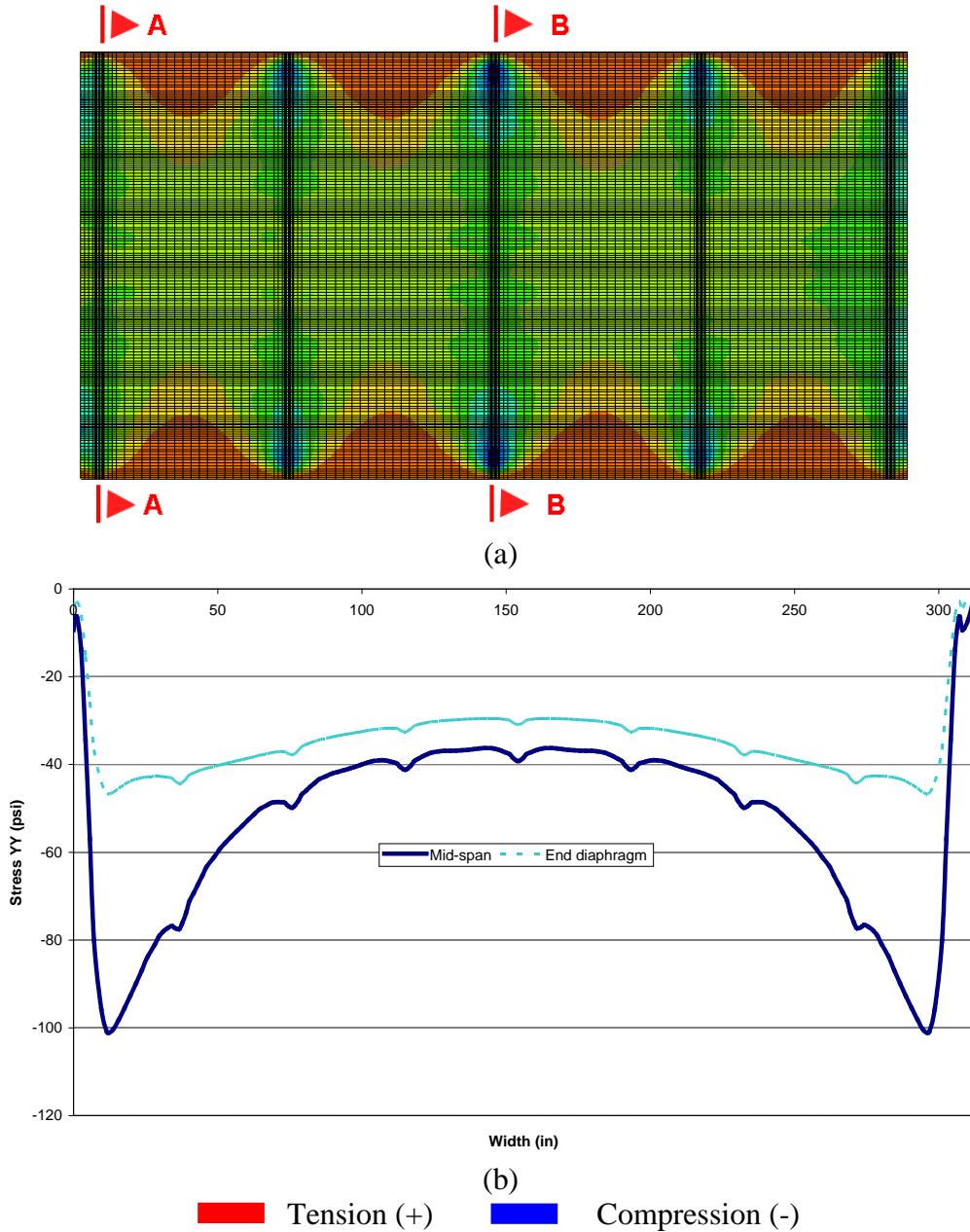


Figure 9-18. Transverse stress distribution (a) at the deck bottom surface and (b) along the width of the deck bottom surface over mid-span (Section B-B) and end-diaphragm (Section A-A) after second stage posttension

Stage 7: Barriers are placed

Analysis in Chapter 8 showed that with single-stage posttension application (current MDOT practice), barrier loads generated tensile stresses within the 6-in thick cast-in-place concrete deck, particularly close to interior beams at mid-span. During this analysis step, barrier load is applied to the structure that is posttensioned following the proposed two-staged procedure. The maximum compressive stress within the 6-in. thick concrete deck remains at 75 psi; whereas

tensile stress magnitudes are increased to 14 psi from 6 psi (Figure 9-19). Also, clamping compressive stress in shear keys between the fascia and the first interior beams increases to 241 psi from 231 psi; whereas tensile stress remains at 8 psi.

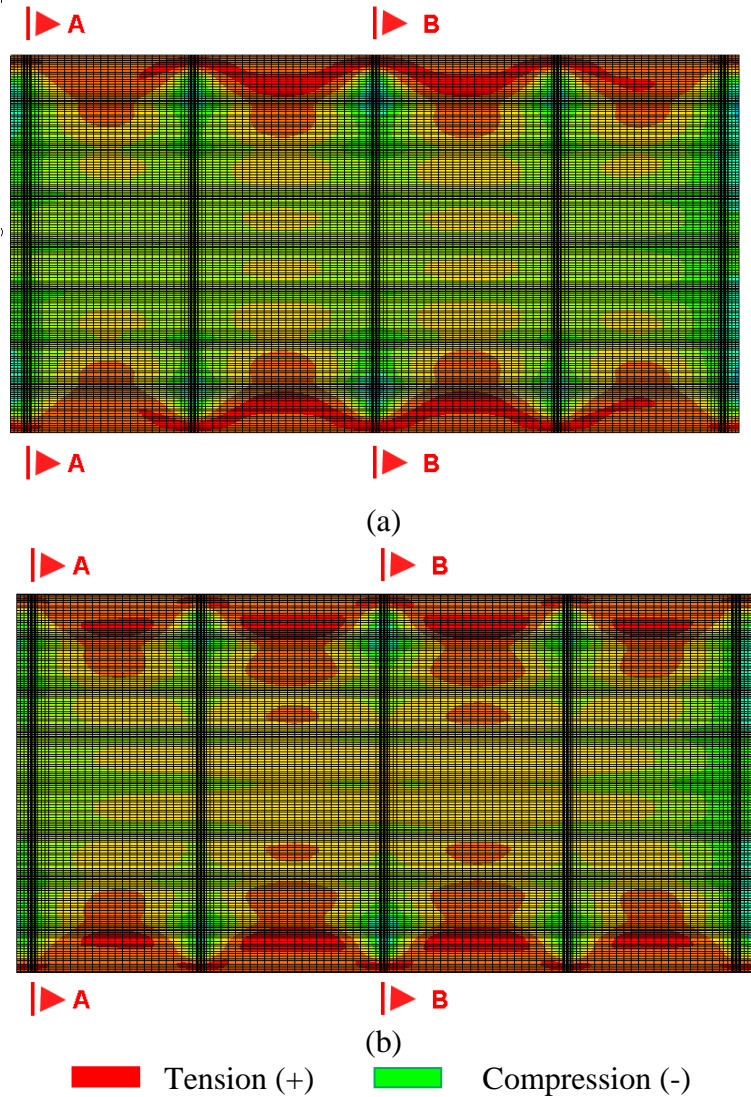


Figure 9-19. Transverse stress distribution at the cast-in-place concrete deck top surface (a) before and (b) after the barriers are placed

9.5.1 Service Load Analysis

Service I load combinations utilized in the analysis are as follows:

Combo 1: 1.0 DEAD + 1.0 NTG

Combo 2: 1.0 DEAD + 1.0 PTG

Combo 3: 1.0 DEAD + 1.0 LL

where

NTG: Negative thermal gradient loading

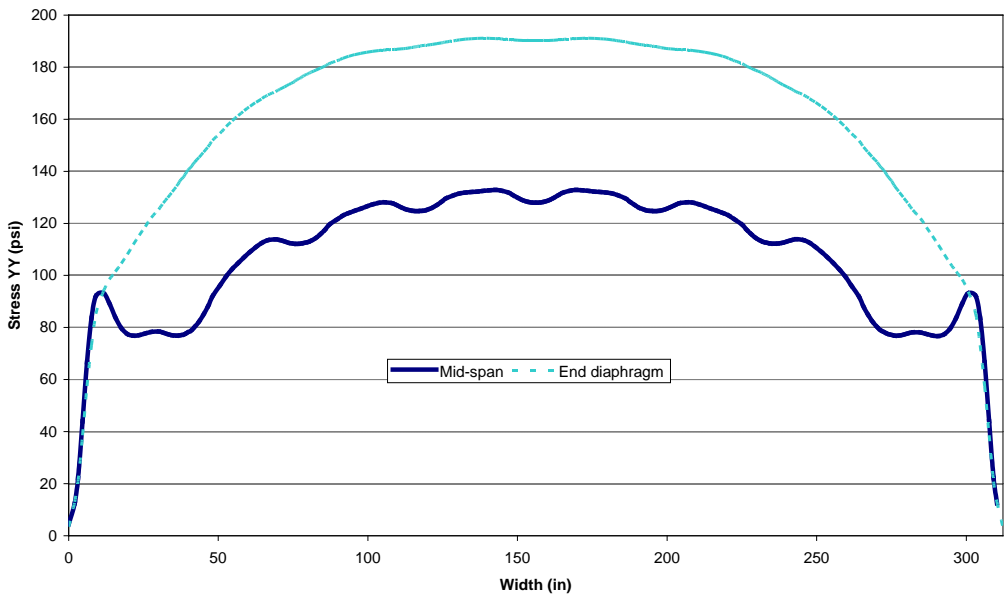
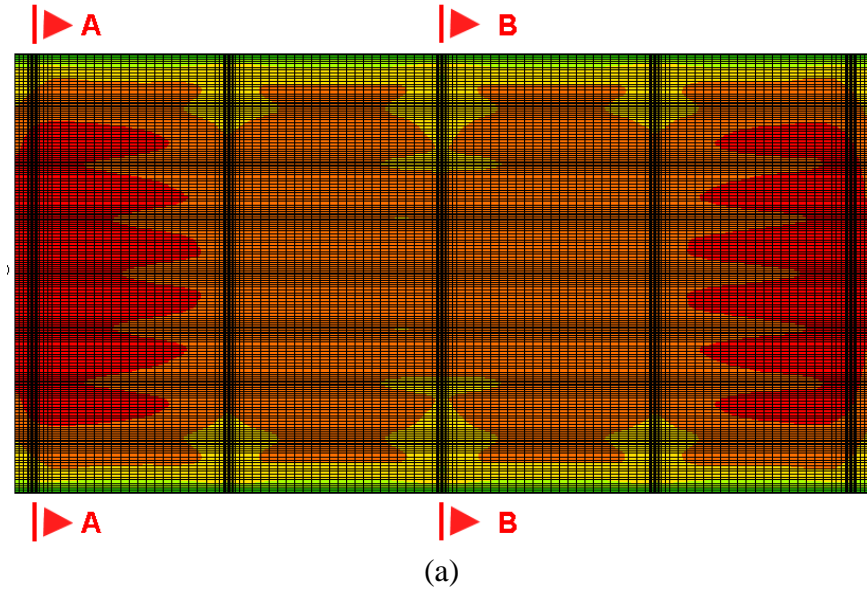
PTG: Positive thermal gradient loading

DEAD: Dead load of all components

LL: HL-93 live load with impact and multiple presence factors

9.5.1.1 Load Combination 1: 1.0 DEAD + 1.0 NTG

Negative thermal gradient loading is applied to the composite beam-shear key-deck assemblage while the stresses generated under dead loads are retained. Transverse stress distribution at the deck top surface is given in Figure 9-20 (a), and the stress variations at selected sections along the width of the top surface are given in Figure 9-20 (b). Transverse tensile stress of 160 psi is calculated at mid-span close to the interior girders in single-stage posttension application (i.e., according to current MDOT practice). These stresses are decreased to 130 psi in the staged posttension application. Tensile stress of 230 psi documented over the end-diaphragms with single-stage posttension is also decreased to 190 psi when the proposed two-stage posttension is applied. Tensile stresses that are developed at the bottom face of the 6-in cast-in-place slab with single-stage posttension are now completely diminished (Figure 9-21b). Clamping stresses developed in the shear keys are minimally affected by the negative thermal gradient loading. The maximum clamping compressive stress at the shear key located between fascia and the first interior beams is decreased to 217 psi from 241 psi, whereas tensile stress remains at 8 psi.



■ Tension (+) ■ Compression (-)

Figure 9-20. Transverse stress distribution (a) at the top surface of the deck and (b) along the width of the deck top surface over mid-span (Section B-B) and end-diaphragm (Section A-A) under service I load combination 1

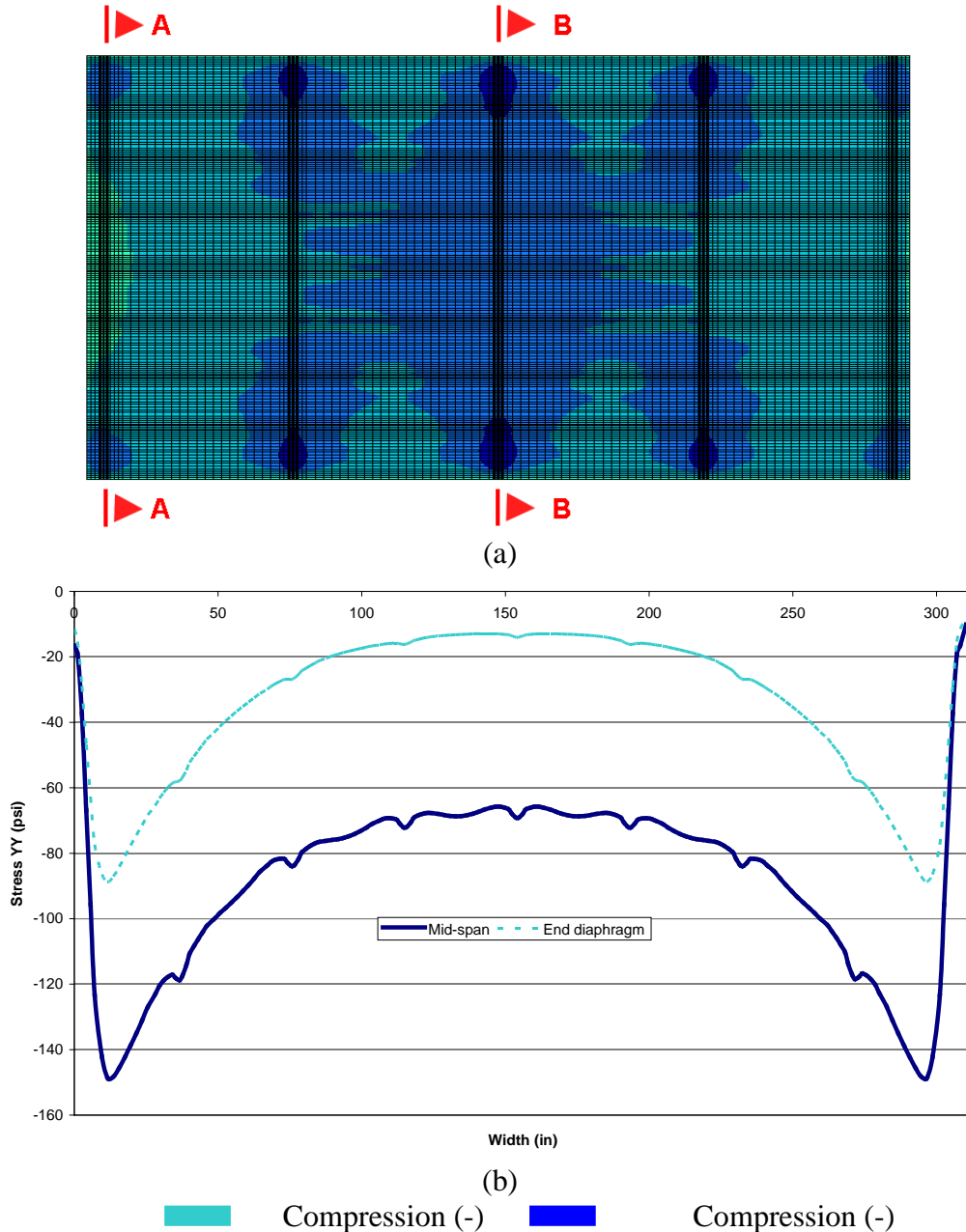


Figure 9-21. Transverse stress distribution (a) at the bottom surface of the 6-in thick deck and (b) along the width of the deck bottom surface over mid-span (Section B-B) and end-diaphragm (Section A-A) under service I load combination 1

9.5.1.2 Load Combination 2: 1.0 DEAD + 1.0 PTG

Negative thermal gradient loading is removed, and positive thermal gradient loading is applied to the composite beam-shear key-deck assemblage while the stresses generated under dead loads are retained. The deck top surface is now uniformly under compression (Figure 9-22) while tensile stresses form at portions of the 6-in. thick deck bottom surface (Figure 9-23).

Compressive stress magnitudes calculated at the top surface of the deck under single-stage posttension are increased by more than 30 psi when two-stage posttension is implemented. The maximum transverse tensile stress magnitude of 166 psi developed at mid-span during single-stage posttension is now decreased to lower than 100 psi. At end diaphragm locations, only at locations close to the fascia beams, tensile stresses are observed with a maximum magnitude of 106 psi (Figure 9-23b).

The application of positive gradient loading affects the clamping stresses in the shear keys between the fascia and the first interior beams. The maximum tensile stress magnitudes at the top of grout layers located between the fascia and the first interior beams increased to 100 psi from -10 psi (Figure 9-24). For this particular load case, precompressing the deck did not help reduce the tensile stress magnitudes developed at the top of shear keys.

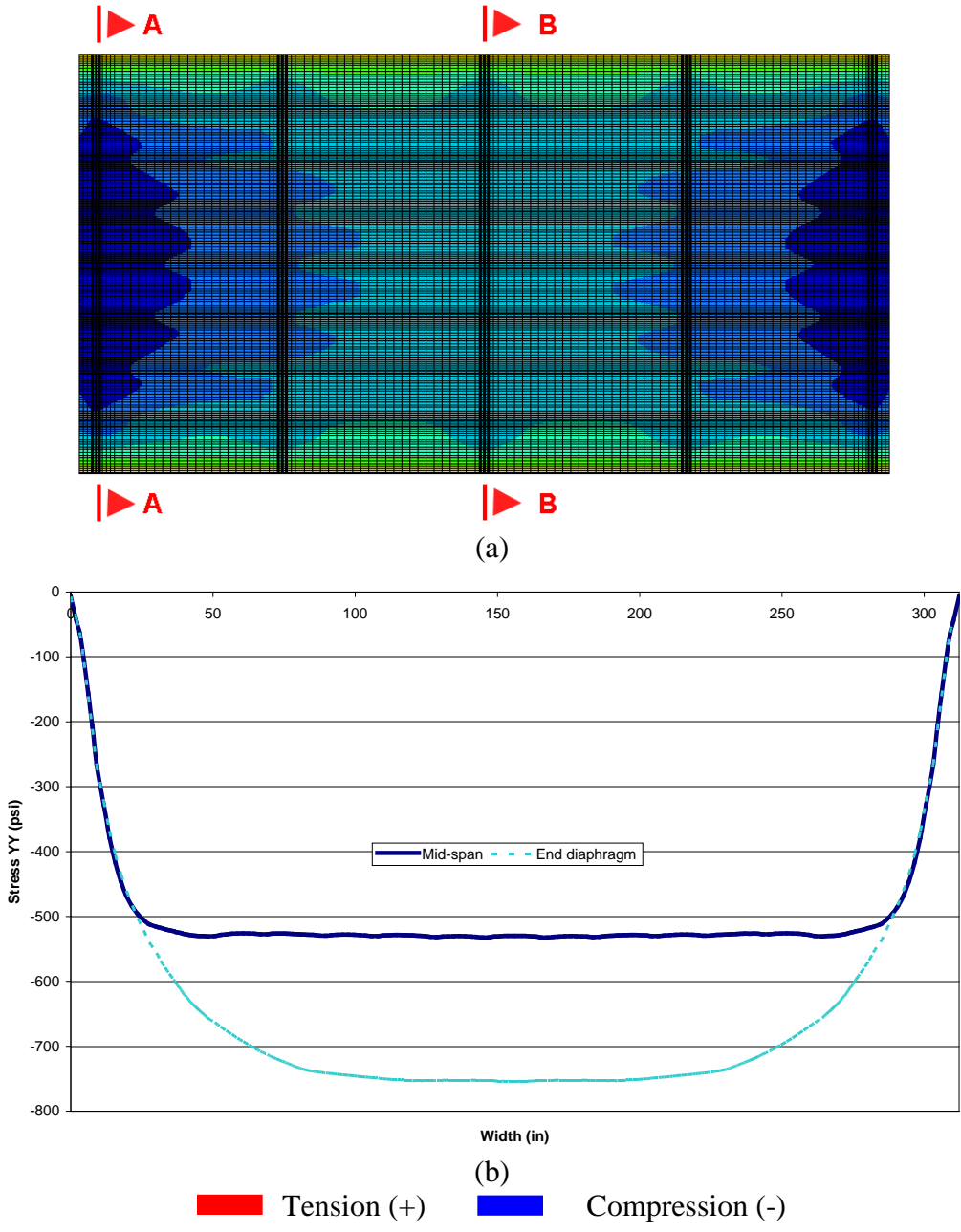


Figure 9-22. Transverse stress distribution (a) at the top surface of the deck and (b) along the width of the deck top surface over mid-span (Section B-B) and end-diaphragm (Section A-A) under service I load combination 2

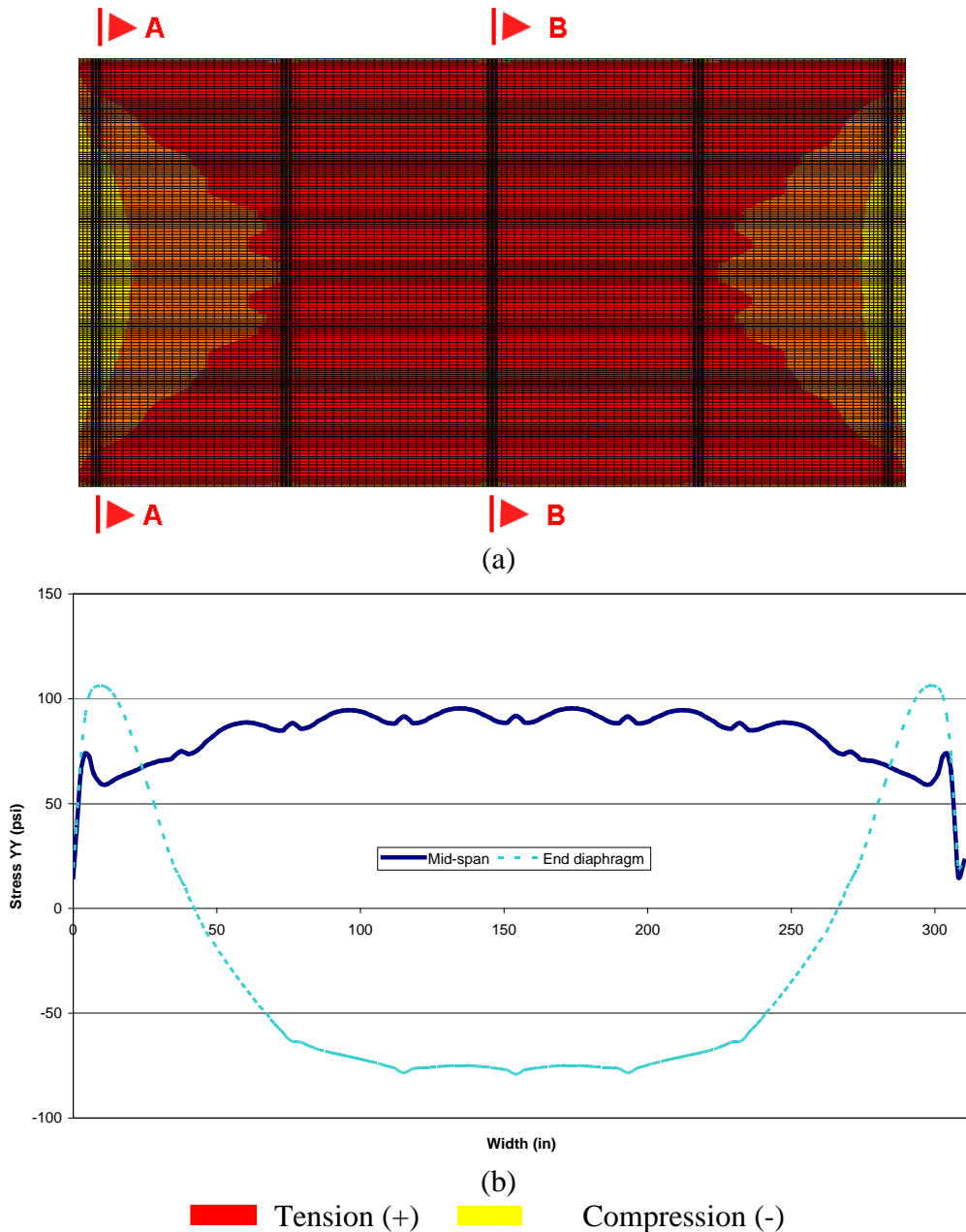
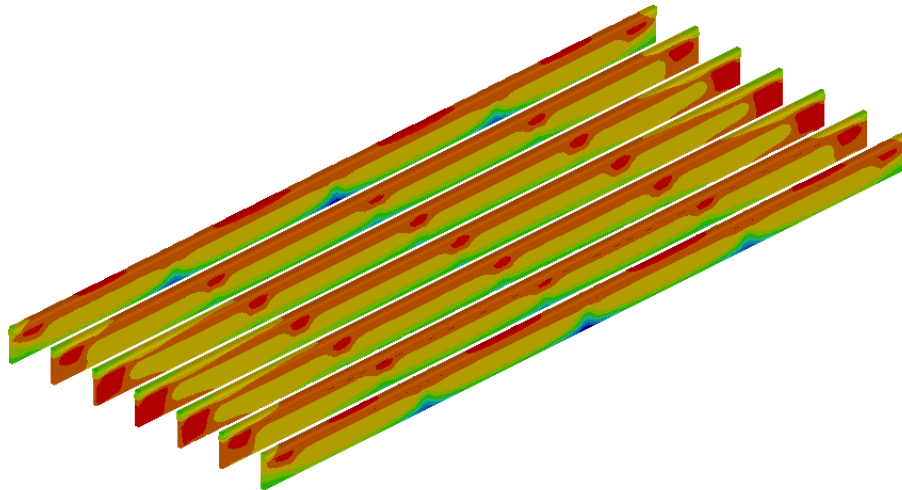
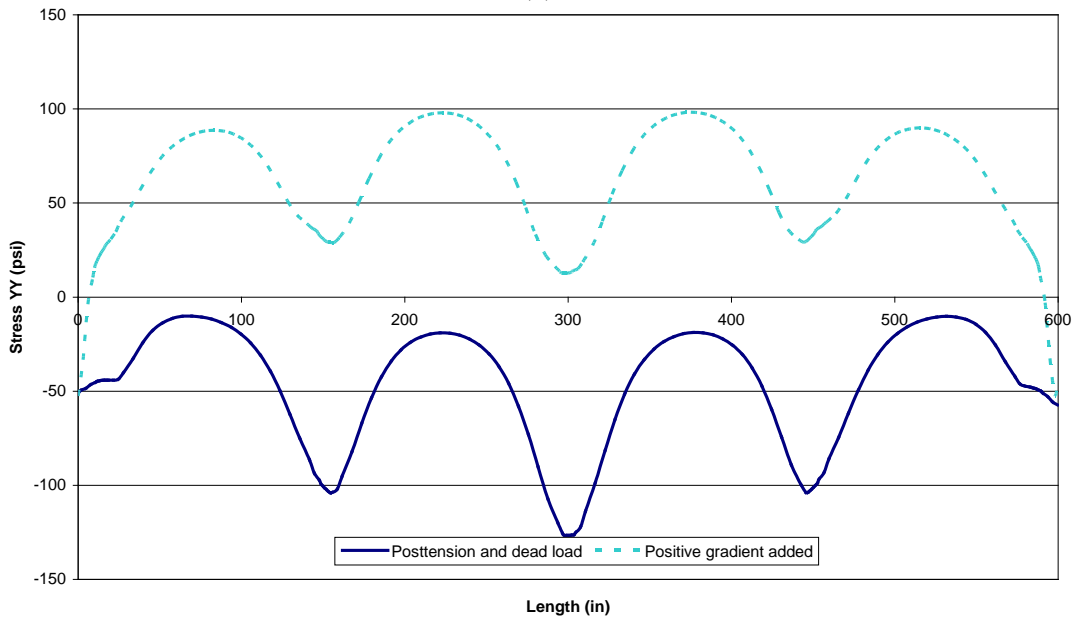


Figure 9-23. Transverse stress distribution (a) at the bottom surface of the cast-in-place deck and (b) along the width of the deck bottom surface over mid-span (Section B-B) and end-diaphragm (Section A-A) under service I load combination 2



(a)



(b)

■ Tension (+) ■ Compression (-)

Figure 9-24. Clamping stress (a) profile on grout layers under positive thermal gradient loading and (b) distribution along the length of grout layers with and without positive gradient loading (stress plots are extracted using shear key top fiber nodes; compression-negative, tension-positive)

9.5.1.3 Combination 3: 1.0 DEAD + 1.0 LL

Single-Lane Loaded

At this step, the thermal gradient load is removed, and the HL-93 load is applied on a single lane of the bridge while the dead load stresses generated in the earlier stages are retained. The maximum transverse tensile stress at the top surface of the deck over the end diaphragm is decreased to 12 psi from 30 psi; whereas it is reduced from 20 psi to 11 psi at mid-span (Figure

9-25). Transverse tensile stresses are completely diminished at the cast-in-place deck bottom surface (Figure 9-26). Grout clamping stresses do not change significantly under a single lane live load. On the grout layers between the fascia and the first interior beams, the maximum compressive clamping stress is increased to 273 psi from 241 psi; whereas tensile stress magnitude is increased to 10 psi.

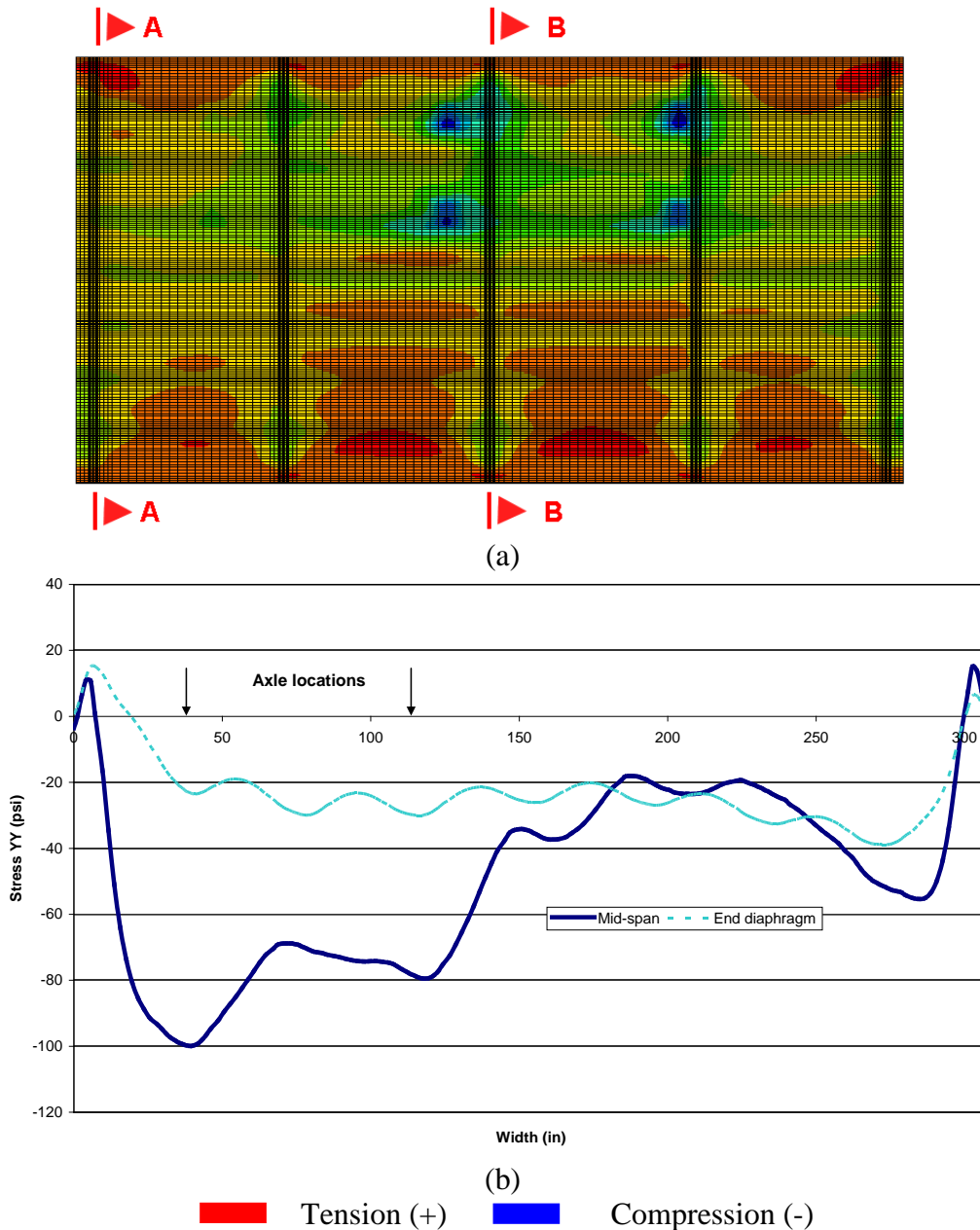


Figure 9-25. Transverse stress distribution (a) at the deck top surface and (b) along the width of the deck top surface over mid-span (Section B-B) and end-diaphragm centerline (Section A-A) under service I load combination 3 with a single lane live load

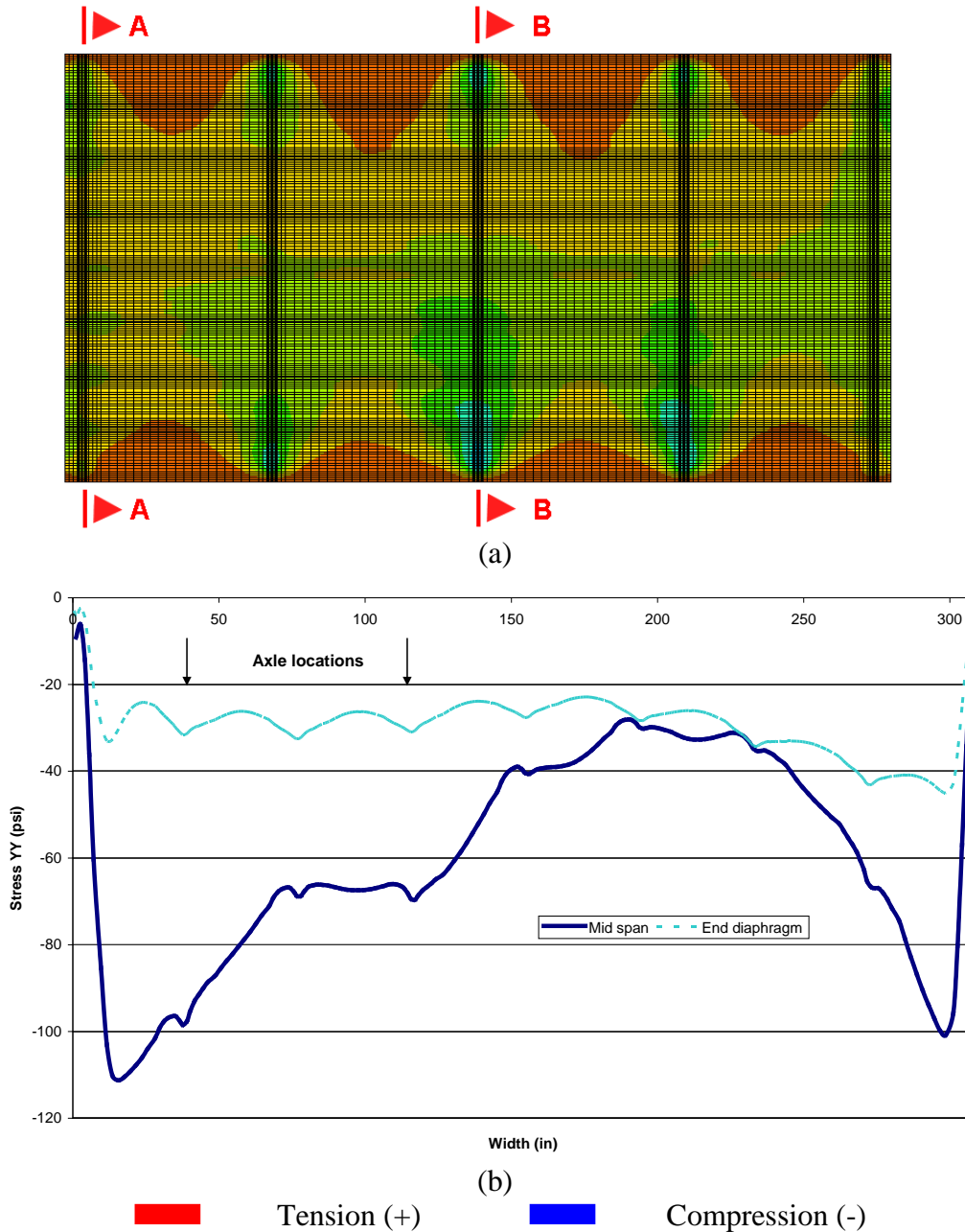


Figure 9-26. Transverse stress distribution (a) at the 6-in. deck bottom surface and (b) along the width of the deck bottom surface over mid-span (Section B-B) and end-diaphragm centerline (Section A-A) under service I load combination 3 with a single lane live load

Two-Lane Loaded

With the live load on both lanes of the bridge, mid-span regions of both top and bottom surfaces of the 6-in thick deck are now under compression. Transverse tensile stresses at the deck top surface and at specific concentrated locations are observed with a maximum of 21 psi (Figure 9-27-a). The entire bottom surface of the cast-in-place deck is under compression (Figure 9-28).

Under this load combination, grout clamping stresses do not change significantly. On the grout layers between the fascia and the first interior beams, the maximum compressive clamping stress is increased to 248 psi from 241 psi, and tensile stress magnitude remained at 10 psi.

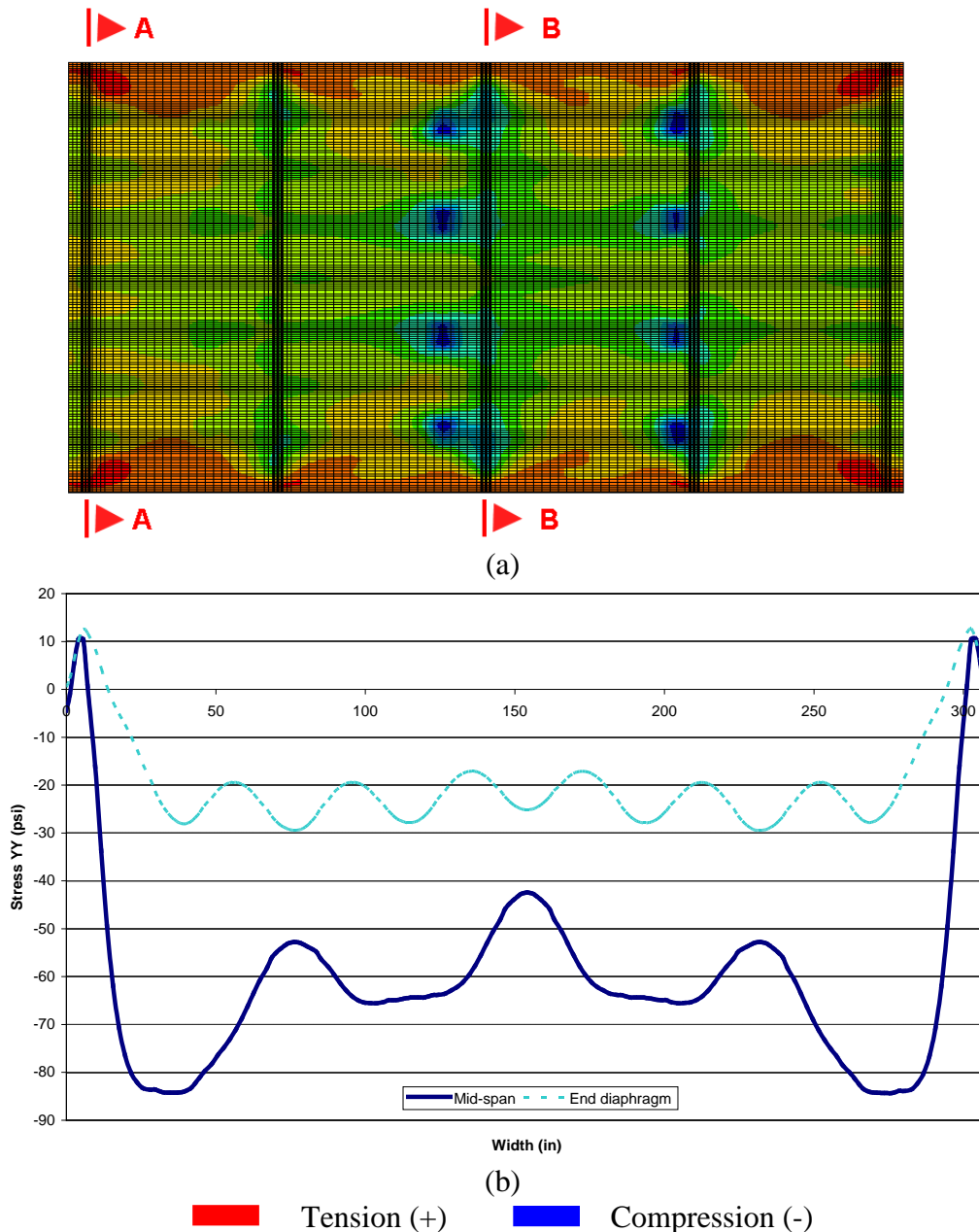


Figure 9-27. Transverse stress distribution (a) at the deck top surface and (b) along the width of the deck top surface over mid-span (Section B-B) and end-diaphragm (Section A-A) under service I load combination 3 with live load on two lanes

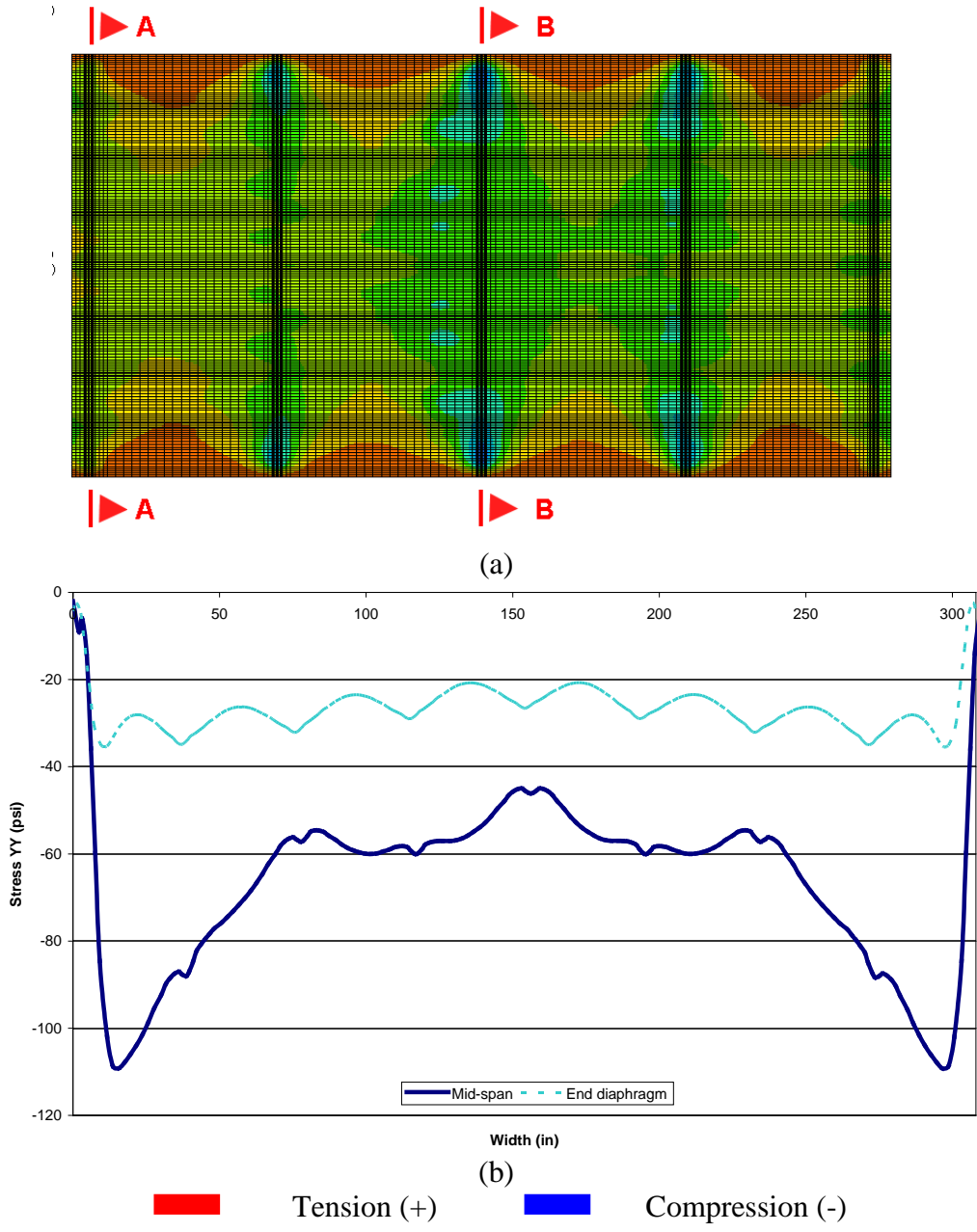


Figure 9-28. Transverse stress distribution (a) at the 6-in. deck bottom surface and (b) along the width of the deck bottom surface over mid-span (Section B-B) and end-diaphragm (Section A-A) under service I load combination 3 with live load on two lanes

9.6 SUMMARY AND CONCLUSIONS

In order to identify and document the longitudinal reflective deck crack initiation and progression, the bridge that carries Oakland Drive over I-94 in Portage, Michigan was monitored during construction. Cracks along the beam-shear key interface were observed before posttensioning and remained cracked after posttension. Cracks that stemmed from the top surface of the deck above the abutments were documented before any live or barriers loads. An analysis model, herein referred to as the macromechanical model was presented. The analysis model is suitable for calculating the required posttension levels using the concepts of mechanics of materials and macromechanics. Based on the results of the macromechanical model analysis, further FE analysis was performed evaluating the effects of staged posttension application on the deck and grout stresses.

Stress analyses of the single-stage and two-stage posttension are compared to document the effectiveness of two-stage posttension. Under thermal gradient loads, transverse stresses along the bottom surface of the deck and at the top deck surface undoubtedly diminished with the application of two-stage posttension (Figure 9-29 and Figure 9-30). Observed deck top surface tensile stresses at mid-span and end-diaphragm locations with single-stage posttension and single lane live load are completely diminished (Figure 9-31). With two-stage posttension, tensile stresses only developed at regions within the proximity of the fascias.

The application of second stage of posttension following deck placement reduced deck stresses under dead and live loads. A similar benefit is not observed under positive gradient loading and transverse tensile stress magnitudes calculated along the top of the shear keys closest to fascias increased by 5 psi. Compressive stress magnitudes decreased by about the same amount (Figure 9-32).

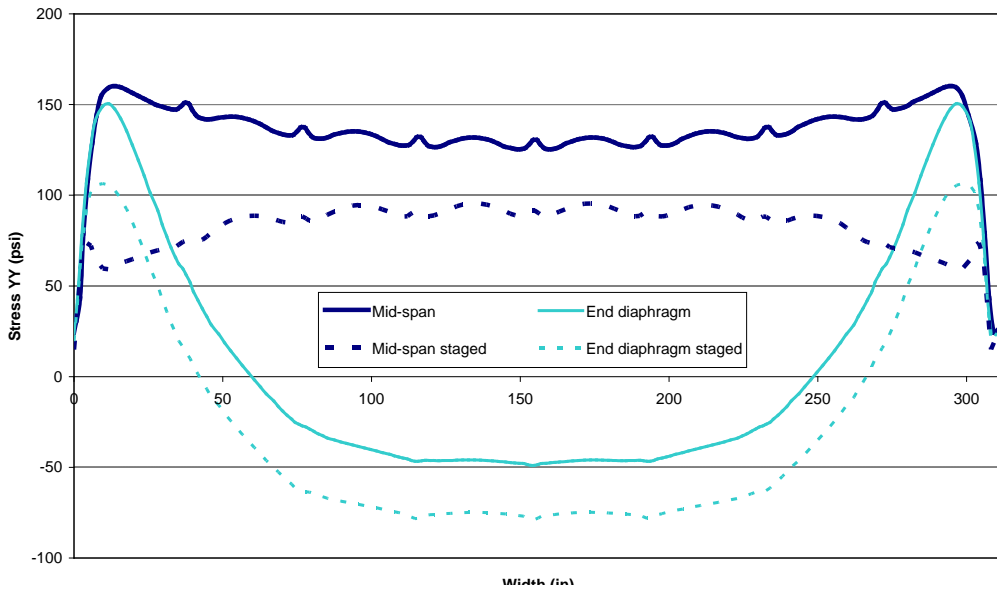


Figure 9-29. Transverse stress distribution along the width of the 6-in cast-in-place concrete deck bottom surface with and without staged posttension under service I load combination 2

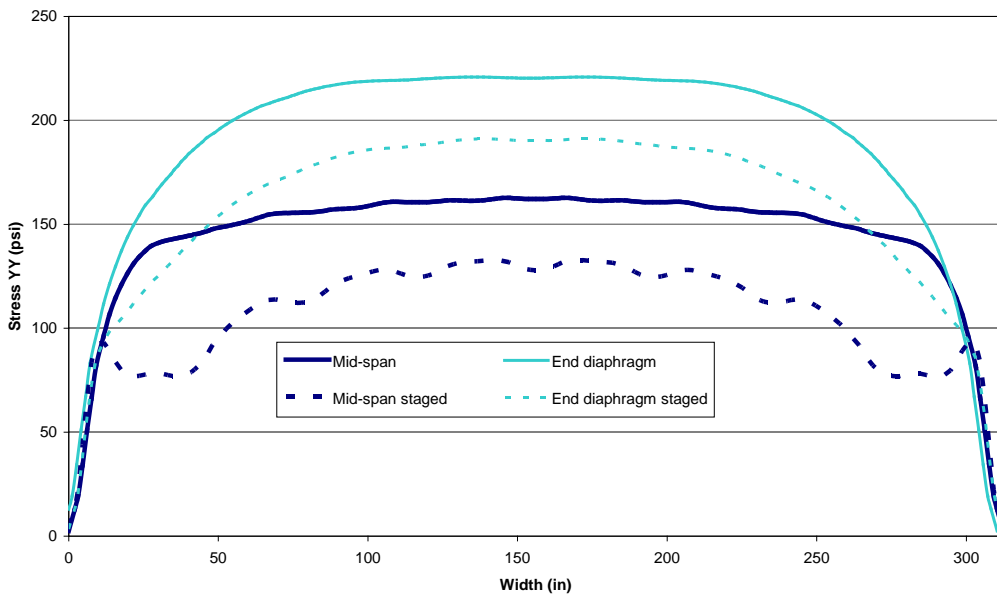


Figure 9-30. Transverse stress distribution along the width of the deck top surface with and without staged posttension under service I load combination 1

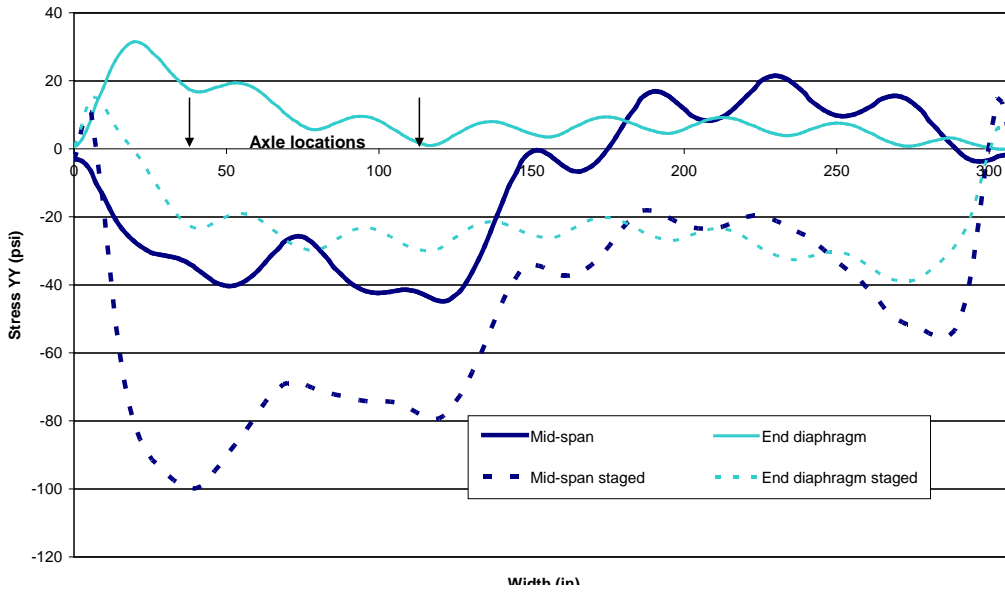


Figure 9-31. Transverse stress distribution along the width of the deck top surface with and without staged posttension under service I load combination 3 with a single lane live load

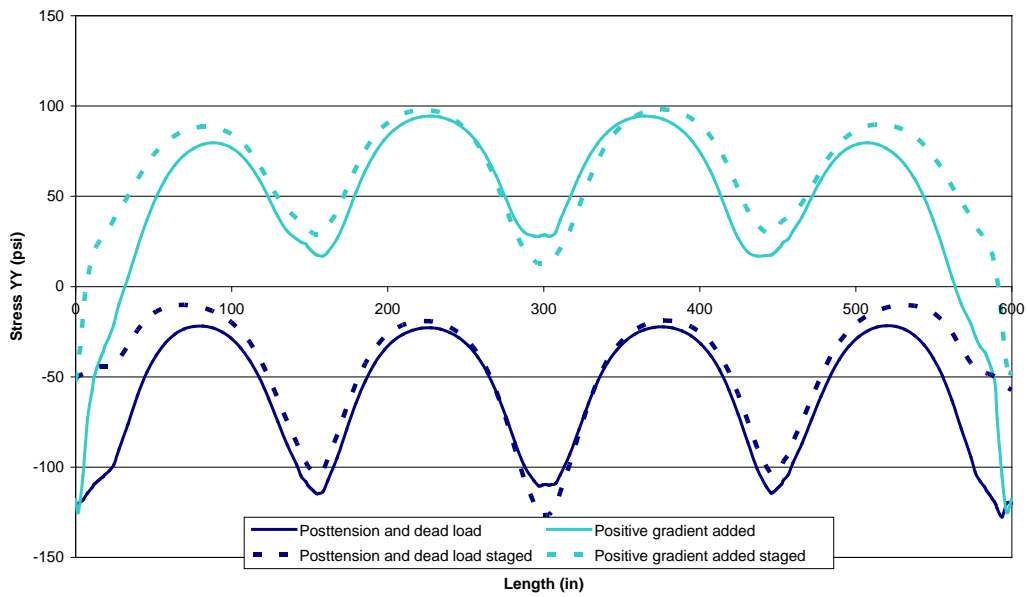


Figure 9-32. Clamping stress distribution along the length of the shear key top surface with and without staged posttension under positive gradient loading

The following conclusions and recommendations are generated from the derivations and analyses presented in this chapter:

1. The macromechanical model, once the ABDE matrices are provided, becomes a very useful and simplified tool in developing an analysis model for orthotropic deck systems such as the side-by-side box-beam bridge decks.
2. The critical moment and shear along the shear keys can be calculated from the analysis results obtained from the macromechanical models of the side-by-side box beam bridge.
3. The critical moments and shear along the shear keys can be used for calculating the transverse posttension requirements based on the proposed service criteria of zero tensile stress on the deck under gravity loading. This process will most likely abate reflective deck cracking.
4. A two-stage transverse posttensioning is recommended corresponding to before and after the six-inch concrete deck is placed.
5. Transverse tensile deck stresses that occur under live load can be eliminated except at specific isolated regions within the proximity of the fascias when recommended two-stage posttensioning is implemented.
6. There is no effective way of reducing tensile stresses in the deck that occur under positive thermal gradient loading.

10 CAPACITY EVALUATION OF A BOX-BEAM BRIDGE WITH DISTRESSED BEAMS

10.1 OVERVIEW

The objective of finite element (FE) modeling and analysis of distressed beams is to simulate various damaged scenarios under dead and live loads. Rating trucks recommended in the MDOT Analysis Guide (2003) and the AASHTO LRFR (2003) are used. Simulation of beam damage scenarios in a full bridge superstructure model helps develop recommendations for load rating considering the structural system interaction rather than the behavior of a single box-beam.

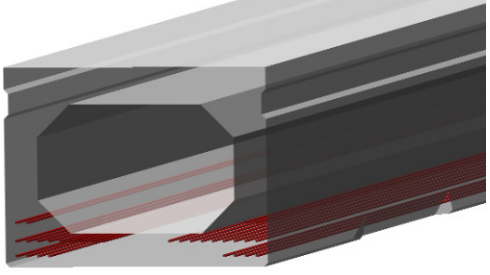
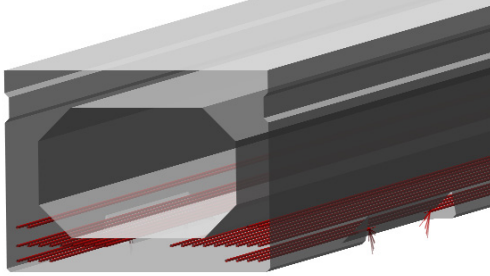
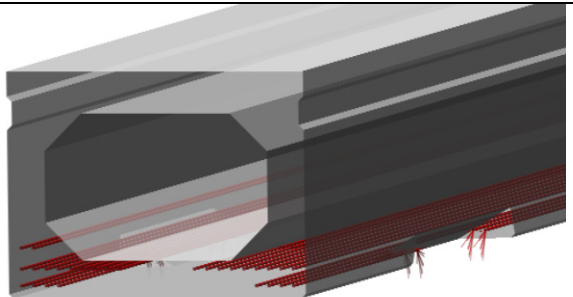
Distresses commonly observed during bridge inspections are incorporated into the full bridge FE models following similar procedures used in Phase I of this project. In the case of flexure critical models, distresses are incorporated at mid-span and quarter point locations of a beam. In the shear critical models, distresses are incorporated at beam ends. Concrete distress is modeled by gradually reducing the elasticity modulus from a depth of distress penetration to the surface. In the case of a broken tendon, strands are discontinued within the distress zone.

Four different distress levels are modeled (Table 10-1 and Table 10-2) again corresponding to the observed states during field inspection. Level one designates the undamaged sound box-beam. Level two is limited to the concrete section loss due to minor spall along bottom corners of a box beam cross-section. Level three designates similar spall as in level two but with one broken tendon within the distressed region. The distress length along the beam is taken as 50 inches for flexure and 17 inches for shear for both level two and three (Figure 10-1). Level four represents a major spall incorporating two broken tendons along the bottom corner of the distressed region. At level four, the length of distress along the beam is increased to 62 and 23 inches for flexure and shear critical models, respectively (Figure 10-2).

Table 10-1. Distress Level Summary in FE Analysis

Case	Distress Level Summary	Figure
1	Control condition; as built properties, no loss of prestressing strand.	None
2	Spall along bottom corner of box-beam. Length of spall is 50 inches and 17 inches for flexure critical and shear critical models, respectively.	Figure 10-1
3	Spall along bottom corner of box-beam. Length of spall is 50 inches and 17 inches for flexure critical and shear critical models, respectively. One broken tendon within distressed zone.	Figure 10-1
4	Spall along bottom corner of box-beam. Length of spall is 62 inches and 23 inches for flexure critical and shear critical models, respectively. Two broken tendons within distressed zone.	Figure 10-2

Table 10-2. Distress Observed During Field Inspection and Used in FE Models

Distress Level	Observed During Field Inspection	Finite Element Model
2		
3		
4		

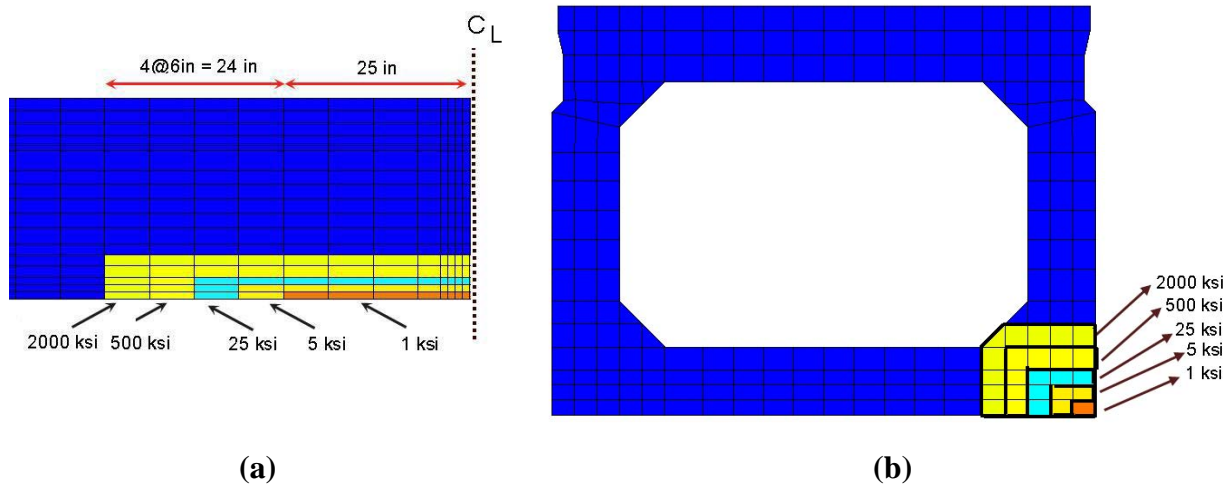


Figure 10-1. Finite element model of distress levels 2 and 3: (a) enlarged view of half of the distressed zone along length and (b) section view of the distressed zone (note: broken strands are not visible)

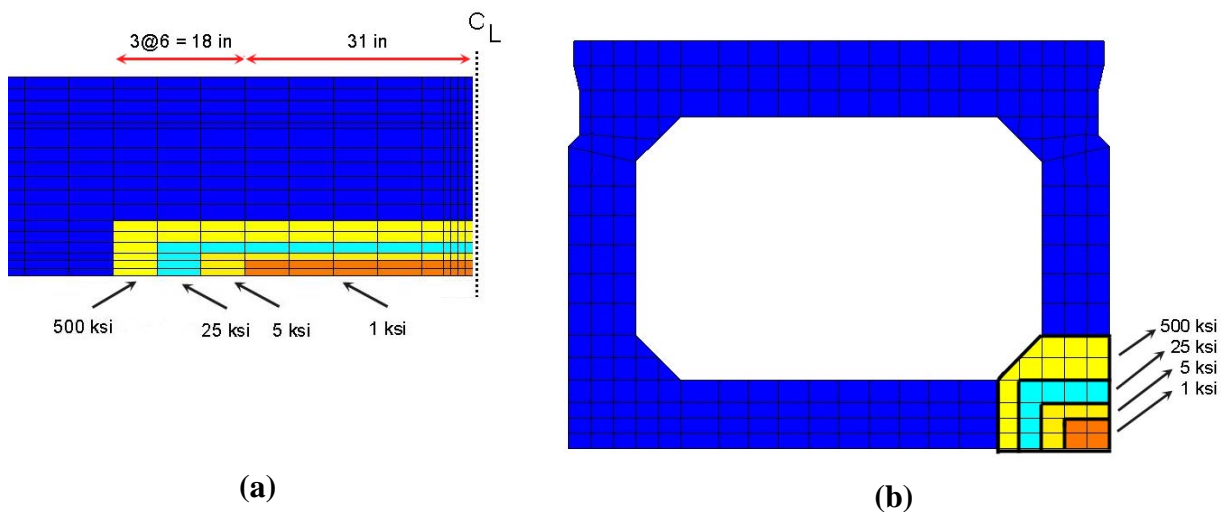


Figure 10-2. Finite element model of distress level 4: (a) enlarged view of half of the distressed zone along length and (b) section view of the distressed zone (note: broken strands are not visible)

This chapter also investigates the influence of posttension and grout loss in the shear key as another form of distress. The length of the grout void in shear keys due to loss of grout is taken equal to the length of the beam distress zone.

The details of the configuration and the material properties of a side-by-side box-beam bridge for construction simulation and service load analysis was given in Chapter 8. The same bridge configuration is used in this chapter for capacity evaluation and load rating following the AASHTO LRFR (2003) procedures. Michigan specific rating trucks are selected from the MDOT Bridge Analysis Guide (2003). According to the AASHTO LRFR (2003), the

methodology for the Load and Resistance Factor Rating (LRFR) of a bridge is comprised of three distinct procedures: (1) design load rating, (2) legal load rating, and (3) permit load rating (Figure 10-3).

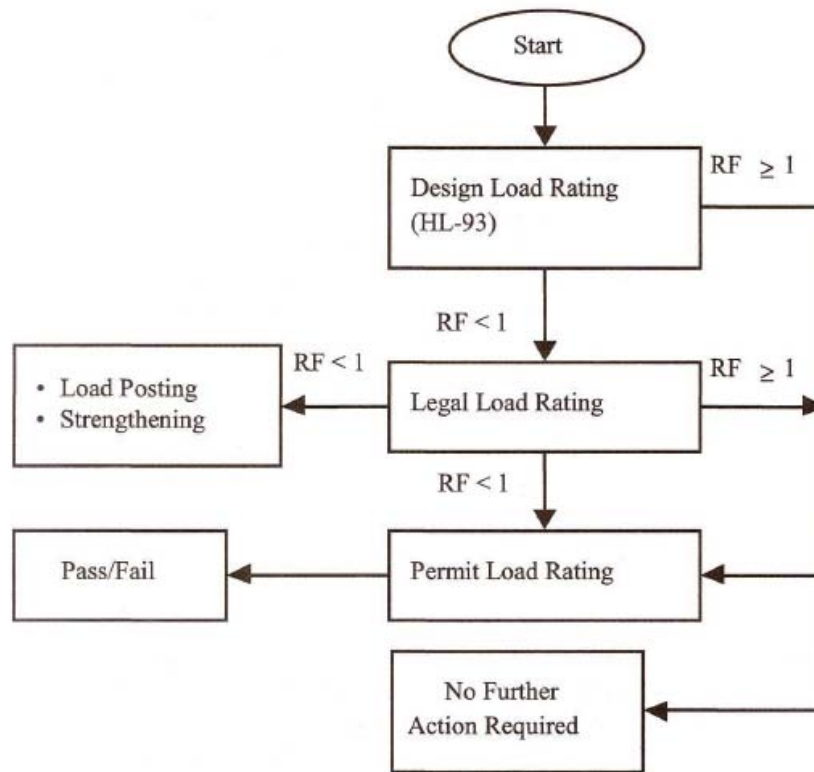


Figure 10-3. LRFR decision making flow chart (AASHTO LRFR 2003)

Design load rating serves as the first-level of load capacity assessment of existing bridges with respect to the design loads given in the AASHTO LRFD bridge design specifications. Permit load rating is required for the review of permit applications for a passage of vehicles with special axle configurations and/or weight limits. Legal load rating provides a safe load capacity for a given AASHTO or state specific truck configuration.

In this project, design load rating is performed using the AASHTO LRFD (2004) live load configuration (i.e., HL-93). Legal load configurations given in the AASHTO LRFR (2003) and the Michigan Bridge Analysis Guide (MDOT 2003) are considered for legal load rating. This analysis considers truck # 21 of the Michigan Bridge Analysis Guide, which shows that a moment of 769 k-ft with a weight of 151.4 kips and a moment/weight ratio of 5.08 governs the legal load rating for the bridge configuration. In both flexure and shear critical configurations,

truck positions generating maximum internal stress resultants (bending moment and shear) are established (Figure 10-4 through Figure 10-8). Analysis is performed by incrementally and uniformly increasing the HL-93 load while monitoring stresses within the fracture critical zone. The analysis is terminated when the tensile stress within the fracture critical zone reached the tensile stress limit.

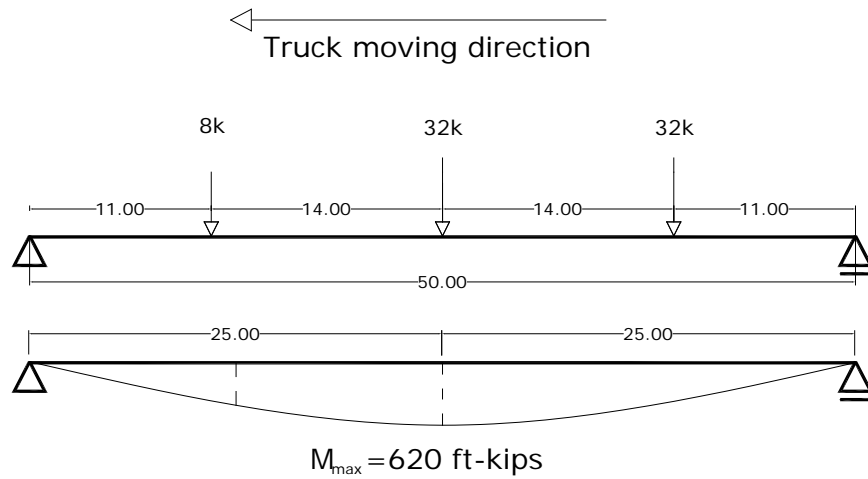


Figure 10-4. Axle load configuration of HL-93 generating maximum moment at mid-span (Note: Lane load that generates additional 200 ft-kips moment at mid-span is not shown)

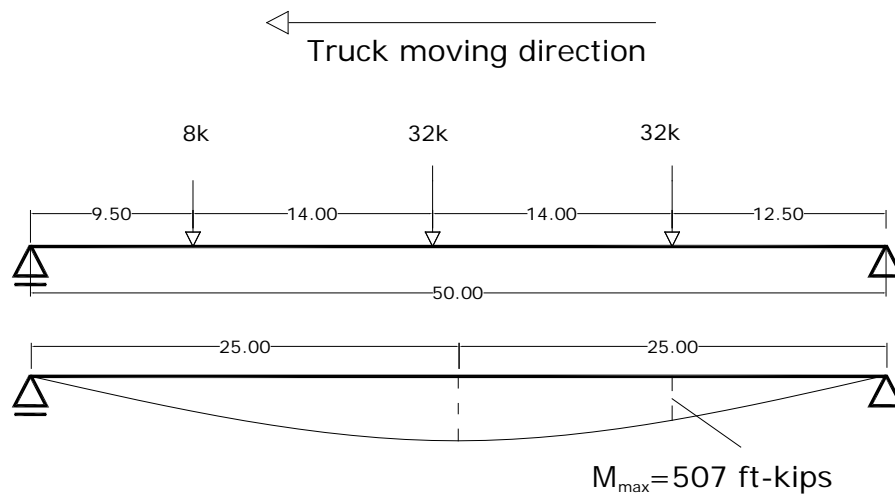


Figure 10-5. Axle load configuration of HL-93 generating maximum moment at quarter point (Note: Lane load that generates additional 150 ft-kips moment at quarter point is not shown)

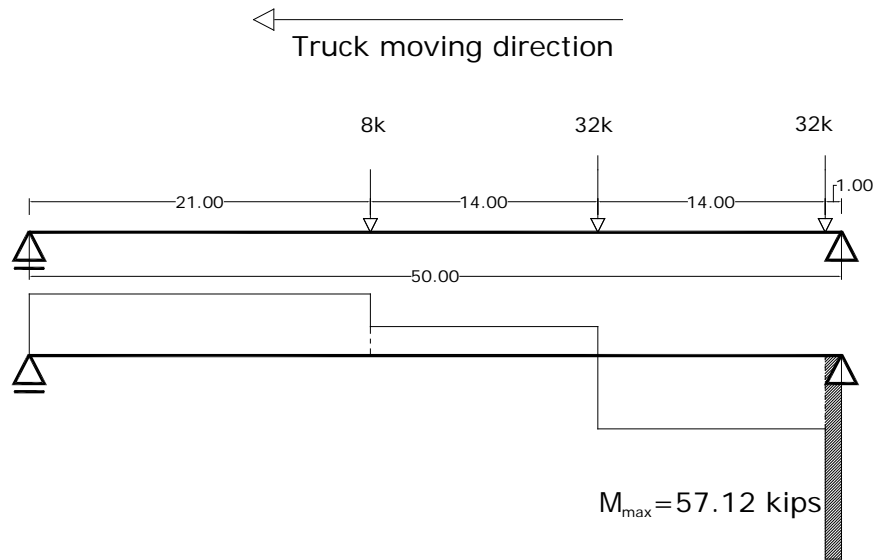


Figure 10-6. Axle load configuration of HL-93 generating maximum shear 1 ft away from the support (Note: Lane load that generates additional 15.36 kips shear 1 ft away from the support is not shown)

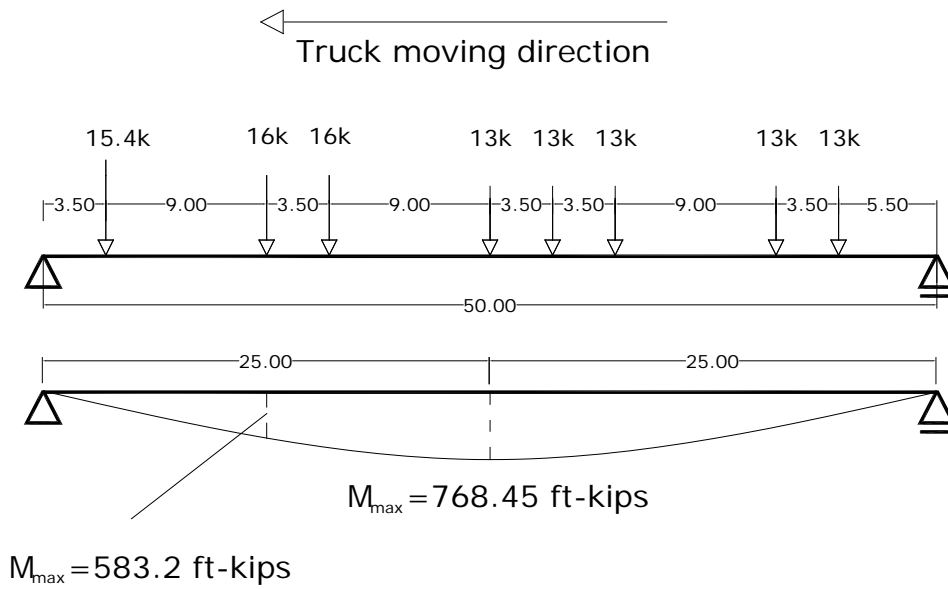


Figure 10-7. Axle load configuration of Truck 21 generating maximum moment at mid-span and quarter point

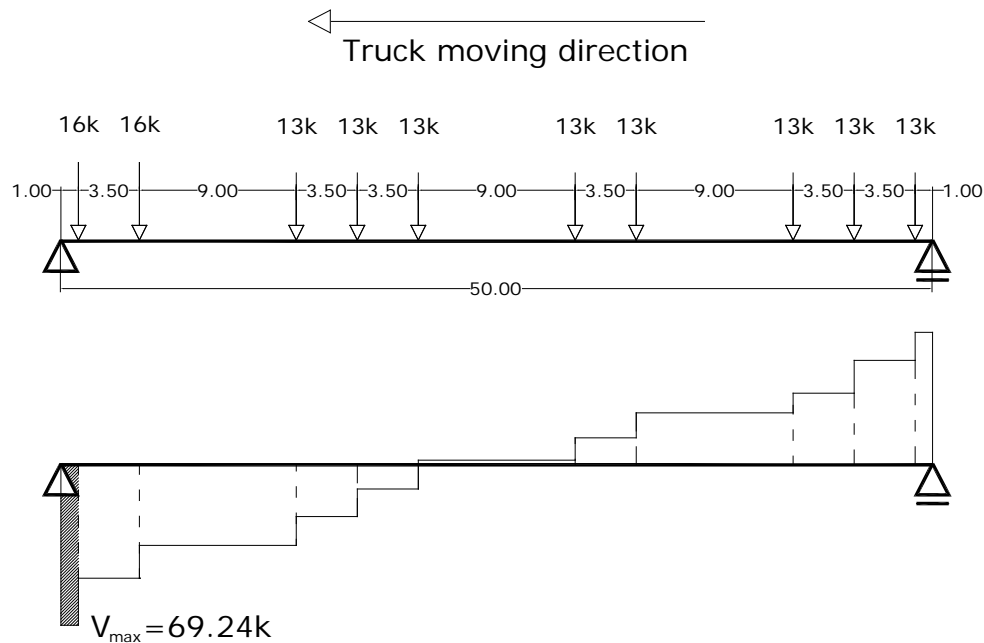


Figure 10-8. Axle load configuration of Truck 21 generating maximum shear 1 ft away from the support

The nonlinear nature of this bridge structural system also requires stages analysis. The first three steps of simulation included positioning box-beams, mortar grouting shear keys, and applying transverse posttension. Next, deck elements and barrier loads are activated resulting in the beam stresses due to the dead load of the structure. Finally, 150 percent of the live load is applied within six increments. This allows calculation of the beam stress levels at 25, 50, 75, 100, 125 and 150 percent of the live load. Design and evaluation is governed by Service III limit state. Hence, the maximum load applied on the bridge is determined when the beam stress reaches the threshold tensile stress limit of $0.19\sqrt{f'_c}$ (ksi). The moment acting on the beam is calculated using element stresses when maximum tensile stress limit is reached; hence the service moment capacity. It should be noted that live load demand is obtained when 100 percent of the live load is acting on the bridge, yet the bridge still may not have reached its ultimate capacity. The behavior is linearly elastic until the first crack occurs, and thus superposition is valid within the live load increments. This means, with the bridge response being D at the end of the dead load

step and (D+L) at the increment when 100 percent of the live load is acting, live load demand can be found by subtracting dead load demand from the total demand (i.e., D+L-D = L).

Beam capacities are defined independently for the flexure critical and shear critical beams. In flexural critical beams, live load capacity is defined as the percentage of truck load that generates a maximum tensile stress equal to the allowable tensile stress limit of $0.19\sqrt{f_c'}$, for moderate corrosion conditions, at or near the bottom fibers (AASHTO LRFD Section 5.9.4.2). In shear critical beams, the fracture critical zone is defined between 12 to 21 inches from the support. Within this zone, principal stresses are calculated. The beam live load capacity is defined as the percentage of truckload generating a maximum tensile principal stress of $0.19\sqrt{f_c'}$ on the web and within the fracture critical zone.

10.2 FLEXURE CRITICAL DISTRESS AND ASSOCIATED BOX BEAM CAPACITIES

The stress and deformation calculations under dead and live loads are performed assuming elastic behavior of both materials (prestressing steel and concrete). Distress types discussed in Table 10-1 and Table 10-2 are incorporated into a fascia beam of a full bridge model (Figure 10-9). Live loads applied to the FE models are scaled to a proportion of the live load that would generate the allowable tensile stress of 424 psi ($0.19\sqrt{f_c'}$ ksi for 5 ksi concrete).

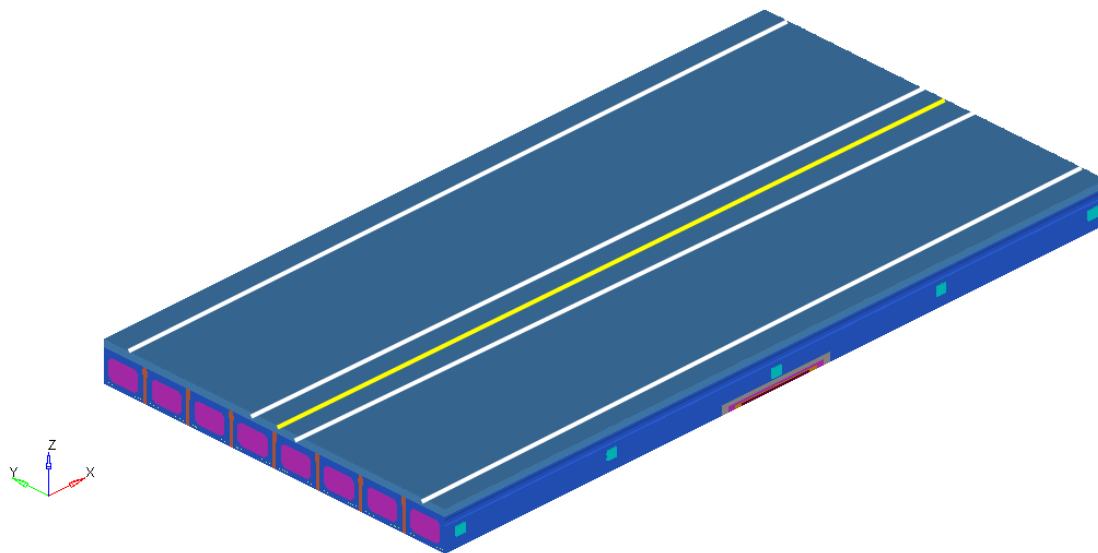


Figure 10-9. 3D view of the model showing distress on fascia beam and design lanes

Table 10-3 shows the service moment capacities calculated from the sectional stress distribution obtained from the FE analysis. The moment capacities are calculated at critical cross-sections by taking moments about the strand axis utilizing the longitudinal element stresses. Critical cross-sections are 13 inches away from the mid-span and the quarter points to avoid interfering with the solid diaphragms. In calculating moment capacities, contribution of concrete tensile stresses is neglected. It should be noted that when the tensile stresses below the neutral axis are neglected, assuming a cracked section, the resulting moment capacities calculated from sectional analysis will be lower than equivalent static moment values..

Table 10-3. Service Moment Capacities for Box-beams at Various Distress Levels (ft-kips)

Level	Beam condition	Service moment capacities of beam with distress at specified locations			
		Live load			
		HL-93		Truck 21	
		Distress location		Distress location	
		Mid-span	Quarter point	Mid-span	Quarter point
1	Undamaged	609	610	610	610
2	Spall	594	611	596	610
3	Spall + 1 broken tendon	559	615	560	615
4	Spall + 2 broken tendons	522	616	524	615

According to Table 10-3, when the distress is at the mid-span, the moment capacity of the section decreases with increasing level of distress. When the distresses are at the quarter point, greater live loads are required to reach the threshold tensile stress level of 424 psi at the beam bottom flange, thus the beam capacity remains practically unchanged (610 – 616 ft-kips). According to the analysis results, the quarter point distress does not control beam capacity. When simulating distress levels 3 and 4, FE models allowed redevelopment of strands beyond the distress regions. However, there are no studies on strand redevelopment, and it is advised to remove strands when evaluating beam capacity with broken strands.

It should also be noted that, in calculating the service moment capacity from the FE analysis results, prestressing strand stress (f_{pe}), after all losses, is taken as 163.4 ksi. In the AASHTO LRFR strength limit state, the average stress in prestressing steel at the time for which the

nominal resistance of the member required (f_{ps}) should be used. For the cross-section, this value is calculated analytically as 262 ksi with the following formulas:

$$f_{ps} = f_{pu} \left(1 - k \frac{c}{d_p}\right) \quad (10-1)$$

$$c = \frac{A_{ps} f_{pu}}{0.85 f_c' \beta_1 b + k A_{ps} \frac{f_{pu}}{d_p}} \quad (10-2)$$

Where:

A_{ps} = area of prestressing steel (1.53 in²)

b = width of beam (36 in.)

c = distance from the extreme compression fiber to neutral axis (for rectangular section behavior)

d_p = distance from the extreme compression fiber to the centroid of prestressing tendons (31 in.)

f_c' = specified concrete compressive strength at 28 days (5 ksi)

f_{pe} = average stress in prestressing steel after all losses (163.4 ksi)

f_{ps} = average stress in prestressing steel at the time for which the nominal resistance of member is required

f_{pu} = specified tensile strength of prestressing steel (270 ksi)

k = factor used in calculation of average stress in prestressing steel for Strength Limit State (0.28 for low-relaxation strands)

β_1 = factor for concrete strength (0.8)

Then, the nominal flexural capacity of the section is calculated analytically as 992 ft-kips with;

$$M_n = A_{ps} f_{ps} \left(d_p - \frac{\beta_1 c}{2}\right) \quad (10-3)$$

The nominal moment capacities of box beams with various distress levels are shown in Table 10-4. Although the section is selected 13 inches away from the mid-span of the FE model,

nominal moment capacity of the undamaged beam, calculated using FE analysis results, is 98 percent accurate when compared with the analytical results (i.e. $976/992 \times 100 = 98.3\%$).

Table 10-4. Nominal Moment Capacities of Box-beams with Various Distress Levels (ft-kips)

Level	Beam condition	Nominal moment capacities of beam with distress at specified locations			
		Live load			
		HL-93 loading		Truck 21	
		Distress location		Distress location	
		Mid-span	Quarter point	Mid-span	Quarter point
1	Undamaged	976	979	979	979
2	Spall	953	979	956	979
3	Spall + 1 broken tendon	896	986	898	986
4	Spall + 2 broken tendons	838	987	840	987

When distress is defined at mid-span, the nominal moment capacity of the beam decreases gradually as the level of damage increases. When distresses occur at the quarter point, moment capacity of the beam is independent of the damage level and remains constant. Moment capacity with quarter point distresses is governed by the mid-span stresses.

Demands under dead load and 100 percent of live load are given in Table 10-5 and Table 10-6 for mid-span and quarter point distresses, respectively. Demand under dead and live load varies within each distress level due to change in the stiffness of the fascia beam. There is a slight difference in the HL-93 and Truck 21 demands, since Truck 21 causes slightly greater moments within the critical section investigated. Maximum demands occur at regions close to mid-span, irrespective of damage level at quarter point.

Table 10-5. Moment Demands for Distress Levels One through Four at Mid-span

Level	Beam condition	Moment demand at critical section (ft-kips)			
		DL	LL (HL-93)	DL	LL MDOT Truck 21)
1	Undamaged	320	238	320	243
2	Spall	324	228	324	232
3	Spall + 1 broken tendon	312	229	312	233
4	Spall + 2 broken tendons	300	225	300	228

Table 10-6. Moment Demands for Distress Levels One through Four at Quarter Point

Level	Beam condition	Moment demand at critical section (ft-kips)			
		DL	LL (HL-93)	DL	LL (MDOT Truck 21)
1	Undamaged	320	238	320	243
2	Spall	319	239	319	243
3	Spall + 1 broken tendon	320	239	320	243
4	Spall + 2 broken tendons	320	239	320	243

The flexural load rating factor for each level of distress is calculated according to the rating formulas given in the AASHTO LRFR (2003) and the MDOT Bridge Analysis Guide (2003). Following AASHTO LRFR procedures, Strength I and Service III Limit States are considered for design and legal load rating calculations. Design and legal load ratings of the box-beam are calculated using the following equation:

$$RF = \frac{C - (\gamma_{DC})DC - (\gamma_{DW})DW \pm (\gamma_P)P}{(\gamma_L)(LL + IM)} \quad (10-4)$$

For the strength limit states

$$C = \phi_c \phi_s \phi R_n \quad (10-5)$$

Where the lower limit shall apply:

$$\phi_c \phi_s \geq 0.85 \quad (10-6)$$

For the Service Limit States:

$$C = f_R \quad (10-7)$$

Where:

RF = Rating factor

C = Capacity

f_R = Allowable stress in the LRFD code

R_n = Nominal member resistance (as inspected)

DC = Dead-load effect due to structural components and attachments

- DW = Dead-load effect due to wearing surface and utilities
- P = Permanent loads other than dead loads
- LL = Live load effect
- IM = Dynamic load allowance (0.33)
- γ_{DC} = LRFD load factor for structural components and attachments (1.25 for Strength I, 1.0 for Service III Limit States)
- γ_{DW} = LRFD load factor for wearing surface and utilities
- γ_p = LRFD load factor for permanent loads other than dead loads = 1.0
- γ_L = Evaluation live-load factor
 1.75 for design inventory,
 1.35 for design operating,
 1.80 for legal live loads of unknown ADTT,
 0.80 for design loads of Service III
 1.00 for legal loads of Service III
- ϕ_c = Condition factor (1.0)
- ϕ_s = System factor (1.0)
- ϕ = LRFD resistance factor (1.0)

Michigan operating load ratings based on the load factor method are calculated according to the following formula (Michigan Bridge Analysis Guide 2003):

$$RF = (C - A_1 D) / [A_2 L (1 + I)] \quad (10-8)$$

Where:

RF = the rating factor for the live-load carrying capacity

C = the capacity of the member, M_n

D = the dead load effect on the member, M_{DL}

L = the live load effect on the member, M_{LL}

I = impact factor

A_1 = factor for dead load

A_2 = factor for live load

Rating factors are given in Table 10-7 and Table 10-8 for distresses at mid-span and quarter point locations, respectively. Although AASHTO LRFR does not require checking legal load rating if the load factor for inventory design load rating is greater than 1.0, legal load ratings are also calculated for comparison purposes. Rating factors decrease as expected with the increased level of damage at mid-span. The Service III legal load rating gives an indication of how much reserve capacity is left for Truck 21 since it uses factor 1.0 for both dead and live loads. For the undamaged case, while the system can carry an additional 20 percent of Truck # 21 at level 4 its capacity to satisfactorily carry the truck decreases by about 2 percent. Spall alone (Level 2) is not a major cause of capacity degradation. Beam capacity reduction is significant if broken tendons are present (Level 3 and 4). Distress at quarter points is not of major concern since the system behavior is still governed by the stresses within the mid-span region. Rating factors remain an almost constant; independent of any damage observed at quarter points (Table 10-8).

Table 10-7. Rating Factors for Distress Levels One through Four at Mid-span

Level	Beam condition	Design Load Rating* (HL-93)		Legal Load Rating (Truck 21)		MDOT Operating Rating (Truck 21)
		Strength I	Service III	Strength I	Service III	
1	Undamaged	1.38	1.51	1.32	1.20	1.79
2	Spall	1.37	1.48	1.32	1.17	1.78
3	Spall + 1 broken tendon	1.26	1.35	1.21	1.07	1.63
4	Spall + 2 broken tendons	1.18	1.24	1.13	0.98	1.52

* For operating, multiply the Strength I Limit State rating with 1.75/1.35

Table 10-8. Rating Factors for Distress Levels One through Four at Quarter Points

Level	Beam condition	Design Load Rating* (HL-93)		Legal Load Rating (Truck 21)		MDOT Operating Rating (Truck 21)
		Strength I	Service III	Strength I	Service III	
1	Undamaged	1.39	1.53	1.32	1.20	1.79
2	Spall	1.39	1.53	1.32	1.20	1.78
3	Spall + 1 broken tendon	1.40	1.54	1.34	1.21	1.80
4	Spall + 2 broken tendons	1.41	1.55	1.34	1.21	1.81

* For operating, multiply the Strength I Limit State rating with 1.75/1.35

10.3 SHEAR CRITICAL DISTRESS AND BOX BEAM CAPACITIES

In the analysis, the PC box-beam is assumed to reach shear capacity upon the crack formation within the shear critical region of the beams. The diagonal tension crack initiates when principal tensile stress reaches the critical tensile stress of 424 psi within the shear critical region.

Under the investigated set of moving loads and span length, critical principal stresses occur near mid-span irrespective of the distress levels at beam ends. The beams are expected to fail under flexure rather than shear. Thus, rating factors (Table 10-7 and Table 10-8) calculated using limiting stresses at the beam mid-span should be considered when evaluating a bridge with flexure-critical span length.

10.4 INFLUENCE OF GROUT LOSS AND BROKEN POSTTENSION STRANDS

Other damage parameters of interest include evaluation of the effect of shear key grout loss and broken transverse posttension strands on the box-beam capacity. Analysis of moment and shear critical distress scenarios demonstrated that flexure governs beam capacity for the selected span. Hence, the effect of shear key grout and/or posttension loss only at the mid-span will be analyzed. Inspection of bridges built in the 1950s with partial depth shear keys showed that the shear key itself was primarily intact (Figure 10-10). Current Michigan box-beam bridges utilize full-depth shear keys. Inspection of a box-beam bridge with full-depth shear key shows grout spall (Figure 10-11). Hence, the impact of grout loss on structural capacity is evaluated. Only grout loss below the first seven inches from the top of the beam is considered in the analysis. In order to define shear key grout loss, the elasticity modulus of the grout is reduced gradually following a similar approach that was applied for distress definition in box beams (Figure 10-12). Grout loss is defined on shear key elements between the investigated fascia and the first interior beam at mid-span (Figure 10-13).

Broken posttension strands at one location are incorporated by removing the horizontal force at the mid-span diaphragm location. A final evaluation included the investigation of broken posttension strands and grout loss simultaneously. The purpose of the analysis is to develop an understanding of the influence of the loss of grout and/or posttension on beam capacity; hence undamaged beam configuration is used in the investigations.



Figure 10-10. a) A portion of shear key grout remain intact with the beam and (b) beam surface after shear key grout cleanly fall off



Figure 10-11. Shear key grout loss

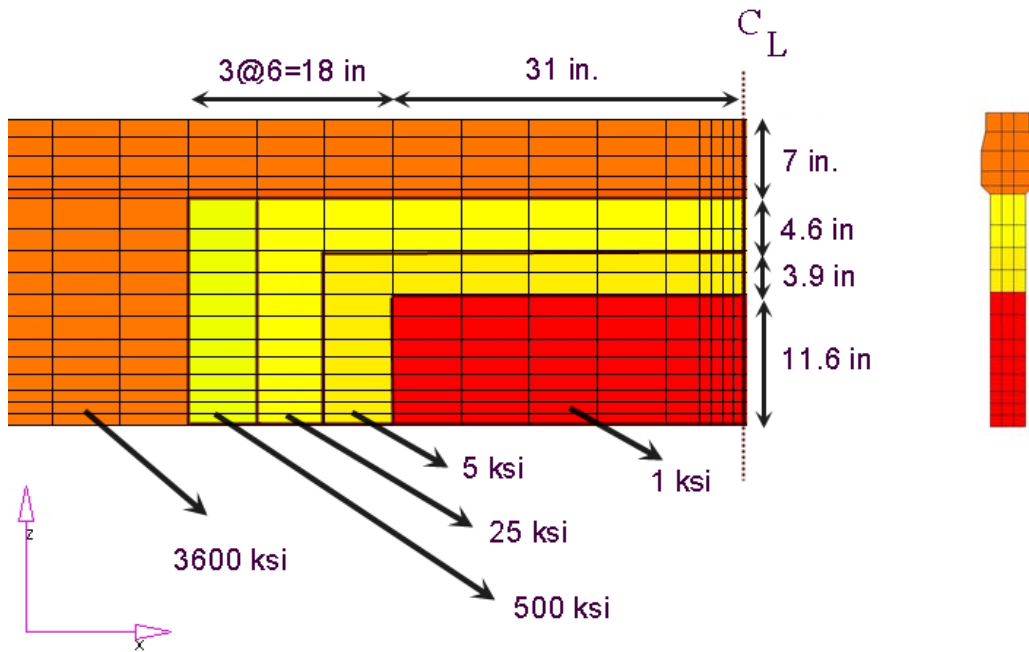


Figure 10-12. Shear key grout loss definition

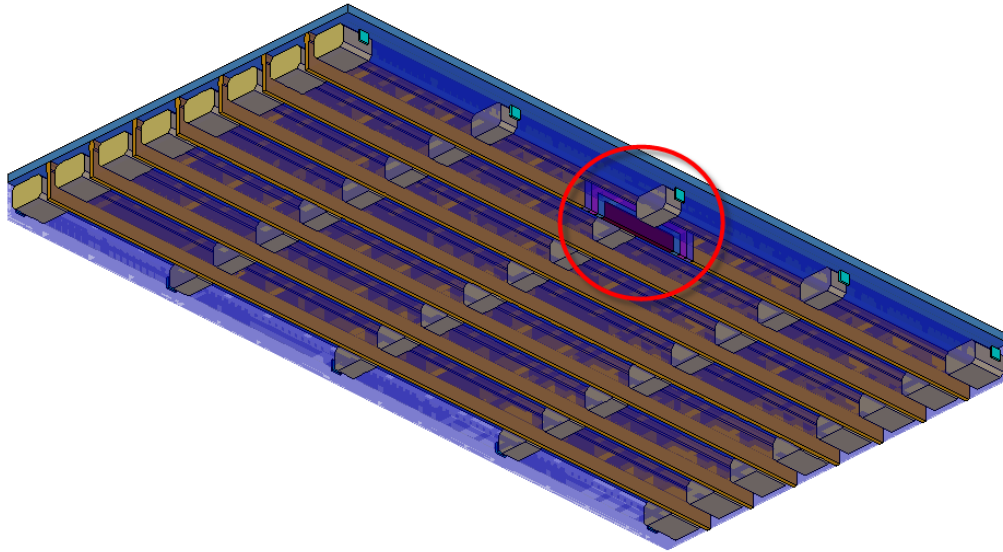


Figure 10-13. Distress at shear key between a fascia and the first interior beam at mid-span

Analysis results of the investigated cases are summarized in Table 10-9: moment due to dead load and 100 percent live load (HL-93), nominal moment capacity, and inventory design load rating. Results of the undamaged beam with no grout or posttension loss are also included for comparison purposes.

Table 10-9. Moments due to Dead and Live Loads, Nominal Moment Capacities, and Rating Factors for Distress at Mid-span

Damage parameter investigated	Moment demand at critical section under dead and live loads (ft-kips)		Nominal Moment Capacity (ft-kips)	Inventory Design Load Rating* (HL-93)	
	DL	LL (HL-93)		Strength I	Service III
Undamaged structure	320	238	976	1.38	1.51
Grout loss	330	233	975	1.38	1.49
Broken PT strand	298	238	928	1.33	1.47
Grout loss + broken PT	304	234	928	1.34	1.46

* For operating, multiply the Strength I Limit State rating with 1.75/1.35

The nominal moment capacity of the fascia beam is independent of the damage to the grout layer. With relatively less stiff connection between the fascia and the first interior beam, the dead load demand increases by around 3 percent due to partial distribution of barrier weight. Due to restrictions in the AASHTO LRFD for positioning live loads close to the barriers and considering tire contact area, a major portion of the wheel loads is placed on the first interior

beam. With the reduction in shear key stiffness due to grout loss, there is a 2 percent reduction in live load demand on the fascia beam.

In the case of broken posttension strands, the nominal moment capacity of the beam decreases by about 5 percent (i.e., from 976 ft-kips to 928 ft-kips). When posttension is applied, transverse compressive stresses develop in the beams. Due to Poisson's effect, longitudinal compressive stresses develop in the beam compensating some of the tensile stresses developed under applied loads (Figure 10-13 and Figure 10-14). Therefore, transverse posttension helps increase the nominal moment capacity of the beam. When transverse posttension is broken, structural system stiffness does not change because perfect bond between beams and shear keys is assumed in the analysis. There is no change in load distribution, but loss of posttension altered the beam stress distributions and resulted in lower dead load moments. Live load (HL-93) demand remains the same for both undamaged and broken posttension strand cases. This is because posttension acting on the mid-span diaphragm location first increases the beam capacity; then the beam capacity returns to original because of posttension loss. Normal stress distribution along the beam height, under 100 percent HL-93 load, remains the same for both undamaged and broken posttension strand cases (Figure 10-15).

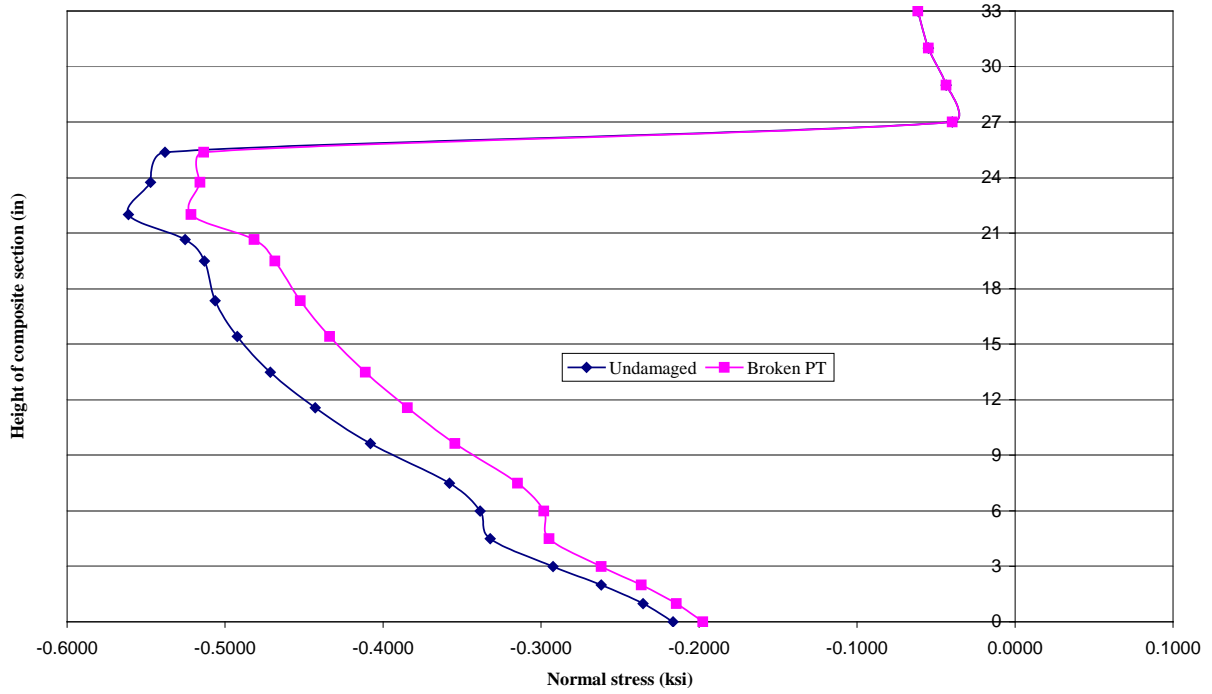


Figure 10-14. Normal stress distribution through the depth of deck-beam composite cross-section under dead load + prestress (tensile +; compression -)

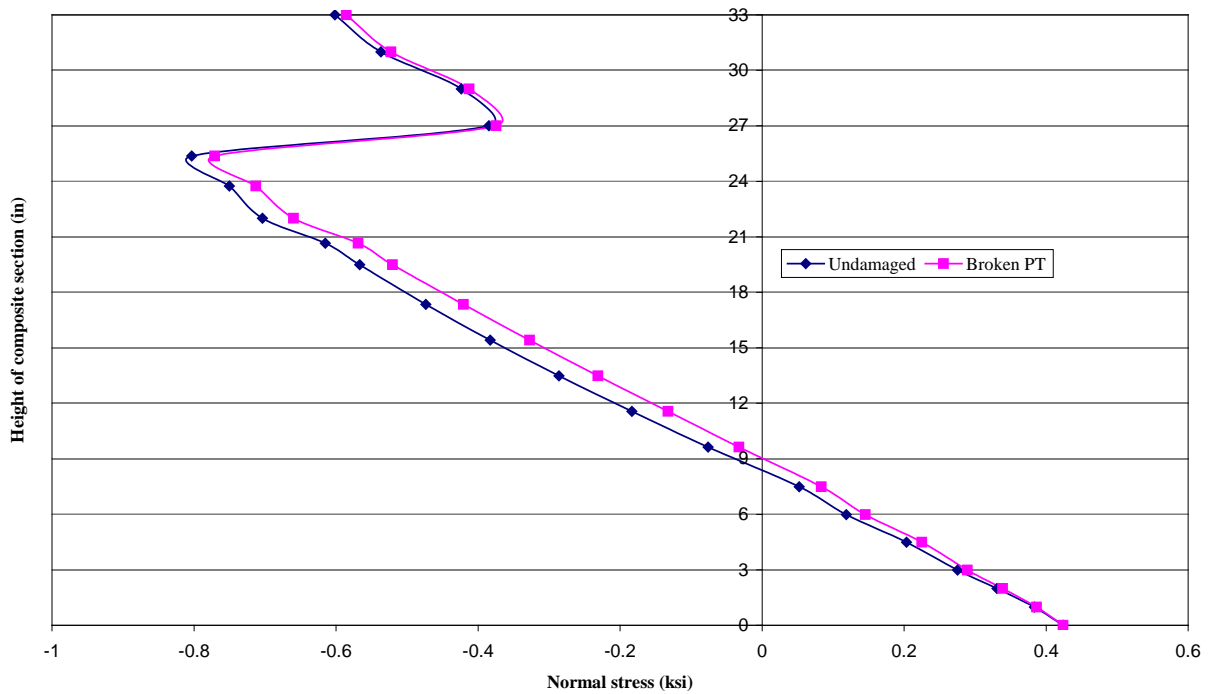


Figure 10-15. Normal stress distribution through the depth of deck-beam composite cross-section under service loads that develop 424 psi extreme fiber tensile stress (Tensile +, Compressive -)

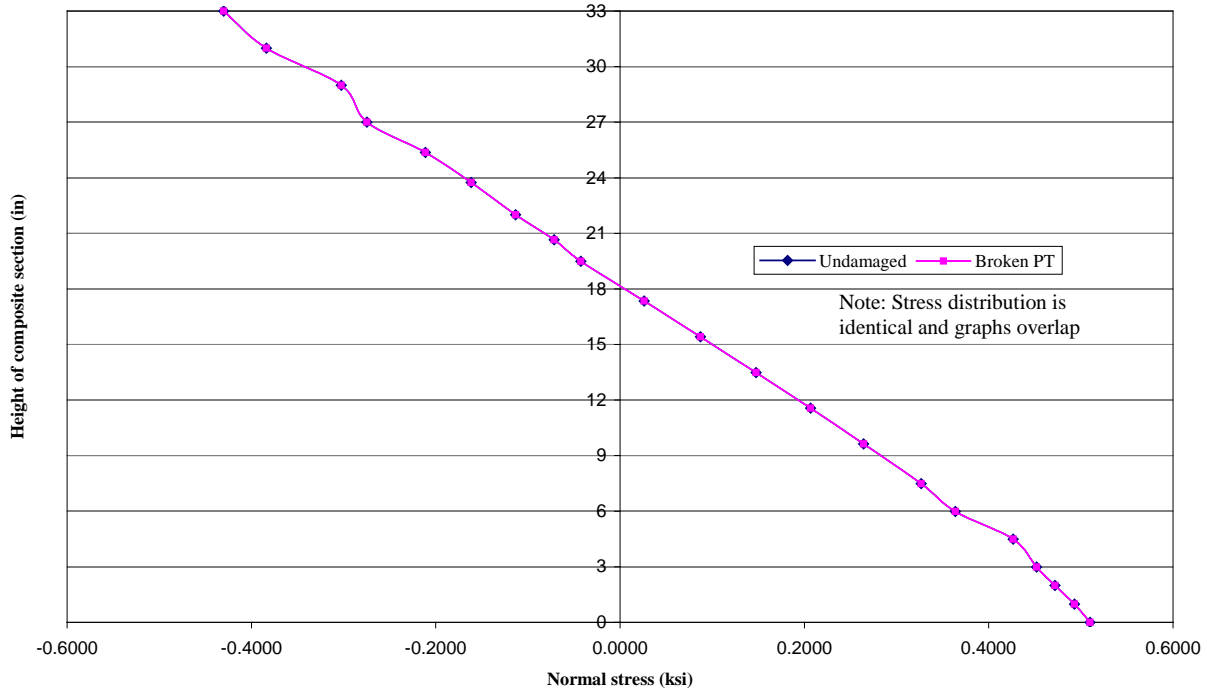


Figure 10-16. Normal stress distribution through the depth of deck-beam composite cross-section only under 100 percent live load (Tensile +, Compressive -)

When all the damage scenarios are considered, most critical is the loss of grout, provided that the bond between shear keys and the beams remain intact once the posttension is lost.

10.5 SUMMARY AND CONSLUSIONS

FE analyses are carried out investigating the effects of various distresses that may occur within the beam or some other components such as the shear key and posttension strands. FE modeling and analysis is performed for an eight-beam, two-lane, 50-ft long bridge under dead loads and live loads, as recommended in the AASHTO LRFD (2004) and the Michigan Bridge Analysis Guide (MDOT 2003). The live load is applied in increments until the tensile stress limit of $0.19\sqrt{f'_c}$ (424 psi) is reached. Flexural capacity is calculated from sectional analysis utilizing the uniaxial stress data obtained from FE analysis. Nominal moment capacity and load demands for distress levels one through four at mid-span are given in Table 10-10.

Table 10-10. Nominal Moment Capacity and Load Demands Based on FE Results (Distress at Mid-span)

Distress Level	Beam condition	Moment Capacity (ft-kips)	Dead Load Demand (ft-kips)	Live Load Demand (ft-kips)	
				HL-93	Truck 21
1	Undamaged	976	320	238	243
2	Spall	953	324	228	232
3	Spall + 1 broken tendon	896	312	229	233
4	Spall + 2 broken tendons	838	300	225	228

Flexural capacities of box beams with distresses at mid-span as well as the dead and live load demands are also calculated at the critical cross-section, in accordance with the AASHTO LRFD (2004) (Table 10-11). Beam distress is defined by reducing the distress width considering the modular ratio between sound concrete and distressed region. The number of prestressing tendons is modified to model the broken tendon cases. Dead load demand is calculated for two separate cases: where barrier load is equally distributed over eight beams, or is solely acting on fascias (i.e., no load transfer). These dead load distributions defined the upper and lower bounds of the dead load demands.

Table 10-11. Nominal Moment Capacity and Load Demands Based on the AASHTO LRFD (2004) (Distress at Mid-span)

Distress Level	Beam condition	Moment Capacity (ft-kips)	Dead Load Demand (ft-kips)		Live Load Demand (ft-kips)	
			Barrier Load Distributed (Lower Bound)	Barrier Load Not Distributed (Upper bound)	HL-93	Truck 21
1	Undamaged	992	282	394	266	269
2	Spall	975	282	394	266	269
3	Spall + 1 broken tendon	886	282	394	266	269
4	Spall + 2 broken tendons	793	282	394	266	269

Capacities obtained from the FE models and the AASHTO LRFD closely correlate with a minimum accuracy of 95% for distress level 4 (i.e. $793/838 \times 100 = 94.6\%$). For distress levels 3 and 4, where broken tendons are present, capacities obtained from FE results exceed those obtained from LRFD due to stress redistribution of broken tendons. However, with LRFD, only sectional analysis can be performed, and it is assumed that tendons are lost through the beam

length. Dead load demands obtained from FE fall within the upper and lower bounds established based on load distribution. Live load demands obtained by LRFD are 11% percent higher than those calculated by FE results. Analytical calculations are based on the distribution factors recommended by the AASHTO LRFD (2004), whereas FE analysis is more refined and accounts for the structural system behavior of Michigan design.

Rating factors given in Table 10-7 for distresses at mid-span are presented again in Table 10-12 for comparison purposes. Load ratings performed with analytical results of lower and upper bound dead load demands are given in Table 10-13 and Table 10-14, respectively.

Table 10-12. Rating Factors for Distress Levels One through Four at Mid-span Obtained from FE Results

Distress Level	Beam condition	Design Load Rating (HL-93)		Legal Load Rating (Truck 21)		MDOT Operating Rating (Truck 21)
		Strength I	Service III	Strength I	Service III	
1	Undamaged	1.38	1.51	1.32	1.20	1.78
2	Spall	1.37	1.48	1.32	1.17	1.78
3	Spall + 1 broken tendon	1.26	1.35	1.21	1.07	1.63
4	Spall + 2 broken tendons	1.18	1.24	1.13	0.98	1.52

Table 10-13. Rating Factors for Distress Levels One through Four at Mid-span Obtained Analytically Using AASHTO LRFR Specifications for Lower Bound Dead Load Demand

Distress Level	Beam condition	Design Load Rating (HL-93)		Legal Load Rating (Truck 21)		MDOT Operating Rating (Truck 21)
		Strength I	Service III	Strength I	Service III	
1	Undamaged	1.37	1.58	1.32	1.25	1.79
2	Spall	1.34	1.53	1.28	1.21	1.74
3	Spall + 1 broken tendon	1.15	1.27	1.10	1.01	1.48
4	Spall + 2 broken tendons	0.95	1.00	0.91	0.79	1.22

Table 10-14. Rating Factors for Distress Levels One through Four at Mid-span Obtained Analytically Using AASHTO LRFR Specifications for Upper Bound Dead Load Demand

Distress Level	Beam condition	Design Load Rating (HL-93)		Legal Load Rating (Truck 21)		MDOT Operating Rating (Truck 21)
		Strength I	Service III	Strength I	Service III	
1	Undamaged	1.07	1.06	1.03	0.83	1.37
2	Spall	1.04	1.01	1.00	0.80	1.32
3	Spall + 1 broken tendon	0.84	0.74	0.81	0.59	1.07
4	Spall + 2 broken tendons	0.65	0.47	0.62	0.37	0.80

For cases where it is assumed that the barrier load is distributed uniformly to the eight beams, load ratings obtained from FE results and analytical calculations are very close to each other for distress levels one and two (Table 10-12 and Table 10-13). The discrepancy between the two ratings is higher when broken tendons are involved (Level 3 and 4). This is again due to stress redistribution of prestressing tendons in FE analysis and constant demand under dead and live load in analytical calculations regardless of distress observed. When barrier load is acting solely on the fascia beam, critical ratings are observed. For legal load rating, a rating factor less than one is observed even for the undamaged scenario (Table 10-14) since dead load demand is increased by around 40 percent (i.e. 282 ft-kips to 394 ft-kips) while the live load factor is increased to 1.0 from 0.80

According to the results:

1. Nominal moment capacity and hence the load rating of the beam decreases gradually as the level of distress increases at mid-span. Beam capacity reduction is significant when broken strands are present (Level 3 and 4).
2. When distresses occur at quarter points, the moment capacity of the beam is governed by the stresses that occur close to mid-span (i.e., beam capacity is independent of the quarter point damage level considered in this analysis). Rating factors remain almost constant with the quarter point damage scenarios considered in this analysis. Two broken strands with some spall constitute the most critical damage considered in the analysis (Table 10-8).

3. For the investigated set of moving loads and span length, critical principal stresses occur near mid-span irrespective of the beam end distress levels considered in this study. The rating factors calculated for the example bridge are independent of the beam end distresses (Table 10-7 and Table 10-8).
4. Loss of grout influences the load demands on the fascia beam; thus load distribution. The fascia beam has to carry greater dead load due to barrier weight and less live load since majority of the axle loads are acting on the interior beams.
5. Posttension does not influence load distribution if shear keys are intact. However, it helps increase beam capacity by countering the tensile stresses.
6. Lateral posttension is required to increase the system redundancy and is important when the bond between beams and the shear key is not capable of transferring tensile stresses.

11 SUMMARY AND CONCLUSIONS

This project consisted of six tasks. The first task was the review and synthesis of literature. Capacity evaluation and load testing of distressed bridges or beams, properties of shear key and repair materials, durability of shear key and repair materials, properties of cementitious materials that have a potential to be used for shear keys, and design parameters for the transverse design of box-beam bridge superstructures are the topics covered under literature review. The literature review was jointly conducted by Western Michigan University (WMU) and Michigan Technological University (MTU). The WMU research team synthesized the information related to capacity evaluation and load testing of distressed bridges or beams, mechanical properties of shear key grout and repair materials, properties of cementitious materials that have a potential use as shear key grout, and design parameters for the transverse design of box-beam bridge superstructures.

Literature revealed that for uncracked beams fatigue is not a concern. Fatigue may become a concern for bridges subjected to frequent loading generating tensile fiber stress in excess of $6(f_c')^{1/2}$ psi or strand stress greater than $0.06f_{pu}$. Transverse connection of precast elements in a box-beam bridge governs the load transfer between beams. Transverse connection is established by the contribution and interaction of grouted full-depth shear keys, transverse posttension and a cast-in-place concrete deck. The effectiveness of transverse connection is a function of the shear key grout and posttension spacing. In this case, when the elasticity modulus of the shear key grout is lower than the parent material, the transfer connection efficiency of the shear key at a posttension location increases with decreasing thickness. Specifically, mechanical properties of grout material at the time of posttension govern the stress distribution along the joint; hence the load transfer and the tightness of the joint to prevent moisture ingress. Shear key grout mixes can be specified for required strength and modulus at the time of transverse posttension application.

The second task was to evaluate the load capacity of a salvaged box-beam. WMU was solely responsible for performing the task and deliverables. A 50-year old box-beam was salvaged from the bridge (S11-38101) that carries Hawkins road over I-94 during a beam replacement activity. The visible beam distress, specifically wide longitudinal cracking at the beam soffit, was the reason for replacement. The beam was carefully removed and load testing was

performed. Analysis of load test data indicated that with all the visible distress, the beam capacity still exceeded the required design capacity. However, the beam was designed for a lower load (i.e., H-15) than the currently required load. A related finding that will be helpful in load capacity assessment was the use of camber measurement for calculating remaining prestress. Prestress estimation using camber measurements overestimated the remaining prestress by 40 to 50 percent. The testing of the salvaged beam also demonstrated the need to implement inspection procedures that will help reveal concealed corrosion, characterize material properties, and also quantify the load transfer ability along the shear keys.

The third task was MTU responsibility. This task included conducting a survey of commonly used repair materials and shear key grouts for prestressed box beam bridges, and a laboratory evaluation of selected materials. The intended result of the laboratory evaluation was development of required material characteristics from the perspective of dimensional stability and durability of prestressed box beam bridges. Based on the survey conducted at the start of the project, four repair materials and three shear key grouts were selected for evaluation. Detailed evaluation of fresh and hardened concrete properties was conducted in the laboratory. An extensive durability evaluation was performed to assess sorptivity, shrinkage, and resistance to freezing and thawing cycles of repair materials as well as shear key grouts. It was observed that the selected materials showed variations in performance in comparison with each other.

The laboratory analysis indicated that selection of a particular repair material would depend upon the intended application. All repair materials exhibited lower sorption values in comparison to normal concrete but exhibited a large variation in shrinkage values in comparison with normal concrete. Among the shear key grouts evaluated, it was observed that the masonry cement based grout exhibited the lowest strengths whereas SET 45 exhibited higher strengths as well as lower shrinkage values.

The fourth task was to evaluate mechanical properties of shear key grout and specified repair materials. WMU was responsible for performing the task and deliverables. Mechanical properties of repair and manufactured grout materials (e.g., set gout and set-45) identified for this propose were documented based on manufacturers' technical data sheets. To form the shear-keys, type R-2 grout mix is specified and commonly used in Michigan box-beam bridges.

Specimens were prepared and tests were performed to document the mechanical properties of R-2 grout. The compressive strength of grout was evaluated. In addition, an ultrasonic pulse velocity (UPV) test was performed in compliance with ASTM C597 to determine the dynamic modulus of elasticity and the Poisson's ratio of the Type R-2 grout. In cementitious materials, the dynamic modulus determined in accordance with ASTM C469 is expected to be greater than the static modulus. However, for the grout materials the measured dynamic modulus was lower than the static modulus determined following the ASTM C469 procedure. Additional testing was performed for investigative purposes. The uniaxial stress-strain response showed a hysteretic strain hardening behavior not expected of sound cementitious material. Consequently, the elastic modulus at low strain is lower than at high strain during the load cycle. The static modulus test (ASTM C469) cannot capture this behavior and calculates a nominal modulus value. Other repair materials also showed a similar behavior, and further investigations are recommended.

The fifth task was the simulation of construction process stages. WMU was responsible for performing the task and deliverables. While simulating the construction process stages, box-beam bridge transverse connection design and material parameters were also investigated using sub-assembly models. The parameters investigated in these simulations were: grout mechanical properties, posttension force magnitude and location, number of diaphragms, and the bridge width. The sub-assembly models developed for this purpose were 50 ft. long, 27×36-in. box beams connected with shear keys and posttension at diaphragm locations. Two sub-assembly models were developed, one with three beams and the other with four beams. Simulations showed that load transfer occurs primarily through the stiffer portions of the bridge superstructure (i.e., through the diaphragms). In this respect, the AASHTO LRFD (2004) Section 5.14.1.2.8 recommendations regarding transverse normal interface stress distribution were found to be vague. Compliance with this recommendation, requiring the development of a minimum clamping stress of 250 psi at shear keys along the beam length, could not be achieved with the current beam and posttension provisions. A comprehensive redesign of transverse connection is needed for achieving this level of uniform clamping stress along the shear key. Every stage of the side-by-side box-beam construction process was simulated using advanced pre/post processing capabilities of HyperMesh and FE analysis capabilities of ABAQUS. Stresses

developed in beams, shear keys, and the deck were evaluated and documented. Further, to assure shear key functionality and strength requirements, a rational analysis and design model was developed. Changes to construction procedures were suggested, and these suggested changes were re-evaluated with construction process simulations. The proposed rational design procedure established the posttension requirements based on minimizing the tensile stresses at the shear key under gravity loading. With the proposed design, posttension application is recommended in two stages before and after 6-in. cast-in-place concrete deck placement. With the two-stage posttension scheme, transverse tensile deck stresses that occur under live load were eliminated except at some isolated regions within the proximity of the fascias.

The sixth and final task was to evaluate flexural and shear capacity of distressed beams considering structural system behavior. WMU was responsible for performing the task and deliverables. Effects of three major distress types were evaluated. These were spall, spall with single broken strand, and spall with two broken strands. Distresses were incorporated along the corner of the beam's bottom flange. In addition to beam distresses, impact of the shear key grout loss and/or transverse posttension loss on beam capacity was investigated. Analysis results showed that, for the selected span length of 50 ft., the capacity was reduced only when the distresses were at the midspan. Partial loss of grout alters the dead and live load demands on the fascia beam due to reduced stiffness. It was shown that posttension did not influence the load distribution provided that shear keys were intact. However, posttension contributes to the beam capacity and provides redundancy to the systems especially when a weak bond exists between the grout and beams.

11.1 RECOMMENDATIONS

The following key recommendations are based on the findings from the project tasks of the literature review, load testing of a salvaged box-beam, testing of grout and repair material properties, and the development of subsequent finite element modeling and simulations:

1. Among the fresh properties of utmost importance is workability in case of polymer based repair materials. Repair materials which do not need excessive force for proper placement and consolidation should be selected.

2. Repair materials with shrinkage values comparable to the substrate concrete should be selected. In this study all the repair materials did not necessarily exhibit the required behavior and, hence, it is essential to select a repair material based on its intended use. It is necessary to evaluate the shrinkage behavior of a selected repair material prior to application on site.
3. To protect exposed steel from corrosion, repair materials evaluated in this study can be adopted for use because all of them exhibited high resistance to chloride ion transport as well as low sorption values.
4. When selecting a shear key grout it is essential to determine the early age compressive strength as well as its early age shrinkage properties based on the load applied to it. A more detailed understanding of shear key grout from a material standpoint as well as the total design of the shear key itself is recommended.
5. Adequate load transfer and achieving a watertight connection along the transverse joint cannot be achieved with the currently specified grout with nonlinear hysteretic behavior. Revisions to grout material specifications are recommended.
6. In-service bridge beam load capacity assessment should be based on material characterization, load transfer evaluation along the shear keys, and estimation or assessment of concealed corrosion.
7. The recommended load analysis procedure and the associated design criteria requiring a two-stage posttension process should be implemented for improved durability performance of side-by-side box-beam bridges.

Intentionally left blank

12 SUGGESTIONS FOR FUTURE RESEARCH

The focus of this work has been the investigation of safety of in-service side-by-side box-beam bridges with distressed beams, selection of materials for repair and the repair techniques, and investigation of drawbacks as well as benefits of current design and construction procedures. As with similar projects dealing with complex bridge structures, several questions remain unanswered, and continuation work is needed. The list of tasks that is outlined below should be considered.

- Load testing data of a fifty-year old salvaged beam indicated that, even with a wide long longitudinal crack at the bottom flange, the experimental beam capacity exceeded the design capacity. Visual inspection of the salvaged beam while in place was not adequate to identify/evaluate the strand corrosion, condition of transverse tie rods, and other material related distress within the box-beam cavity. Further, there was no quantifiable evaluation of load transfer between girders. Future projects are suggested for incorporating inspection procedures based on innovative technologies for acquiring quantifiable data for load rating of bridges.
- Shear key grout specifications need to be reevaluated and revised. For example, the required grout compressive strength in 24 hours is 4000 psi according to the AASHTO LRFD (2004) Section 5.14.1.2.8. The AASHTO Standard Specifications (2002) require 5000 psi in 24 hours. Grout materials tested during this project could not satisfy the strength required by the AASHTO LRFD or Standard. Also, AASHTO LRFD (2004) requires a clamping stress level of 250 psi at the shear key upon posttension application. The concern with the grout materials tested is not their strength, but the nonlinear strain hardening behavior. Consequently, grout modulus under levels of posttension stresses is very low. Grout modulus at the time of posttension is important as it governs the load distribution between the beams as well as tightening the joint for water intrusion. A future project is suggested to formulate grout composition, mechanical property variation with time, behavior under various load levels, and appraisal of AASHTO stipulations.
- Construction process numerical simulation results illustrated the benefits of implementing two-stage transverse posttension on side-by-side box-beam bridges. First, an implementation project is recommended utilizing the design and posttension

stipulations developed in this study. Also, development of design charts is proposed for a robust design of unremarkable side-by-side box beam bridges. These should be based on the recommended analysis and posttension design procedures. Hence, three future projects are recommended: an implementation project for developing design charts to be included in the MDOT Bridge Design Guide, the implementation of the proposed design and construction procedures on a new superstructure replacement construction, and the instrumentation and monitoring of the replacement bridge for long-term performance.

13 REFERENCES

- AASHTO. (2002). *Standard Specifications for Highway Bridges*, 17th Edition, American Association of State Highway and Transportation Officials, 444 North Capitol Street, N.W., Suite 249, Washington, D. C.
- AASHTO. (2004). *AASHTO LRFD Bridge Design Specifications*, Third Edition, American Association of State Highway and Transportation Officials, 444 North Capitol Street, N.W., Suite 249, Washington, D. C.
- ABAQUS/Standard User's Manual - Version 6.7. (2008). Hibbitt, Karlson & Sorensen, Inc., Pawtucket, RI. (<http://www.abaqus.com>).
- ACI. (2005). "ACI 548 Polymer Modified Concrete ". American Concrete Institute, Detroit, MI.
- ACI 503.1 (1992). "Standard specification for bonding hardened concrete, steel, wood, brick and other materials to hardened concrete with a multi-component epoxy adhesive." American Concrete Institute, Detroit, MI, 1992.
- Aktan, H., Ahlborn, T. M., Gilbertson, C. G., and Attanayake, U. (2005) "Condition Assessment and Methods of Abatement of Prestressed Concrete Box-Beam Deterioration – Phase I." *MDOT RC-1470*, Michigan Department of Transportation, Lansing, MI.
- Al-Zahrani, M. M., Maselhuddin, M., Al-Duaijan, A. U., and Ibrahim, M. (2003). "Mechanical Properties and Durability Characteristics of Polymer-and Cement-Based Materials." *Cement and Concrete Composites*, 25, 527-537.
- Arandigoyen, M., Alvarez, J. I. (2007). "Pore structure and mechanical properties of cement–lime mortars." *Cement and Concrete Research* 37 (2007) 767–775.
- Attanayake, U. (2006). "Macromechanical modeling of precast orthotropic bridge superstructure systems." *Ph.D Dissertation*, Wayne State University, Detroit, Michigan.
- Attanayake, U. and Aktan, H. M. (2009). "Side-by-side Box-beam Bridge Superstructure – Rational Transverse Posttension Design," *CD-ROM, paper # 09-3420*, 88th TRB Annual Meeting, Transportation Research Board of National Academies, Washington, D. C.
- Attanayake, U. and Aktan, H. (2008). "Issues with Reflective Deck Cracks in Side-by-Side Box-Beam Bridges." *The 4th Concrete Bridge Conference*, Hyatt Regency, St. Louis, Missouri, May 4 – 7.
- Attanayake, U. and Aktan, H. M. (2007). "Macromechanical modeling of precast orthotropic bridge superstructure systems." *CD-ROM, paper # 07-3209*, 86th Annual Meeting, Transportation Research Board of National Academies, Washington, D. C.

- Baluch, M. H., Rahman, M. K., and Al-Gadhib, A. H. (2002). "Risks of Cracking and Delamination in Patch Repair." *Journal of Materials in Civil Engineering* 14(4), 294-302.
- Barboza, A. d. S. R. and El Debs, E. E. (2006). "Load-bearing capacity of mortar joints between precast elements." *Magazine of Concrete Research*, 58 (9), 589-599.
- Beushausen, H.-D., and Alexander, M. G. (2007). "Performance of Concrete Patch Repair System" *Advances in Construction Materials 2007*, C. U. Grosse, ed., Springer 255-262.
- Civjan, S. A., Jirsa, J. O., Carrasquillo, R. L., and Fowler, D. W. (1998). "Instrument to Evaluate Remaining Prstress in Damaged Prestressed Concrete Bridge Girders." *PCI Journal*, 43(2), 62-71.
- Deshpande, Y. S. (2006). "Evaluation of Commercial Rapid-Setting Materials and Development of Rapid-Setting Self-Compacting Concrete for Dowel Bar Retrofit Applications " Ph.D., Purdue University.
- Dong, X. (2002). "Traffic forces and temperature effects on shear key connection for adjacent box girder bridge." Ph.D Dissertation, University of Cincinnati, Ohio.
- Dragosavic, M. (1978). "Load bearing capacity of joints between precast elements." *RILEM-CEB-CIB Symposium Mechanical and Insulating Properties of Joints of Precast Reinforced Concrete Elements*. RILEM/CEB, Athens. pp. 29-40.
- El-Remaily, A., Tadros, M. K., Yamane, T., and Krause, G. (1996). "Transverse Design of Adjacent Precast Prestressed Concrete Box-beam Bridges." *PCI Journal*, 41(4), 96-113.
- Emberson, N. K., and Mays, G. C. (1990). "Significance of property mismatch in the patch repair of structural concrete Part I: Properties of Repair Systems." *Magazine of Concrete Research*, 45(152), 147-160.
- Ghrici, M., Kenai, S., Said-Mansour, M. (2007). "Mechanical properties and durability of mortar and concrete containing natural pozzolana and limestone blended cements." *Cement & Concrete Composites* 27(2007) 542–549.
- Gulyas, R. J., Wirthlin, G. J., and Champa, J. T. (1995). "Evaluation of keyway grout test methods for precast concrete bridges." *PCI Journal*, Vol. 40, No. 1, pp. 44-57.
- Harries, K. A. (2006). "Full-scale Testing Program on De-commissioned Girders from the LakeView Drive Bridge." FHWA-PA-2006-008-EMG001, University of Pittsburgh, Department of Civil and Environmental Engineering, 949 Benedum Hall, Pittsburgh, PA 15261.
- Hassan, K. E., Robery, P. C., and Al-Alawi, L. (2000). "Effect of Hot-Dry Curing Environment on the Intrinsic Properties of Repair Materials " *Cement and Concrete Composites*, 22, 453-458.

Hawkins, N.M., and Fuentes, B.F. (2003). "Structural Condition Assessment and Service Load Performance of Deteriorated Pretensioned Deck Beam Bridges." FHWA-IL-UI-285, Illinois Department of Transportation, Springfield, IL 62704.

<http://www.fhwa.dot.gov/hfl/about.cfm> (Accessed: September 2008).

<http://www.trb.org/trbnet/ProjectDisplay.asp?ProjectID=1673> (Accessed: September 2008)

Huckelbridge, A. A. Jr., El-Esnawi, H., and Moses, F. (1995). "Shear-Key Performance in Multibeam Box-beam Bridges." *Journal of Performance of Constructed Facilities*, 9(4), 271-285.

HyperMesh user's manual – version 8.0. (2007). Altair Engineering, Inc., 1820 E Big Beaver, Troy, Michigan 48083. (<http://www.altair.com>).

Issa, M.A., Valle, C.L., Abdalla, H.A., Islam, S., and Issa, M.A. (2003). "Performance of Transverse Joint Grout Materials in Full-Depth Precast Concrete Bridge Deck Systems." *PCI Journal*, Vol. 48, No. 4, pp.92-103.

Jones, R. M. (1975). *Mechanics of composite Materials*, first edition, McGraw-Hill, New York.

Kollar, L. P. and Springer, G. S. (2003). *Mechanics of Composite Structures*. Cambridge University press.

Kosednar, J., and Mailvaganam, N. P. (2005). "Selection and Use of Polymer-Based Materials in the Repair of Concrete Structures." *Journal of Performance of Constructed Facilities*, 19(3), 229-233.

Kuhlmann, L. A., and Foor, N. C. (1984). "Chloride Permeability Versus Air Content of Latex Modified Concrete." *Cement, Concrete, and Aggregates*, 6(1), 11-16.

Kuhn, P., and Chiarto, P. T., "Shear Lag in Box-beams Methods of Analysis and Experimental Investigations." Report No 739, *National Advisory Committee of Aeronautics*.

Lall, J., Alampalli, S., and DiCocco, E. F. (1998). "Performance of Full-Depth Shear Keys in Adjacent Prestressed Box Beam Bridges," *PCI Journal*, Vol. 43, No. 2, pp. 72-79.

Lavelle, J. A. (1988). "Acrylic latex-Modified Portland Cement " *ACI Materials Journal* (1), 4-8.

Mangat, P. S., and O'Flaherty, F. J. (2000). "Influence of Elastic Modulus on Stress Redistribution and Cracking in Repair Patches " *Cement and Concrete Research*, 30(1), 125-136.

MDOT. (2003a). *Bridge Design Manual*. Michigan Department of Transportation, Lansing, Michigan.

MDOT. (2003b). *Standard Specification for Construction*. Michigan Department of Transportation, Lansing, Michigan.

MDOT. (2005a). *Bridge Design Guide*. Michigan Department of Transportation, Lansing, Michigan.

MDOT. (2005b). *Bridge Analysis Guide*. Michigan Department of Transportation, Lansing, Michigan.

Miller, R., Hlavacs, G. M., Long, T., and Greuel, A. (1999). "Full-Scale Testing of Shear-Keys for Adjacent Box-beam Bridges." *PCI Journal*, 44(6), 80-90.

Miller, R., and Parekh, K. (1994). "Destructive Testing of Deteriorated Prestressed Box Bridge Beam." *Transportation Research Record 1460*, Transportation Research Board, 2101 Constitution Avenue, NW, Washington, DC.

Mirza, J., Mirza, M. S., and Lapointe, R. (2002). "Laboratory and Field Performance of Polymer-Modified Cement-Based Repair Mortars in Cold Climates." *Constructino and Building Materials* (16), 363-374.

Ohama, Y. (1995a). *Handbook of Polymer-Modified Concrete and Mortars-Properties and Process Technology* Noyes Publication Park Ridge, New Jersey

Ohama, Y. (1995b). "Polymer-Modified Mortars and Concretes." *Concrete Admixtures Handbook*, V. S. Ramachandran, ed., Noyes Publications, Park Ridge, N.J.

Parameswaran, S. (2004). "Investigating the Role of Material Properties and Their Variability in the Selection of Repair Material," Purdue University West Lafayette.

PCI (2003). *Precast Prestressed Bridge Design Manual*. Precast/Prestressed Concrete Institute, 175 W. Jackson Boulevard, Chicago, IL 60604

Pinelle, D. J. (1995). "Curing Stresses in Polymer-Modified Repair Mortars." *Cement, Concrete, and Aggregates*, 17(2), 195-200.

Rao, C., and Frantz, G. C. (1996). "Fatigue Tests of 27-Year-Old Prestressed Concrete Bridge Box-beams." *PCI Journal*, 41(5), 74-83.

Scholz. D. P., Wallenfelsz, J. A., Lijeron, C., and Roberts-Wallmann, C. (2007). "Recommendations for the Connection Between Full-Depth Precast BridgeDeck Panel Systems and Precast I-Beams." FHWA/VTRC 07-CR17, Virginia Transportation Research Council, 530 Edgemont Road, Charlottesville, VA 22903.

Vambersky, J. N. J. A. (1990). "Mortar Joints Loaded in Compression." *Proceeding of International Seminar on Prefabrication of Concrete Structures*. Delft University Press. pp. 167-180.

Vaysburd, A. M. (2006). "Holistic system approach to design and implementation of concrete repair." *Cement and Concrete Composites*, 28, 671-678.

Young, B., and Kreider, R. (2006). "Laboratory and Field Evaluations of Rapid Setting Patching Materials for Portland Cement Concrete." NTPEP Report 9005.1, AASHTO.

Yurtdas, I., Peng, H., Burlion, N., Skoczylas, F. (2005). "Influence of water by cement ratio on mechanical properties of mortars is submitted by drying." *Cement and Concrete Research* 36 (2006) 1286–1293.